Secondary aerosol formation from dimethyl sulfide - improved mechanistic understanding based on smog chamber experiments and modelling

Robin Wollesen de Jonge[1], Jonas Elm[2], Bernadette Rosati[2,4], Sigurd Christiansen[2], Noora Hyttinen[3], Dana Lüdemann[1], Merete Bilde[2], and Pontus Roldin[1]

[1]Division of Nuclear Physics, Lund University, P.O. Box 118, Lund, Sweden
[2]Department of Chemistry, Aarhus University, Langelandsgade 140, Aarhus, Denmark
[3]Nano and Molecular Systems Research Unit, University of Oulu, P.O. Box 3000, FI-90014 Oulu, Finland
[4]Faculty of Physics, University of Vienna, Boltzmanngasse 5, AT-1090 Vienna, Austria

Correspondence: Robin Wollesen de Jonge (robin.wdejonge@nuclear.lu.se)

S1 Reaction mechanism

Table S1: Multiphase DMS mechanism. Reactions related to the MCMv3.3.1 isoprene chemistry scheme have been excluded.

#	Reaction	Rate	Ref.
1	$O \rightarrow O_3$	$5.6D\text{-}34 \cdot [N_2] \cdot (T/300)^{-2.6} \cdot [O_2]$ $+6.0D\text{-}34 \cdot [O_2] \cdot (T/300)^{-2.6} \cdot [O_2]$	[1]
2	$O + O_3 \rightarrow DUMMY$	$8.0D\text{-}12 \cdot exp(-2060/T)$	[1]
3	$O + NO \rightarrow NO_2$	KMT01	[1]
4	$O + NO_2 \rightarrow NO$	$5.5D\text{-}12 \cdot exp(188/T)$	[1]
5	$O + NO_2 \rightarrow NO_3$	KMT02	[1]
6	$O1D \rightarrow O$	$3.2D\text{-}11 \cdot exp(67/T) \cdot [O_2] + 2.0D\text{-}11 \cdot exp(130/T) \cdot [N_2]$	[1]
7	$NO + O_3 \rightarrow NO_2$	$1.4D\text{-}12 \cdot exp(-1310/T)$	[1]
8	$NO_2 + O_3 \rightarrow NO_3$	$1.4D\text{-}13 \cdot exp(-2470/T)$	[1]
9	$NO + NO \rightarrow NO_2 + NO_2$	$3.3D\text{-}39 \cdot exp(530/T) \cdot [O_2]$	[1]
10	$NO + NO_3 \rightarrow NO_2 + NO_2$	$1.8D\text{-}11 \cdot exp(110/T)$	[1]
11	$NO_2 + NO_3 \rightarrow NO + NO_2$	$4.50D\text{-}14 \cdot exp(-1260/T)$	[1]
12	$NO_2 + NO_3 \rightarrow [N_2]O5$	KMT03	[1]

[1] MCMv3.3.1 ; [2] Hoffmann et al. (2016) ; [3] Wu et al. (2014) ; [4] Berndt et al. (2019) ; [5] Kukui et al. (2003)

[6] Atkinson et al. (2007) ; [7] Sander et al. (2006) ; [8] Atkinson et al. (2008) ; [9] Braeuer et al. (2013) ; [10] Jacobson (2005)

[11] Demore et al. (1997) ; [12] Berndt et al. (2020) ; [13] Kahan et al. (2012) ; [14] Burkholder et al. (2015)

[E] Estimate based on equilibrium coefficients ; [C] Based on pKa value from COSMO*therm* ; [A] Assumed

. . . multiphase DMS mechanism continued

#	Reaction	Rate	Ref.
13	O1D $\rightarrow$ OH + OH	2.14D-10·H_2O	[1]
14	OH + O_3 $\rightarrow$ HO_2	1.70D-12·exp(-940/T)	[1]
15	OH + H_2 $\rightarrow$ HO_2	7.7D-12·exp(-2100/T)	[1]
16	OH + CO $\rightarrow$ HO_2	KMT05	[1]
17	OH + H_2O_2 $\rightarrow$ HO_2	2.9D-12·exp(-160/T)	[1]
18	HO_2 + O_3 $\rightarrow$ OH	2.03D-16·$(T/300)^{4.57}$·exp(693/T)	[1]
19	OH + HO_2 $\rightarrow$ DUMMY	4.8D-11·exp(250/T)	[1]
20	HO_2 + HO_2 $\rightarrow$ H_2O_2	2.20D-13·KMT06·exp(600/T)+1.90D-33·M·KMT06·exp(980/T)	[1]
21	OH + NO $\rightarrow$ HONO	KMT07	[1]
22	OH + NO_2 $\rightarrow$ HNO_3	KMT08	[1]
23	OH + NO_3 $\rightarrow$ HO_2 + NO_2	2.0D-11	[1]
24	HO_2 + NO $\rightarrow$ OH + NO_2	3.45D-12·exp(270/T)	[1]
25	HO_2 + NO_2 $\rightarrow$ HO_2NO_2	KMT09	[1]
26	OH + HO_2NO_2 $\rightarrow$ NO_2	3.2D-13·exp(690/T)·1.0	[1]
27	HO_2 + NO_3 $\rightarrow$ OH + NO_2	4.0D-12	[1]
28	OH + HONO $\rightarrow$ NO_2	2.5D-12·exp(260/T)	[1]
29	OH + HNO_3 $\rightarrow$ NO_3	KMT11	[1]
30	O + SO_2 $\rightarrow$ SO_3	4.0D-32·exp(-1000/T)·M	[1]
31	OH + SO_2 $\rightarrow$ HSO_3	KMT12	[1]
32	HSO_3 $\rightarrow$ HO_2 + SO_3	1.3D-12·exp(-330/T)·[O_2]	[1]
33	SO_3 $\rightarrow$ H_2SO_4	1.20D-15·H_2O	[1]
34	O_3 $\rightarrow$ O1D	J(1)	[1]
35	O_3 $\rightarrow$ O	J(2)	[1]
36	H_2O_2 $\rightarrow$ OH + OH	J(3)	[8] [13]
37	NO_2 $\rightarrow$ NO + O	J(4)	[1]
38	NO_3 $\rightarrow$ NO	J(5)	[1]
39	NO_3 $\rightarrow$ NO_2 + O	J(6)	[1]
40	HONO $\rightarrow$ OH + NO	J(7)	[1]
41	HNO_3 $\rightarrow$ OH + NO_2	J(8)	[1]
42	[N_2]O5 $\rightarrow$ NO_2 + NO_3	KMT04	[1]
43	HO_2NO_2 $\rightarrow$ HO_2 + NO_2	KMT10	[1]
44	DMS + NO_3 $\rightarrow$ $CH_3SCH_2O_2$ + HNO_3	1.9D-13·exp(520/T)	[1]
45	DMS + OH $\rightarrow$ $CH_3SCH_2O_2$	1.12D-11·exp(-250/T)	[1]
46	\t DMS + OH $\rightarrow$ $HODMSO_2$	KMT18	[1]
47	DMS + OH $\rightarrow$ CH_3SOHCH_3	KMT18	[2]
48	CH_3SOHCH_3 $\rightarrow$ DMS + OH	(1.7D-42·O_2·exp(7810/T)/(1D0+5.5D-31·O_2·	[2]

[1] MCMv3.3.1 ; [2] Hoffmann et al. (2016) ; [3] Wu et al. (2014) ; [4] Berndt et al. (2019) ; [5] Kukui et al. (2003)

[6] Atkinson et al. (2007) ; [7] Sander et al. (2006) ; [8] Atkinson et al. (2008) ; [9] Braeuer et al. (2013) ; [10] Jacobson (2005)

[11] Demore et al. (1997) ; [12] Berndt et al. (2020) ; [13] Kahan et al. (2012) ; [14] Burkholder et al. (2015)

[E] Estimate based on equilibrium coefficients ; [C] Based on pKa value from COSMO*therm* ; [A] Assumed

. . . multiphase DMS mechanism continued

#	Reaction	Rate	Ref.
		exp(7640/T)))/(8.3D-29·T·exp(5136/T))	
49	$CH_3SOHCH_3 \rightarrow HODMSO_2$	8.5D-13·[O_2]	[2]
50	$CH_3SOHCH_3 \rightarrow CH_3SOH + CH_3O_2$	5D5	[2]
51	$CH_3SOH + OH \rightarrow CH_3SO$	5D-11	[2]
52	$DMS + Cl \rightarrow CH_3SCH_2O_2 + HCl$	0.45·3.4D-10	[2]
53	$DMS + Cl \rightarrow CH_3SCH_3Cl$	0.55·3.4D-10	[2]
54	$DMS + ClO \rightarrow DMSO + Cl$	0.73·1.7D-15·exp(340/T)	[2]
55	$DMS + ClO \rightarrow CH_3SCH_2O_2 + HOCl$	0.27·1.7D-15·exp(340/T)	[2]
56	$DMS + Cl_2 \rightarrow CH_3SCH_2Cl + HCl$	3.4D-14	[2]
57	$CH_3SCH_2Cl + OH \rightarrow CH_3SOH + CH_2ClO_2$	2.5D-12	[2]
58	$CH_3SCH_3Cl + NO_2 \rightarrow DMS + ClNO_2$	2.7D-11	[2]
59	$CH_3SCH_3Cl + NO \rightarrow DMS + ClNO$	1.2D-11	[2]
60	$CH_3SCH_3Cl \rightarrow DMSO + ClO$	4D-18·[O_2]	[2]
61	$CH_3SCH_3Cl \rightarrow DMS + Cl$	9D1	[2]
62	$CH_3SOCH_3Cl \rightarrow DMSO_2 + ClO$	3D-18·[O_2]	[2]
63	$CH_3SOCH_3Cl + NO \rightarrow DMSO + ClNO$	1.2D-11	[2]
64	$CH_3SOCH_3Cl + NO_2 \rightarrow DMSO + ClNO_2$	2.1D-11	[2]
65	$CH_3SOCH_3Cl + CH_3SOCH_3Cl \rightarrow DMSO + DMSO + Cl_2$	3D-11	[2]
66	$CH_3SOCH_3Cl \rightarrow DMSO + Cl$	9D1	[2]
67	$CH_3SCH_2O_2 + HO_2 \rightarrow CH_3SCH_2OOH$	KRO_2HO_2·0.387	[1]
68	$CH_3SCH_2O_2 + NO \rightarrow CH_3SCH_2O + NO_2$	4.9D-12·exp(260/T)	[1]
69	$CH_3SCH_2O_2 + NO_3 \rightarrow CH_3SCH_2O + NO_2$	KRO_2NO_3	[1]
70	$CH_3SCH_2O_2 \rightarrow CH_3SCH_2O$	2·(K298CH_3O_2·1.0D-11)$^{0.5}$ ·RO_2·0.8	[1]
71	$CH_3SCH_2O_2 \rightarrow CH_3SCH_2OH$	2·(K298CH_3O_2·1.0D-11)$^{0.5}$ ·RO_2·0.1	[1]
72	$CH_3SCH_2O_2 \rightarrow CH_3SCHO$	2·(K298CH_3O_2·1.0D-11)$^{0.5}$ ·RO_2·0.1	[1]
73	$CH_3SCH_2O_2 \rightarrow OOCH_2SCH_2OOH$	2.2433D11·exp(-9.8016D3/T)·exp(1.0348E8/T^3)·5D0	[4]
74	$OOCH_2SCH_2OOH \rightarrow HPMTF + OH$	6.097D11·exp(-9.4892D3/T)·exp(1.102E8/T^3)	[4]
75	$OOCH_2SCH_2OOH + NO \rightarrow HOOCH_2S + NO_2 + HCHO$	4.9D-12·exp(260/T)	[1]
76	$OOCH_2SCH_2OOH + HO_2 \rightarrow HOOCH_2SCH_2OOH$	1.13D-13·exp(1300/T)	[1]
77	$HPMTF + OH \rightarrow HOOCH_2SCO$	1.4D-12·exp(0D0/T)	[3]
78	$HOOCH_2SCO \rightarrow HOOCH_2S + CO$	9.2D9·exp(-505.4/T)	[3]
79	$HOOCH_2SCO \rightarrow HCHO + OH + OCS$	1.6D7·exp(-1468.6/T)	[3]
80	$HOOCH_2S + O_3 \rightarrow HOOCH_2SO$	1.15D-12·exp(430/T)	[3]
81	$HOOCH_2S + NO_2 \rightarrow HOOCH_2SO + NO$	6.00D-11·exp(240/T)	[3]
82	$HOOCH_2SO + O_3 \rightarrow SO_2 + HCHO + OH$	4.00D-13	[3]
83	$HOOCH_2SO + NO_2 \rightarrow SO_2 + HCHO + OH + NO$	1.20D-11	[3]
84	$HODMSO_2 + NO \rightarrow DMSO_2 + HO_2 + NO_2$	KRO_2NO	[1]

[1] MCMv3.3.1 ; [2] Hoffmann et al. (2016) ; [3] Wu et al. (2014) ; [4] Berndt et al. (2019) ; [5] Kukui et al. (2003)

[6] Atkinson et al. (2007) ; [7] Sander et al. (2006) ; [8] Atkinson et al. (2008) ; [9] Braeuer et al. (2013) ; [10] Jacobson (2005)

[11] Demore et al. (1997) ; [12] Berndt et al. (2020) ; [13] Kahan et al. (2012) ; [14] Burkholder et al. (2015)

[E] Estimate based on equilibrium coefficients ; [C] Based on pKa value from COSMO*therm* ; [A] Assumed

. . . multiphase DMS mechanism continued

#	Reaction	Rate	Ref.
85	$HODMSO_2 \rightarrow DMSO + HO_2$	8.90D+10·exp(-6040/T)	[1]
86	$CH_3SCH_2OOH + OH \rightarrow CH_3SCHO + OH$	7.03D-11	[1]
87	$CH_3SCH_2OOH \rightarrow CH_3SCH_2O + OH$	J(41)	[1]
88	$CH_3SCH_2O \rightarrow CH_3S + HCHO$	KDEC	[1]
89	$CH_3SCH_2OH + OH \rightarrow CH_3SCHO + HO_2$	2.78D-11	[1]
90	$CH_3SCHO + OH \rightarrow CH_3S + CO$	1.11D-11	[1]
91	$CH_3SCHO \rightarrow CH_3S + CO + HO_2$	J(15)	[1]
92	$DMSO_2 + OH \rightarrow DMSO_2O_2$	4.40D-14	[1]
93	$DMSO + OH \rightarrow MSIA + CH_3O_2$	6.10D-12·exp(800/T)	[1]
94	$DMSO + NO_3 \rightarrow DMSO_2 + NO_2$	2.9D-13	[2]
95	$DMSO + Cl \rightarrow CH_3SOCH_2O_2 + HCl$	1.45D-11	[2]
96	$DMSO + Cl \rightarrow CH_3SOCH_3Cl$	7.4D-11	[2]
97	$CH_3SOCH_2O_2 + NO \rightarrow CH_3SO + HCHO + NO_2$	7.5D-12	[2]
98	$CH_3SOCH_2O_2 + HO_2 \rightarrow CH_3SOCH_2OOH$	1.5D-12	[2]
99	$CH_3S + NO_2 \rightarrow CH_3SO + NO$	6.00D-11·exp(240/T)	[1]
100	$CH_3S + O_3 \rightarrow CH_3SO$	1.15D-12·exp(430/T)	[1]
101	$CH_3S \rightarrow CH_3SOO$	1.20D-16·exp(1580/T)·[O_2]	[1]
102	$HCHO \rightarrow CO + HO_2 + HO_2$	J(11)	[1]
103	$HCHO \rightarrow H_2 + CO$	J(12)	[1]
104	$NO_3 + HCHO \rightarrow HNO_3 + CO + HO_2$	5.5D-16	[1]
105	$OH + HCHO \rightarrow HO_2 + CO$	5.4D-12·exp(135/T)	[1]
106	$DMSO_2O_2 + HO_2 \rightarrow DMSO_2OOH$	KRO_2HO_2·0.387	[1]
107	$DMSO_2O_2 + NO \rightarrow DMSO_2O + NO_2$	KRO_2NO	[1]
108	$DMSO_2O_2 + NO_3 \rightarrow DMSO_2O + NO_2$	KRO_2NO_3	[1]
109	$DMSO_2O_2 \rightarrow CH_3SO_2CHO$	2.00D-12·RO_2·0.2	[1]
110	$DMSO_2O_2 \rightarrow DMSO_2O$	2.00D-12·RO_2·0.6	[1]
111	$DMSO_2O_2 \rightarrow DMSO_2OH$	2.00D-12·RO_2·0.2	[1]
112	$MSIA + OH \rightarrow CH_3O_2 + SO_2$	0D0·9.00D-11	[1]
113	$MSIA + OH \rightarrow CH_3SO_2$	1D-10·exp(0D0/T)	[5]
114	$MSIA + NO_3 \rightarrow CH_3SO_2 + HNO_3$	1D-13	[2]
115	$CH_3O_2 + HO_2 \rightarrow CH_3OOH$	3.8D-13·exp(780/T)·(1-1/(1+498·exp(-1160/T)	[1]
116	$CH_3O_2 + HO_2 \rightarrow HCHO$	3.8D-13·exp(780/T)·(1/(1+498·exp(-1160/T)))	[1]
117	$CH_3O_2 + NO \rightarrow CH_3NO_3$	2.3D-12·exp(360/T)·0.001	[1]
118	$CH_3O_2 + NO \rightarrow CH_3O + NO_2$	2.3D-12·exp(360/T)·0.999	[1]
119	$CH_3O_2 + NO_2 \rightarrow CH_3O_2NO_2$	KMT13	[1]
120	$CH_3O_2 + NO_3 \rightarrow CH_3O + NO_2$	1.2D-12	[1]
121	$CH_3O_2 \rightarrow CH_3O$	2·KCH_3O_2·RO_2·7.18·exp(-885/T)	[1]

[1] MCMv3.3.1 ; [2] Hoffmann et al. (2016) ; [3] Wu et al. (2014) ; [4] Berndt et al. (2019) ; [5] Kukui et al. (2003)

[6] Atkinson et al. (2007) ; [7] Sander et al. (2006) ; [8] Atkinson et al. (2008) ; [9] Braeuer et al. (2013) ; [10] Jacobson (2005)

[11] Demore et al. (1997) ; [12] Berndt et al. (2020) ; [13] Kahan et al. (2012) ; [14] Burkholder et al. (2015)

[E] Estimate based on equilibrium coefficients ; [C] Based on pKa value from COSMO*therm* ; [A] Assumed

…multiphase DMS mechanism continued

#	Reaction	Rate	Ref.
122	$CH_3O_2 \rightarrow CH_3OH$	$2\cdot KCH_3O_2\cdot RO_2\cdot 0.5\cdot(1\text{-}7.18\cdot \exp(-885/T))$	[1]
123	$CH_3O_2 \rightarrow HCHO$	$2\cdot KCH_3O_2\cdot RO_2\cdot 0.5\cdot(1\text{-}7.18\cdot \exp(-885/T))$	[1]
124	$CH_3SO + NO_2 \rightarrow CH_3O_2 + SO_2 + NO$	1.20D-11·0.25	[1]
125	$CH_3SO + NO_2 \rightarrow CH_3SO_2 + NO$	1.20D-11·0.75	[1]
126	$CH_3SO + O_3 \rightarrow CH_3O_2 + SO_2$	4.00D-13	[1]
127	$CH_3SO \rightarrow CH_3SOO_2$	3.12D-16·exp(1580/T)·$[O_2]$	[1]
128	$CH_3SOO + NO \rightarrow CH_3SO + NO_2$	1.1D-11	[1]
129	$CH_3SOO + NO_2 \rightarrow CH_3SO + NO_3$	2.2D-11	[1]
130	$CH_3SOO \rightarrow CH_3O_2 + SO_2$	5.60D+16·exp(-10870/T)	[1]
131	$CH_3SOO \rightarrow CH_3S$	3.50D+10·exp(-3560/T)	[1]
132	$CH_3SOO + HO_2 \rightarrow CH_3SOOH$	4D-12	[2]
133	$CH_3SOO \rightarrow CH_3SO_2$	1D0	[2]
134	$DMSO_2OOH + OH \rightarrow CH_3SO_2CHO + OH$	1.26D-12	[1]
135	$DMSO_2OOH + OH \rightarrow DMSO_2O_2$	3.60D-12	[1]
136	$DMSO_2OOH \rightarrow DMSO_2O + OH$	J(41)	[1]
137	$DMSO_2O \rightarrow CH_3SO_2 + HCHO$	KDEC	[1]
138	$CH_3SO_2CHO + OH \rightarrow CH_3SO_2 + CO$	1.78D-12	[1]
139	$CH_3SO_2CHO \rightarrow CH_3SO_2 + CO + HO_2$	J(15)	[1]
140	$DMSO_2OH + OH \rightarrow CH_3SO_2CHO + HO_2$	5.23D-13	[1]
141	$DMSO_2OH + OH \rightarrow DMSO_2O$	1.40D-13	[1]
142	$CH_3OOH \rightarrow CH_3O + OH$	J(41)	[1]
143	$OH + CH_3OOH \rightarrow CH_3O_2$	5.3D-12·exp(190/T)·0.6	[1]
144	$OH + CH_3OOH \rightarrow HCHO + OH$	5.3D-12·exp(190/T)·0.4	[1]
145	$CH_3NO_3 \rightarrow CH_3O + NO_2$	J(51)	[1]
146	$OH + CH_3NO_3 \rightarrow HCHO + NO_2$	4.0D-13·exp(-845/T)	[1]
147	$CH_3O \rightarrow HCHO + HO_2$	7.2D-14·exp(-1080/T)·$[O_2]$	[1]
148	$CH_3O_2NO_2 \rightarrow CH_3O_2 + NO_2$	KMT14	[1]
149	$CH_3OH + OH \rightarrow HO_2 + HCHO$	2.85D-12·exp(-345/T)	[1]
150	$CH_3SO_2 + O_3 \rightarrow CH_3SO_3$	3.00D-13	[1]
151	$CH_3SO_2 \rightarrow CH_3O_2 + SO_2$	5.00D+13·exp(-9673/T)	[1]
152	$CH_3SO_2 \rightarrow CH_3SO_2O_2$	1.03D-16·exp(1580/T)·$[O_2]$	[1]
153	$CH_3SO_2 + OH \rightarrow MSA$	5D-11	[2]
154	$CH_3SO_2 + NO_2 \rightarrow CH_3SO_3 + NO$	2.2D-11	[2]
155	$CH_3SOO_2 + HO_2 \rightarrow CH_3SO_2 + OH$	$KAPHO_2\cdot 0.44$	[1]
156	$CH_3SOO_2 + HO_2 \rightarrow CH_3SOOOH$	$KAPHO_2\cdot 0.41$	[1]
157	$CH_3SOO_2 + HO_2 \rightarrow MSIA + O_3$	$KAPHO_2\cdot 0.15$	[1]
158	$CH_3SOO_2 + NO \rightarrow CH_3SO_2 + NO_2$	1.00D-11	[1]

[1] MCMv3.3.1 ; [2] Hoffmann et al. (2016) ; [3] Wu et al. (2014) ; [4] Berndt et al. (2019) ; [5] Kukui et al. (2003)

[6] Atkinson et al. (2007) ; [7] Sander et al. (2006) ; [8] Atkinson et al. (2008) ; [9] Braeuer et al. (2013) ; [10] Jacobson (2005)

[11] Demore et al. (1997) ; [12] Berndt et al. (2020) ; [13] Kahan et al. (2012) ; [14] Burkholder et al. (2015)

[E] Estimate based on equilibrium coefficients ; [C] Based on pKa value from COSMO*therm* ; [A] Assumed

. . . multiphase DMS mechanism continued

#	Reaction	Rate	Ref.
159	$CH_3SOO_2 + NO_2 \rightarrow CH_3SOO_2NO_2$	1.20D-12·(T/300)$^{-0.9}$	[1]
160	$CH_3SOO_2 + NO_3 \rightarrow CH_3SO_2 + NO_2$	KRO_2NO_3·1.74	[1]
161	$CH_3SOO_2 \rightarrow CH_3SO$	9.10D+10·exp(-3560/T)	[1]
162	$CH_3SOO_2 \rightarrow CH_3SO_2$	1.00D-11·RO_2·0.7	[1]
163	$CH_3SOO_2 \rightarrow$ MSIA	1.00D-11·RO_2·0.3	[1]
164	$CH_3SO_3 + HO_2 \rightarrow$ MSA	5.00D-11	[1]
165	$CH_3SO_3 \rightarrow CH_3O_2 + SO_3$	5.00D+13·exp(-9946/T)	[1]
166	$CH_3SO_2O_2 + HO_2 \rightarrow CH_3SO_2OOH$	$KAPHO_2$·0.41	[1]
167	$CH_3SO_2O_2 + HO_2 \rightarrow CH_3SO_3 + OH$	$KAPHO_2$·0.44	[1]
168	$CH_3SO_2O_2 + HO_2 \rightarrow$ MSA + O_3	$KAPHO_2$·0.15	[1]
169	$CH_3SO_2O_2 + NO \rightarrow CH_3SO_3 + NO_2$	1.00D-11	[1]
170	$CH_3SO_2O_2 + NO_2 \rightarrow CH_3SO_4NO_2$	1.20D-12·(T/300)$^{0.9}$	[1]
171	$CH_3SO_2O_2 + NO_3 \rightarrow CH_3SO_3 + NO_2$	KRO_2NO_3·1.74	[1]
172	$CH_3SO_2O_2 \rightarrow CH_3SO_2$	3.01D+10·exp(-3560/T)	[1]
173	$CH_3SO_2O_2 \rightarrow CH_3SO_3$	1.00D-11·RO_2·0.7	[1]
174	$CH_3SO_2O_2 \rightarrow$ MSA	1.00D-11·RO_2·0.3	[1]
175	$CH_3SOOOH + OH \rightarrow CH_3SOO_2$	9.00D-11	[1]
176	$CH_3SOOOH \rightarrow CH_3SO_2 + OH$	J(41)	[1]
177	$CH_3SOO_2NO_2 + OH \rightarrow$ MSIA + NO_2	1.00D-11	[1]
178	$CH_3SOO_2NO_2 \rightarrow CH_3SOO_2 + NO_2$	5.40D+16·exp(-13112/T)	[1]
179	MSA + OH $\rightarrow CH_3SO_3$	2.24D-14	[1]
180	$CH_3SO_2OOH + OH \rightarrow CH_3SO_2O_2$	3.60D-12	[1]
181	$CH_3SO_2OOH \rightarrow CH_3SO_3 + OH$	J(41)	[1]
182	$CH_3SO_4NO_2 + OH \rightarrow CH_3SO_2O_2 + HNO_3$	3.60D-13	[1]
183	$CH_3SO_4NO_2 \rightarrow CH_3SO_2O_2 + NO_2$	5.40D+16·exp(-13112/T)	[1]
184	$Cl + O_3 \rightarrow ClO$	2.8D-11·exp(-250/T)	[9] [2] [6]
185	$Cl + H_2 \rightarrow HCl + HO_2$	3.9D-11·exp(-2310/T)	[9] [2] [6]
186	$Cl + HO_2 \rightarrow HCl$	3.4D-11	[9] [2] [6]
187	$Cl + HO_2 \rightarrow ClO + OH$	6.3D-11·exp(-570/T)	[9] [2] [6]
188	$Cl + H_2O_2 \rightarrow HCl + HO_2$	1.1D-11·exp(-980/T)	[9] [2] [6]
189	$Cl_2 + OH \rightarrow HOCl + Cl$	3.6D-12·exp(-1200/T)	[9] [2] [6]
190	$ClO + O_3 \rightarrow ClO_2$	1.13D-17·exp(-3600·(1D0/T-1D0/298D0))	[9] [2]
191	$ClO + O_3 \rightarrow OClO$	1.48D-18·exp(-4000·(1D0/T-1D0/298D0))	[9] [2]
192	$ClO + OH \rightarrow HO_2 + Cl$	0.94·7.3D-12·exp(300/T)	[9] [2] [6]
193	$ClO + OH \rightarrow HCl$	0.06·7.3D-12·exp(300/T)	[9] [2] [6]
194	$ClO + HO_2 \rightarrow HOCl$	2.2D-12·exp(340/T)	[9] [2] [6]
195	$ClO + ClO \rightarrow Cl_2$	1D-12·exp(-1590/T)	[9] [2] [6]

[1] MCMv3.3.1 ; [2] Hoffmann et al. (2016) ; [3] Wu et al. (2014) ; [4] Berndt et al. (2019) ; [5] Kukui et al. (2003)

[6] Atkinson et al. (2007) ; [7] Sander et al. (2006) ; [8] Atkinson et al. (2008) ; [9] Braeuer et al. (2013) ; [10] Jacobson (2005)

[11] Demore et al. (1997) ; [12] Berndt et al. (2020) ; [13] Kahan et al. (2012) ; [14] Burkholder et al. (2015)

[E] Estimate based on equilibrium coefficients ; [C] Based on pKa value from COSMO*therm* ; [A] Assumed

. . . multiphase DMS mechanism continued

#	Reaction	Rate	Ref.
196	$ClO + ClO \rightarrow Cl + ClO_2$	3D-11·exp(-2450/T)	[9] [2] [6]
197	$ClO + ClO \rightarrow Cl + OClO$	3.5D-13·exp(-1370/T)	[9] [2] [6]
198	$ClO + ClO \rightarrow Cl_2O_2$	KMT46, 1.52D-15	[9] [2]
199	$Cl \rightarrow ClO_2$	KMT47·[O_2], 5.17D-14·[O_2]	[9] [2]
200	$ClO_2 \rightarrow Cl$	2.8D-10·exp(-1820/T)·[N_2]	[9] [2] [6]
201	$Cl + ClO_2 \rightarrow Cl_2$	0.95·2.42D-10	[9] [2] [7]
202	$Cl + ClO_2 \rightarrow ClO + ClO$	0.05·2.42D-10	[9] [2] [7]
203	$Cl_2O_2 \rightarrow ClO + ClO$	KMT48, 2.87D-3	[9] [2]
204	$Cl_2O_2 + O_3 \rightarrow ClO + ClO_2$	1D-19	[9] [2] [6]
205	$Cl_2O_2 + Cl \rightarrow Cl_2 + ClO_2$	7.6D-11·exp(65/T)	[9] [2] [6]
206	$OClO + OH \rightarrow HOCl$	1.4D-12·exp(600/T)	[9] [2] [6]
207	$Cl + OClO \rightarrow ClO + ClO$	3.2D-11·exp(170/T)	[9] [2] [6]
208	$ClO + OClO \rightarrow Cl_2O_3$	KMT49, 1.08D-19	[9] [2]
209	$Cl_2O_3 \rightarrow ClO + OClO$	KMT50 + J(65), 6.17D-2	[9] [2]
210	$HCl + OH \rightarrow Cl$	1.7D-12·exp(-230/T)	[9] [2] [6]
211	$HOCl + OH \rightarrow ClO$	5.60D-13·exp(-500·(1D0/T-1D0/298D0))	[9] [2] [7]
212	$HOCl + Cl \rightarrow HCl + ClO$	0.76·1.62D-12·exp(-130·(1D0/T-1D0/298D0))	[9] [2] [7]
213	$HOCl + Cl \rightarrow Cl_2 + OH$	0.24·1.62D-12·exp(-130·(1D0/T-1D0/298D0))	[9] [2] [7]
214	$ClO + NO \rightarrow Cl + NO_2$	6.2D-12·exp(295/T)	[9] [2] [6]
215	$OClO + NO \rightarrow ClO + NO_2$	1.16D-13·exp(350/T)	[9] [2] [6]
216	$Cl + NO_3 \rightarrow ClO + NO_2$	2.40D-11	[9] [2] [6]
217	$ClO + NO_3 \rightarrow ClO_2 + NO_2$	0.68·4.61D-13	[9] [2] [6]
218	$ClO + NO_3 \rightarrow OClO + NO_2$	0.32·4.61D-13	[9] [2] [6]
219	$Cl + NO \rightarrow ClNO$	KMT51, 1.92D-12	[9] [2]
220	$Cl + ClNO \rightarrow Cl_2 + NO$	8.11D-11·exp(100·(1D0/T-1D0/298D0))	[9] [2] [7]
221	$Cl + NO_2 \rightarrow ClNO_2$	KMT52, 5.80D-14	[9] [2]
222	$ClNO_2 + OH \rightarrow HOCl + NO_2$	3.62D-14·exp(-1250·(1D0/T-1D0/298D0))	[9] [2] [7]
223	$ClO + NO_2 \rightarrow ClNO_3$	KMT53, 1.85D-19	[9] [2]
224	$ClNO_3 \rightarrow ClO + NO_2$	1.47D-3·exp(-11438·(1D0/T-1D0/298D0)) + J(70)	[9] [2]
225	$ClNO_3 + OH \rightarrow ClO + HNO_3$	0.5·1.2D-12·exp(-330/T)	[9] [2] [6]
226	$ClNO_3 + OH \rightarrow HOCl + NO_3$	0.5·1.2D-12·exp(-330/T)	[9] [2] [6]
227	$ClNO_3 + Cl \rightarrow Cl_2 + NO_3$	6.2D-12·exp(145/T)	[9] [2] [6]
228	$Cl + CH_4 \rightarrow CH_3O_2 + HCl$	6.6D-12·exp(-1240/T)	[9] [2]
229	$Cl + CH_3OOH \rightarrow CH_3O_2 + HCl$	5.7D-11	[9] [2]
230	$Cl + CH_3O_2 \rightarrow HCHO + ClO$	0.5·1.60D-10	[9] [2] [7]
231	$Cl + CH_3O_2 \rightarrow HO_2 + HCl + HCOOH$	0.5·1.60D-10	[9] [2] [7]
232	$ClO + CH_3O_2 \rightarrow ClO_2 + HCHO + HO_2$	1.63D-12·exp(-238·(1D0/T-1D0/298D0))	[9] [2]

[1] MCMv3.3.1 ; [2] Hoffmann et al. (2016) ; [3] Wu et al. (2014) ; [4] Berndt et al. (2019) ; [5] Kukui et al. (2003)

[6] Atkinson et al. (2007) ; [7] Sander et al. (2006) ; [8] Atkinson et al. (2008) ; [9] Braeuer et al. (2013) ; [10] Jacobson (2005)

[11] Demore et al. (1997) ; [12] Berndt et al. (2020) ; [13] Kahan et al. (2012) ; [14] Burkholder et al. (2015)

[E] Estimate based on equilibrium coefficients ; [C] Based on pKa value from COSMO*therm* ; [A] Assumed

. . . multiphase DMS mechanism continued

#	Reaction	Rate	Ref.
233	$Cl + HCHO \rightarrow HCl + CO + HO_2$	7.23D-11·exp(-34·(1D0/T-1D0/298D0))	[9] [2]
234	$ClO + HCHO \rightarrow HOCl + CO + HO_2$	8.7D-16·exp(-2100·(1D0/T-1D0/298D0))	[9] [2]
235	$Cl + CH_3CHO \rightarrow HCl + CH_3CO_3$	8D-11	[9] [2]
236	$Cl_2 \rightarrow Cl + Cl$	J(61)	[9] [2] [7]
237	$ClO \rightarrow Cl + O$	J(62)	[9] [2] [7]
238	$OClO \rightarrow ClO + O$	J(63)	[9] [2] [7]
239	$Cl_2O_2 \rightarrow Cl + ClO_2$	J(64)	[9] [2] [7]
240	$Cl_2O_3 \rightarrow ClO + OClO$	J(65)	[9] [2] [6]
241	$HOCl \rightarrow Cl + OH$	J(66)	[9] [2] [6]
242	$ClNO \rightarrow Cl + NO$	J(67)	[9] [2] [6]
243	$ClNO_2 \rightarrow Cl + NO_2$	J(68)	[9] [2] [6]
244	$ClNO_3 \rightarrow Cl + NO_3$	J(69)	[9] [2] [7]
245	$ClNO_3 \rightarrow ClO + NO_2$	J(70)	[9] [2] [7]
246	$CH_3SOCH_2OOH \rightarrow CH_3SO + HCHO + OH$	J(41)	[9] [2]
247	$CH_3SCH_2Cl \rightarrow CH_3S + CH_2ClO_2$	J(71)	[9] [2]
248	$CH_3SOOH \rightarrow CH_3SO + OH$	J(41)	[9] [2]
249	$CH_3Cl + OH \rightarrow CH_2ClO_2$	$7.33D\text{-}18 \cdot T^2 \cdot exp(-809/T)$	[9] [2]
250	$CH_3Cl + Cl \rightarrow CH_2ClO_2 + HCl$	4.85D-13·exp(-1150·(1D0/T-1D0/298D0))	[9] [2]
251	$CH_2ClO_2 + HO_2 \rightarrow CH_2ClOOH$	3.2D-13·exp(820/T)·0.3	[1]
252	$CH_2ClO_2 + HO_2 \rightarrow CHOCl$	3.2D-13·exp(820/T)·0.7	[1]
253	$CH_2ClO_2 + NO \rightarrow CH_2ClO + NO_2$	$KRO_2NO \cdot 1.5$	[9] [2]
254	$CH_2ClO_2 + NO_3 \rightarrow CH_2ClO + NO_2$	KRO_2NO_3	[9] [2]
255	$CH_2ClO_2 \rightarrow CH_2ClO$	$2 \cdot (KCH_3O_2 \cdot 1.9D\text{-}13 \cdot exp(870/T))^{0.5} \cdot RO_2 \cdot 0.6$	[1]
256	$CH_2ClO_2 \rightarrow CH_2ClOH$	$2 \cdot (KCH_3O_2 \cdot 1.9D\text{-}13 \cdot exp(870/T))^{0.5} \cdot RO_2 \cdot 0.2$	[1]
257	$CH_2ClO_2 \rightarrow CHOCl$	$2 \cdot (KCH_3O_2 \cdot 1.9D\text{-}13 \cdot exp(870/T))^{0.5} \cdot RO_2 \cdot 0.2$	[1]
258	$CH_2ClOOH + OH \rightarrow CH_2ClO_2$	1.90D-12·exp(190/T)	[1]
259	$CH_2ClOOH + OH \rightarrow CHOCl + OH$	4.14D-12	[1]
260	$CH_2ClOOH \rightarrow CH_2ClO + OH$	J(41)	[1]
261	$CHOCl + NO_3 \rightarrow CO + Cl + HNO_3$	KNO_3AL	[1]
262	$CHOCl + OH \rightarrow CO + Cl$	6.12D-12	[1]
263	$CHOCl \rightarrow HO_2 + CO + Cl$	J(11)	[1]
264	$CH_2ClO \rightarrow CHOCl + HO_2$	$KROPRIM \cdot [O_2]$	[1]
265	$CH_2ClOH + OH \rightarrow CHOCl + HO_2$	1.08D-12	[1]
266	$DMS + Br \rightarrow CH_3SCH_2O_2 + HBr$	9D-11·exp(-2390/T)	[9] [2]
267	$DMS + Br \rightarrow CH_3SCH_3Br$	KMT54	[9] [2]
268	$DMS + BrO \rightarrow DMSO + Br$	1.5D-14·exp(1000/T)	[9] [2]
269	$CH_3SCH_3Br \rightarrow DMSO + BrO$	$1D\text{-}18 \cdot [O_2]$	[9] [2]

[1] MCMv3.3.1 ; [2] Hoffmann et al. (2016) ; [3] Wu et al. (2014) ; [4] Berndt et al. (2019) ; [5] Kukui et al. (2003)

[6] Atkinson et al. (2007) ; [7] Sander et al. (2006) ; [8] Atkinson et al. (2008) ; [9] Braeuer et al. (2013) ; [10] Jacobson (2005)

[11] Demore et al. (1997) ; [12] Berndt et al. (2020) ; [13] Kahan et al. (2012) ; [14] Burkholder et al. (2015)

[E] Estimate based on equilibrium coefficients ; [C] Based on pKa value from COSMO*therm* ; [A] Assumed

. . . multiphase DMS mechanism continued

#	Reaction	Rate	Ref.
270	$CH_3SCH_3Br \rightarrow DMS + Br$	1.02D4	[9] [2]
271	$DMSO + BrO \rightarrow DMSO_2 + Br$	1D-14	[9] [2]
272	$Br + O_3 \rightarrow BrO$	1.7D-11·exp(-800/T)	[9] [2] [6]
273	$Br + HO_2 \rightarrow HBr$	7.7D-12·exp(-450/T)	[9] [2] [6]
274	$Br + H_2O_2 \rightarrow HBr + HO_2$	5D-16	[9] [2] [6]
275	$Br_2 + OH \rightarrow HOBr + Br$	2D-11·exp(240/T)	[9] [2] [6]
276	$BrO + O_3 \rightarrow Br$	0.9·2D-17	[9] [2] [6]
277	$BrO + O_3 \rightarrow OBrO$	0.1·2D-17	[9] [2] [6]
278	$BrO + OH \rightarrow Br + HO_2$	1.8D-11·exp(250/T)	[9] [2] [6]
279	$BrO + HO_2 \rightarrow HOBr$	4.5D-12·exp(500/T)	[9] [2] [6]
280	$BrO + BrO \rightarrow Br + Br$	0.85·2.7D-12	[9] [2] [6]
281	$BrO + BrO \rightarrow Br_2$	0.15·2.7D-12	[9] [2] [6]
282	$HBr + OH \rightarrow Br$	6.7D-12·exp(155/T)	[9] [2] [6]
283	$Br + NO_2 \rightarrow BrNO_2$	KMT55	[9] [2] [6]
284	$Br + NO_3 \rightarrow BrO + NO_2$	1.6D-11	[9] [2] [6]
285	$BrO + NO \rightarrow Br + NO_2$	8.7D-12·exp(260/T)	[9] [2] [6]
286	$BrO + NO_2 \rightarrow BrNO_3$	KMT56	[9] [2] [6]
287	$BrNO_3 \rightarrow BrO + NO_2$	2.75D-5·exp(-12360·(1D0/T-1D0/298D0)) + J(78)	[9] [2]
288	$BrNO_3 + Br \rightarrow Br_2 + NO_3$	4.9D-11	[9] [2]
289	$HBr + NO_3 \rightarrow Br + HNO_3$	1D-16	[9] [2] [6]
290	$Br + Cl_2O_2 \rightarrow BrCl + ClO_2$	5.9D-12·exp(-170/T)	[9] [2] [6]
291	$Br + OClO \rightarrow BrO + ClO$	2.7D-11·exp(-1300/T)	[9] [2] [6]
292	$BrO + ClO \rightarrow Br + OClO$	1.6D-12·exp(430/T)	[9] [2] [6]
293	$BrO + ClO \rightarrow Br + ClO_2$	2.9D-12·exp(220/T)	[9] [2] [6]
294	$BrO + ClO \rightarrow BrCl$	5.8D-13·exp(170/T)	[9] [2] [6]
295	$Br_2 + Cl \rightarrow BrCl + Br$	3.62D-10·exp(135·(1D0/T-1D0/298D0))	[9] [2]
296	$BrCl + Br \rightarrow Br_2 + Cl$	3.32D-15	[9] [2]
297	$Br + Cl_2 \rightarrow BrCl + Cl$	1.1D-15	[9] [2]
298	$BrCl + Cl \rightarrow Br + Cl_2$	1.45D-11	[9] [2]
299	$Br + CH_3OOH \rightarrow HBr + CH_3O_2$	1.18D-14·exp(-1610·(1D0/T-1D0/298D0))	[9] [2]
300	$BrO + CH_3O_2 \rightarrow Br + HCHO + HO_2$	0.25·6.01D-12·exp(800·(1D0/T-1D0/298D0))	[9] [2]
301	$BrO + CH_3O_2 \rightarrow HOBr + HCOOH$	0.75·6.01D-12·exp(800·(1D0/T-1D0/298D0))	[9] [2]
302	$Br + HCHO \rightarrow HBr + CO + HO_2$	1.161D-12·exp(-800·(1D0/T-1D0/298D0))	[9] [2] [7]
303	$BrO + HCHO \rightarrow HOBr + CO + HO_2$	1.5D-14	[9] [2]
304	$Br + CH_3CHO \rightarrow HBr + CH_3CO_3$	3.841D-12·exp(-460·(1D0/T-1D0/298D0))	[9] [2]
305	$Br_2 \rightarrow Br + Br$	J(72)	[9] [2] [6]
306	$BrO \rightarrow Br + O$	J(73)	[9] [2] [6]

[1] MCMv3.3.1 ; [2] Hoffmann et al. (2016) ; [3] Wu et al. (2014) ; [4] Berndt et al. (2019) ; [5] Kukui et al. (2003)

[6] Atkinson et al. (2007) ; [7] Sander et al. (2006) ; [8] Atkinson et al. (2008) ; [9] Braeuer et al. (2013) ; [10] Jacobson (2005)

[11] Demore et al. (1997) ; [12] Berndt et al. (2020) ; [13] Kahan et al. (2012) ; [14] Burkholder et al. (2015)

[E] Estimate based on equilibrium coefficients ; [C] Based on pKa value from COSMO*therm* ; [A] Assumed

. . . multiphase DMS mechanism continued

#	Reaction	Rate	Ref.
307	OBrO $\rightarrow$ BrO + O	J(74)	[9] [2] [6]
308	HOBr $\rightarrow$ Br + OH	J(75)	[9] [2] [6]
309	$BrNO_2 \rightarrow Br + NO_2$	J(76)	[9] [2] [6]
310	$BrNO_3 \rightarrow Br + NO_3$	J(77)	[9] [2] [6]
311	$BrNO_3 \rightarrow BrO + NO_2$	J(78)	[9] [2] [6]
312	BrCl $\rightarrow$ Br + Cl	J(79)	[9] [2] [6]
313	DMS + IO $\rightarrow$ DMSO + IODINE	3.3D-13·exp(-925/T)	[9] [2]
314	IODINE + IODINE $\rightarrow$ IODINE2	2.99D-11	[9] [2]
315	IODINE + $O_3 \rightarrow$ IO	2.1D-11·exp(-830/T)	[9] [2] [6]
316	IODINE2 + OH $\rightarrow$ IODINE+ HOI	2.1D-10	[9] [2] [6]
317	IODINE + $HO_2 \rightarrow$ HI	1.5D-11·exp(-1090/T)	[9] [2] [6]
318	IO + $HO_2 \rightarrow$ HOI	1.4D-11·exp(540/T)	[9] [2] [6]
319	IO + IO $\rightarrow I_2O_2$	0.485·8.03D-11·exp(500·(1D0/T-1D0/298D0))	[9] [2] [7]
320	IO + IO $\rightarrow$ OIO + IODINE	0.38·8.03D-11·exp(500·(1D0/T-1D0/298D0))	[9] [2] [7]
321	IO + IO $\rightarrow$ IODINE2	0.025·8.03D-11·exp(500·(1D0/T-1D0/298D0))	[9] [2] [7]
322	IO + IO $\rightarrow$ IODINE + IODINE	0.11·8.03D-11·exp(500·(1D0/T-1D0/298D0))	[9] [2] [7]
323	OIO + OH $\rightarrow HIO_3$	0.5·2D-10	[9] [2]
324	OIO + OH $\rightarrow$ HOI	0.5·2D-10	[9] [2]
325	OIO + OIO $\rightarrow I_2O_2$	5D-11	[9] [2]
326	$I_2O_2 \rightarrow$ IO + IO	2D1	[9] [2]
327	HI + OH $\rightarrow$ IODINE	1.6D-11·exp(440/T)	[9] [2] [6]
328	IODINE + NO $\rightarrow$ INO	KMT57	[9] [2] [6]
329	IODINE + $NO_2 \rightarrow INO_2$	KMT58	[9] [2] [6]
330	IODINE + $NO_3 \rightarrow$ IO + NO_2	4.5D-10	[9] [2]
331	IODINE2 + $NO_3 \rightarrow$ IODINE + INO_3	1.5D-12	[9] [2] [6]
332	IO + NO $\rightarrow$ IODINE + NO_2	7.15D-12·exp(300/T)	[9] [2] [6]
333	IO + $NO_2 \rightarrow INO_3$	KMT59	[9] [2] [6]
334	OIO + NO $\rightarrow$ IO + NO_2	1.1D-12·exp(542/T)	[9] [2] [6]
335	HI + $NO_3 \rightarrow$ IODINE + HNO_3	1.3D-12·exp(-1830/T)	[9] [2] [6]
336	INO + INO $\rightarrow$ IODINE2 + NO + NO	8.5D-11·exp(-2620/T)	[9] [2] [6]
337	$INO_2 + INO_2 \rightarrow$ IODINE2 + $NO_2 + NO_2$	4.7D-13·exp(-1670/T)	[9] [2] [6]
338	$INO_2 \rightarrow$ IODINE + NO_2	9.8D-20·M + J(88)	[9] [2]
339	$INO_3 \rightarrow$ IO + NO_2	4.5D-5·exp(-12060/T)·M + J(90)	[9] [2] [6]
340	IODINE2 + Cl $\rightarrow$ IODINE + ICl	2.1D-10	[9] [2]
341	IODINE2 + Br $\rightarrow$ IODINE + IBr	1.2D-10	[9] [2]
342	IODINE + BrO $\rightarrow$ IO + Br	1.2D-11	[9] [2]
343	IO + ClO $\rightarrow$ OClO + IODINE	0.55·4.7D-12·exp(280/T)	[9] [2] [6]

[1] MCMv3.3.1 ; [2] Hoffmann et al. (2016) ; [3] Wu et al. (2014) ; [4] Berndt et al. (2019) ; [5] Kukui et al. (2003)

[6] Atkinson et al. (2007) ; [7] Sander et al. (2006) ; [8] Atkinson et al. (2008) ; [9] Braeuer et al. (2013) ; [10] Jacobson (2005)

[11] Demore et al. (1997) ; [12] Berndt et al. (2020) ; [13] Kahan et al. (2012) ; [14] Burkholder et al. (2015)

[E] Estimate based on equilibrium coefficients ; [C] Based on pKa value from COSMO*therm* ; [A] Assumed

. . . multiphase DMS mechanism continued

#	Reaction	Rate	Ref.
344	IO + ClO → Cl + IODINE	0.25·4.7D-12·exp(280/T)	[9] [2] [6]
345	IO + ClO → ICl	0.2·4.7D-12·exp(280/T)	[9] [2] [6]
346	IO + BrO → OIO + Br	0.8·1.5D-11·exp(510/T)	[9] [2] [6]
347	IO + BrO → IODINE + Br	0.2·1.5D-11·exp(510/T)	[9] [2] [6]
348	C3H7I + OH → $CH_3CIO_2CH_3$	1.6D-12	[9] [2]
349	$CH_3CIO_2CH_3$ + CH_3O_2 → CH_3CIOCH_3 + HCHO + HO_2	2.4D-14	[9] [2]
350	$CH_3CIO_2CH_3$ + $CH_3CIO_2CH_3$ → CH_3CIOCH_3 + CH_3CIOCH_3	5.57D-16·exp(-2200·(1D0/T-1D0/298D0))	[9] [2]
351	$CH_3CIO_2CH_3$ + NO → CH_3CIOCH_3 + NO_2	9.04D-12·exp(360·(1D0/T-1D0/298D0))	[9] [2]
352	CH_3CIOCH_3 → CH_3COCH_3 + IODINE	1D1	[9] [2]
353	C2H5I + OH → CH_3CHIO_2	0.13·3.69D-13·exp(-800·(1D0/T-1D0/298D0))	[9] [2]
354	C2H5I + OH → $CH_2ICH_2O_2$	0.87·3.69D-13·exp(-800·(1D0/T-1D0/298D0))	[9] [2]
355	$CH_2ICH_2O_2$ + CH_3O_2 → CH_2ICH_2OH + HCHO	0.2·2D-12	[9] [2]
356	$CH_2ICH_2O_2$ + CH_3O_2 → CH_2ICHO + CH_3OH	0.2·2D-12	[9] [2]
357	$CH_2ICH_2O_2$ + CH_3O_2 → CH_2ICH_2O + HCHO + HO_2	0.6·2D-12	[9] [2]
358	$CH_2ICH_2O_2$ + $CH_2ICH_2O_2$ → CH_2ICH_2OH + CH_2ICHO	0.43·3.98D-12·exp(1240·(1D0/T-1D0/298D0))	[9] [2]
359	$CH_2ICH_2O_2$ + $CH_2ICH_2O_2$ → CH_2ICH_2O + CH_2ICH_2O	0.57·3.98D-12·exp(1240·(1D0/T-1D0/298D0))	[9] [2]
360	$CH_2ICH_2O_2$ + NO → CH_2ICH_2O + NO_2	9.7D-12	[9] [2]
361	CH_2ICH_2OH + OH → CH_2ICHO + HO_2	4.6D-12	[9] [2]
362	CH_2ICH_2O → CH_2ICHO + HO_2	9.48D-15·exp(-550·(1D0/T-1D0/298D0))·$[O_2]$	[9] [2]
363	CH_2ICHO + OH → CH_2ICO_3	3.1D-12	[9] [2]
364	CH_2ICO_3 + HO_2 → CH_2ICO_3H	0.71·1.41D-11·exp(1040·(1D0/T-1D0/298D0))	[9] [2]
365	CH_2ICO_3 + HO_2 → CH_2ICOOH	0.29·1.41D-11·exp(1040·(1D0/T-1D0/298D0))	[9] [2]
366	CH_2ICO_3 + CH_3O_2 → CH_2ICOOH + HCHO	0.3·1D-11	[9] [2]
367	CH_2ICO_3 + CH_3O_2 → CH_2IO_2 + HCHO + HO_2	0.7·1D-11	[9] [2]
368	CH_2ICO_3 + NO → CH_2IO_2 + NO_2	2D-11·exp(270·(1D0/T-1D0/298D0))	[9] [2]
369	CH_2ICO_3 + NO_2 → $CH_2ICOOONO_2$	KMT62	[9] [2]
370	$CH_2ICOOONO_2$ → CH_2ICO_3 + NO_2	KMT63	[9] [2]
371	$CH_2ICOOONO_2$ + OH → $O_2CHICOOONO_2$	6.26D-13	[9] [2]
372	$O_2CHICOOONO_2$ + NO → CHOI + CO + NO_2 + NO_2	1.36D-11·exp(360·(1D0/T-1D0/298D0))	[9] [2]
373	CH_2ICO_3H + OH → CH_2ICO_3	4.29D-12	[9] [2]
374	CH_2ICOOH + OH → CH_2IO_2	3.59D-12·exp(190·(1D0/T-1D0/298D0))	[9] [2]
375	CH_3CHIO_2 + CH_3O_2 → CH_3CHO + IODINE + HCHO + HO_2	0.6·8.8D-13	[9] [2]
376	CH_3CHIO_2 + CH_3O_2 → CH_3CHIOH + HCHO	0.2·8.8D-13	[9] [2]
377	CH_3CHIO_2 + CH_3O_2 → CH_3CIO + CH_3OH	0.2·8.8D-13	[9] [2]
378	CH_3CHIO_2 + NO → CH_3CHO + IODINE + NO_2	1.87D-11·exp(360·(1D0/T-1D0/298D0))	[9] [2]
379	CH_3CHIOH + OH → CH_3CIO + HO_2	2.77D-12	[9] [2]
380	CH_3CIO + OH → $CIOCH_2O_2$	3.88D-14	[9] [2]

[1] MCMv3.3.1 ; [2] Hoffmann et al. (2016) ; [3] Wu et al. (2014) ; [4] Berndt et al. (2019) ; [5] Kukui et al. (2003)

[6] Atkinson et al. (2007) ; [7] Sander et al. (2006) ; [8] Atkinson et al. (2008) ; [9] Braeuer et al. (2013) ; [10] Jacobson (2005)

[11] Demore et al. (1997) ; [12] Berndt et al. (2020) ; [13] Kahan et al. (2012) ; [14] Burkholder et al. (2015)

[E] Estimate based on equilibrium coefficients ; [C] Based on pKa value from COSMO*therm* ; [A] Assumed

. . . multiphase DMS mechanism continued

#	Reaction	Rate	Ref.
381	$CIOCH_2O_2 + CH_3O_2 \rightarrow IODINE + CO + HCHO + HCHO +$	2D-12	[9] [2]
382	$CIOCH_2O_2 + NO \rightarrow IODINE + CO + HCHO + NO_2$	1.36D-11·exp(360·(1D0/T-1D0/298D0))	[9] [2]
383	$CH_2I_2 + OH \rightarrow CHI_2O_2$	2.75D-14·exp(-929·(1D0/T-1D0/298D0))	[9] [2]
384	$CH_2I_2 + Cl \rightarrow CHI_2O_2 + HCl$	4.7D-13·exp(-1135·(1D0/T-1D0/298D0))	[9] [2]
385	$CHI_2O_2 + HO_2 \rightarrow CHOI + HOI$	0.3·5.87D-12·exp(700·(1D0/T-1D0/298D0))	[9] [2]
386	$CHI_2O_2 + HO_2 \rightarrow COI_2$	0.7·5.87D-12·exp(700·(1D0/T-1D0/298D0))	[9] [2]
387	$CHI_2O_2 + CH_3O_2 \rightarrow CHI_2OH + HCHO$	0.2·2D-12	[9] [2]
388	$CHI_2O_2 + CH_3O_2 \rightarrow COI_2 + CH_3OH$	0.2·2D-12	[9] [2]
389	$CHI_2O_2 + CH_3O_2 \rightarrow CHOI + IODINE + HO_2 + HCHO$	0.6·2D-12	[9] [2]
390	$CHI_2O_2 + CHI_2O_2 \rightarrow CHOI + CHOI + IODINE + IODINE$	7D-12	[9] [2]
391	$CHI_2O_2 + NO \rightarrow CHOI + IODINE + NO_2$	1.7D-11	[9] [2]
392	$CHI_2OH + OH \rightarrow COI_2 + HO_2$	9.34D-13	[9] [2]
393	$COI_2 + OH \rightarrow COI + HOI$	5D-15	[9] [2]
394	$CH_3I + OH \rightarrow CH_2IO_2$	4.3D-12·exp(-1120/T)	[9] [2] [8]
395	$CH_3I + Cl \rightarrow CH_2IO_2 + HCl$	1.01D-12·exp(-1000·(1D0/T-1D0/298D0))	[9] [2] [7]
396	$CH_2IO_2 + HO_2 \rightarrow CH_2IO_2H$	0.85·6.7D-12	[9] [2] [8]
397	$CH_2IO_2 + HO_2 \rightarrow CHOI$	0.15·6.7D-12	[9] [2] [8]
398	$CH_2IO_2 + CH_3O_2 \rightarrow CH_2IOH + HCHO$	0.2·2D-12	[9] [2]
399	$CH_2IO_2 + CH_3O_2 \rightarrow CHOI + CH_3OH$	0.2·2D-12	[9] [2]
400	$CH_2IO_2 + CH_3O_2 \rightarrow CH_2IO + HO_2 + HCHO$	0.6·2D-12	[9] [2]
401	$CH_2IO_2 + CH_2IO_2 \rightarrow CH_2IO + CH_2IO$	1.05D-12	[9] [2]
402	$CH_2IO_2 + NO \rightarrow CH_2IO + NO_2$	1.1D-11	[9] [2]
403	$CH_2IO_2H + OH \rightarrow CH_2IO_2$	3.59D-12·exp(190·(1D0/T-1D0/298D0))	[9] [2]
404	$CH_2IO_2H + OH \rightarrow CHOI + OH$	5.79D-12	[9] [2]
405	$CH_2IOH + OH \rightarrow CHOI + HO_2$	1.06D-12	[9] [2]
406	$CH_2IO \rightarrow CHOI + HO_2$	9.48D-15·exp(-550·(1D0/T-1D0/298D0))·[O_2]	[9] [2]
407	$CHOI + OH \rightarrow IODINE + CO$	1.16D-12	[9] [2]
408	$CHOI + Cl \rightarrow COI + HCl$	7.48D-12·exp(-710·(1D0/T-1D0/298D0))	[9] [2] [8]
409	$COI \rightarrow CO + IODINE$	4.1D-10·exp(-2960/T)·[N_2]	[9] [2] [8]
410	$CO + IODINE \rightarrow COI$	1.3D-33·(T/300)$^{-3.8}$ ·[N_2]	[9] [2] [8]
411	$IODINE2 \rightarrow IODINE + IODINE$	J(80)	[9] [2] [6]
412	$IO \rightarrow IODINE + O$	J(81)	[9] [2] [6]
413	$OIO \rightarrow IODINE$	J(82)	[9] [2]
414	$OIO \rightarrow IO + O$	J(83)	[9] [2]
415	$I_2O_2 \rightarrow IODINE + IODINE$	J(84)	[9] [2]
416	$HI \rightarrow IODINE + HO_2$	J(85)	[9] [2] [6]
417	$HOI \rightarrow IODINE + OH$	J(86)	[9] [2] [6]

[1] MCMv3.3.1 ; [2] Hoffmann et al. (2016) ; [3] Wu et al. (2014) ; [4] Berndt et al. (2019) ; [5] Kukui et al. (2003)

[6] Atkinson et al. (2007) ; [7] Sander et al. (2006) ; [8] Atkinson et al. (2008) ; [9] Braeuer et al. (2013) ; [10] Jacobson (2005)

[11] Demore et al. (1997) ; [12] Berndt et al. (2020) ; [13] Kahan et al. (2012) ; [14] Burkholder et al. (2015)

[E] Estimate based on equilibrium coefficients ; [C] Based on pKa value from COSMO*therm* ; [A] Assumed

. . . multiphase DMS mechanism continued

#	Reaction	Rate	Ref.
418	INO → IODINE + NO	J(87)	[9] [2] [7]
419	$INO_2 \rightarrow IODINE + NO_2$	J(88)	[9] [2] [7]
420	$INO_3 \rightarrow IODINE + NO_3$	J(89)	[9] [2] [7]
421	$INO_3 \rightarrow IO + NO_2$	J(90)	[9] [2] [7]
422	ICl → IODINE + Cl	J(91)	[9] [2] [6]
423	IBr → IODINE + Br	J(92)	[9] [2] [6]
424	$C3H7I \rightarrow IODINE + IC3H7O_2$	J(97)	[9] [2]
425	$C2H5I \rightarrow IODINE + C2H5O_2$	J(98)	[9] [2]
426	$CH_2ICHO \rightarrow CH_2IO_2 + CO + HO_2$	J(11)	[9] [2] [9] [2]
427	$CH_2ICO_3H \rightarrow CH_2IO_2 + OH$	J(41)	[9] [2] [9] [2]
428	$CH_2I_2 \rightarrow IODINE + CH_2IO_2$	J(99)	[9] [2]
429	$CH_3I \rightarrow IODINE + CH_3O_2$	J(96)	[14]
430	$CH_2IO_2H \rightarrow CH_2IO + OH$	J(41)	[9] [2]
431	$CHOI \rightarrow IODINE + CO + HO_2$	J(11)	[9] [2] [9] [2]
432	$CH_2ICl \rightarrow IODINE + CH_2ClO_2$	J(100)	[9] [2] [8]
433	$CH_2IBr \rightarrow IODINE + CH_2BRO_2$	J(101)	[9] [2] [8]
434	$CHBr_3 + OH \rightarrow CBr_3O_2$	1.8D-13·exp(-600·(1D0/T-1D0/298D0))	[9] [2] [7]
435	$CHBr_3 + Cl \rightarrow CBr_3O_2 + HCl$	2.8D-13·exp(850·(1D0/T-1D0/298D0))	[9] [2] [7]
436	$CBr_3O_2 + HO_2 \rightarrow COBr_2 + HOBr$	4.7D-13·exp(710/T)	[9] [2] [8]
437	$CBr_3O_2 + CH_3O_2 \rightarrow CBr_3OH + HCHO$	0.3·6.6D-12	[9] [2]
438	$CBr_3O_2 + CH_3O_2 \rightarrow CBr_3O + HCHO + HO_2$	0.7·6.6D-12	[9] [2]
439	$CBr_3O_2 + CBr_3O_2 \rightarrow CBr_3O + CBr_3O;$	3.3D-13·exp(740/T)	[9] [2] [8]
440	$CBr_3O_2 + NO \rightarrow COBr_2 + Br + NO_2$	1.81D-11·exp(270·(1D0/T-1D0/298D0))	[9] [2] [7]
441	$CBr_3O_2 + NO_2 \rightarrow CBr_3OONO_2$	KMT60	[9] [2] [8]
442	$CBr_3OONO_2 \rightarrow CBr_3O_2 + NO_2$	KMT61	[9] [2] [8]
443	$CBr_3OH + OH \rightarrow CBr_3O$	3.6D-14	[9] [2]
444	$CBr_3O \rightarrow COBr_2 + Br$	4D13·exp(-4600/T)	[9] [2] [8]
445	$DIBRET + Cl \rightarrow DIBRETO_2 + HCl$	4.3D-13·exp(-800·(1D0/T-1D0/298D0))	[9] [2] [7]
446	$CH_3BR + Cl \rightarrow CH_2BRO_2 + HCl$	4.42D-13·exp(-1030·(1D0/T-1D0/298D0))	[9] [2]
447	$COBr_2 + OH \rightarrow COBr + HOBr$	5D-15	[9] [2] [8]
448	COBr → CO + Br	4.1D-10·exp(-2960/T)·[N_2]	[9] [2] [8]
449	CO + Br → COBr	1.3D-33·$(T/300)^{-3.8}$ ·[N_2]	[9] [2] [8]
450	$CHBr_3 \rightarrow Br + DIBRETO_2$	J(93)	[14]
451	$DIBRET \rightarrow Br + CH_2BrO_2$	J(94)	[14]
452	$COBr_2 \rightarrow Br + Br + CO$	J(95)	[14]
453	$CH_2Br_2 + OH \rightarrow CHBr_2O_2$	1.5D-12·exp(-775/T)	[9] [2] [8]
454	$CHBr_2O_2 + HO_2 \rightarrow CHOBr + HOBr$	0.3·5.87D-12·exp(700·(1D0/T-1D0/298D0))	[9] [2] [8]

[1] MCMv3.3.1 ; [2] Hoffmann et al. (2016) ; [3] Wu et al. (2014) ; [4] Berndt et al. (2019) ; [5] Kukui et al. (2003)

[6] Atkinson et al. (2007) ; [7] Sander et al. (2006) ; [8] Atkinson et al. (2008) ; [9] Braeuer et al. (2013) ; [10] Jacobson (2005)

[11] Demore et al. (1997) ; [12] Berndt et al. (2020) ; [13] Kahan et al. (2012) ; [14] Burkholder et al. (2015)

[E] Estimate based on equilibrium coefficients ; [C] Based on pKa value from COSMO*therm* ; [A] Assumed

. . . multiphase DMS mechanism continued

#	Reaction	Rate	Ref.
455	$CHBr_2O_2 + HO_2 \rightarrow COBr_2 + HOBr$	0.7·5.87D-12·exp(700·(1D0/T-1D0/298D0))	[9] [2] [8]
456	$CHBr_2O_2 + CH_3O_2 \rightarrow CHBr_2OH + HCHO$	0.2·2D-12	[9] [2]
457	$CHBr_2O_2 + CH_3O_2 \rightarrow COBr_2 + CH_3OH$	0.2·2D-12	[9] [2]
458	$CHBr_2O_2 + CH_3O_2 \rightarrow CHOBr + Br + HCHO + HO_2$	0.6·2D-12	[9] [2]
459	$CHBr_2O_2 + CHBr_2O_2 \rightarrow CHOBr + CHOBr + Br + Br$	7.0D-12	[9] [2] [8]
460	$CHBr_2O_2 + NO \rightarrow CHOBr + Br + NO_2$	1.7D-11	[9] [2] [8]
461	$CHBr_2OH + OH \rightarrow COBr_2 + HO_2$	9.34D-13	[9] [2]
462	$CH_3SOH + O_3 \rightarrow CH_3O_2 + HO_2 + SO_2$	2D-12	[12]
463	$Cl_2{}^- + Cl(aq) \rightarrow Cl_2(aq) + Cl^-$	2.1D9/(cw·Na)	[9] [2]
464	$Cl_2{}^- + Cl_2{}^- \rightarrow Cl_2(aq) + Cl^- + Cl^-$	1.8D9/(cw·Na)	[9] [2]
465	$Cl^- + O_3(aq) \rightarrow ClO^-$	3D-3/(cw·Na)	[9] [2]
466	$Cl(aq) + H_2O_2(aq) \rightarrow Cl^- + HO_2(aq)$	2D9/(cw·Na)	[9] [2]
467	$Cl_2{}^- + H_2O_2(aq) \rightarrow Cl^- + Cl^- + HO_2(aq)$	5D4·exp(-3340.0·(1D0/T-1D0/298D0))/(cw·Na)	[9] [2]
468	$Cl_2{}^- \rightarrow Cl^- + ClOH^-$	23.4·$m(H_2O)$ + $[OH^-]$·4.5D7	[9] [2]
469	$Cl_2{}^- + HO_2(aq) \rightarrow Cl^- + Cl^-$	1.3D10/(cw·Na)	[9] [2]
470	$Cl_2{}^- + O_2{}^- \rightarrow Cl^- + Cl^-$	6D9/(cw·Na)	[9] [2]
471	$Cl_2{}^- + OH(aq) \rightarrow HOCl(aq) + Cl^-$	1D9/(cw·Na)	[9] [2]
472	$Cl_2{}^- \rightarrow Cl^- + Cl^- + OH(aq)$	$[OH^-]$·4D6	[9] [2]
473	$Cl_3{}^- + HO_2(aq) \rightarrow Cl_2{}^- + Cl^-$	1D9/(cw·Na)	[9] [2]
474	$Cl_3{}^- + O_2{}^- \rightarrow Cl_2{}^- + Cl^-$	3.8D9/(cw·Na)	[9] [2]
475	$Cl_2(aq) + HO_2(aq) \rightarrow Cl_2{}^-$	1D9/(cw·Na)	[9] [2]
476	$Cl_2(aq) + O_2{}^- \rightarrow Cl_2{}^-$	1D9/(cw·Na)	[9] [2]
477	$HOCl(aq) + H_2O_2(aq) \rightarrow Cl^-$	1.1D4/(cw·Na)	[9] [2]
478	$ClO^- + H_2O_2(aq) \rightarrow Cl^-$	1.7D5/(cw·Na)	[9] [2]
479	$HOCl(aq) + HO_2(aq) \rightarrow Cl(aq)$	7.5D6/(cw·Na)	[9] [2]
480	$HOCl(aq) + O_2{}^- \rightarrow Cl(aq)$	7.5D6/(cw·Na)	[9] [2]
481	$ClO^- + O_2{}^- \rightarrow Cl(aq)$	2D8/(cw·Na)	[9] [2]
482	$HOCl(aq) + OH(aq) \rightarrow ClO(aq)$	2D9/(cw·Na)	[9] [2]
483	$ClO^- + OH(aq) \rightarrow ClO(aq)$	8.8D9/(cw·Na)	[9] [2]
484	$Cl_2{}^- + HSO_3{}^- \rightarrow Cl^- + Cl^- + SO_3{}^-$	1.7D8·exp(-400.0·(1D0/T-1D0/298D0))/(cw·Na)	[9] [2]
485	$Cl_2{}^- + SO_3^{2-} \rightarrow Cl^- + Cl^- + SO_3{}^-$	6.2D7/(cw·Na)	[9] [2]
486	$HOCl(aq) + SO_3^{2-} \rightarrow Cl^- + HSO_4{}^-$	7.6D8/(cw·Na)	[9] [2]
487	$HOCl(aq) + HSO_3{}^- \rightarrow Cl^- + HSO_4{}^-$	7.6D8/(cw·Na)	[9] [2]
488	$Cl^- + HSO5^- \rightarrow HOCl(aq) + SO_4{}^{2-}$	1.8D-3·exp(-7352.0·(1D0/T-1D0/298D0))/(cw·Na)	[9] [2]
489	$Cl_2{}^- + NO_2{}^- \rightarrow Cl^- + Cl^- + NO_2(aq)$	6D7/(cw·Na)	[9] [2]
490	$Cl(aq) + Cl^- \rightarrow Cl_2{}^-$	8.5D9/(cw·Na)	[9] [2]
491	$Cl_2{}^- \rightarrow Cl(aq) + Cl^-$	6D4	[9] [2]

[1] MCMv3.3.1 ; [2] Hoffmann et al. (2016) ; [3] Wu et al. (2014) ; [4] Berndt et al. (2019) ; [5] Kukui et al. (2003)

[6] Atkinson et al. (2007) ; [7] Sander et al. (2006) ; [8] Atkinson et al. (2008) ; [9] Braeuer et al. (2013) ; [10] Jacobson (2005)

[11] Demore et al. (1997) ; [12] Berndt et al. (2020) ; [13] Kahan et al. (2012) ; [14] Burkholder et al. (2015)

[E] Estimate based on equilibrium coefficients ; [C] Based on pKa value from COSMO*therm* ; [A] Assumed

. . . multiphase DMS mechanism continued

#	Reaction	Rate	Ref.
492	$Cl_2(aq) + Cl^- \rightarrow Cl_3^-$	2D4/(cw·Na)	[9] [2]
493	$Cl_3^- \rightarrow Cl_2(aq) + Cl^-$	1.1D5	[9] [2]
494	$Cl_2(aq) \rightarrow Cl^- + HOCl(aq)$	m(H_2O)·0.4·exp(-8000.0·(1D0/T-1D0/298D0))	[9] [2]
495	$Cl^- + HOCl(aq) \rightarrow Cl_2(aq)$	$[H^+]$·2.1D4·exp(-3500.0·(1D0/T-1D0/298D0))/(cw·Na)	[9] [2]
496	$HCl(aq) \rightarrow Cl^-$	5D11·exp(6890.0·(1D0/T-1D0/298D0))	[9] [2]
497	$Cl^- \rightarrow HCl(aq)$	$[H^+]$·2.9D5	[9] [2]
498	$HOCl(aq) \rightarrow ClO^-$	1.5D3	[9] [2]
499	$ClO^- \rightarrow HOCl(aq)$	$[H^+]$·5D10	[9] [2]
500	$Cl^- + OH(aq) \rightarrow ClOH^-$	4.3D9/(cw·Na)	[9] [2]
501	$ClOH^- \rightarrow Cl^- + OH(aq)$	6.1D9	[9] [2]
502	$Cl(aq) \rightarrow ClOH^-$	$[OH^-]$·1.8D10 +m(H_2O)·4.1D3	[9] [2]
503	$ClOH^- \rightarrow Cl(aq)$	23D0 + $[H^+]$·2.1D10	[9] [2]
504	$ClOH^- + Cl^- \rightarrow Cl_2^-$	1D4/(cw·Na)	[9] [2]
505	$Cl^- + SO_4^- \rightarrow Cl(aq) + SO_4^{2-}$	2.52D8/(cw·Na)	[9] [2]
506	$Cl(aq) + SO_4^{2-} \rightarrow Cl^- + SO_4^-$	2.1D8/(cw·Na)	[9] [2]
507	$Cl^- + NO_3(aq) \rightarrow Cl(aq) + NO_3^-$	3.4D8·exp(-4300.0·(1D0/T-1D0/298D0))/(cw·Na)	[9] [2]
508	$Cl(aq) + NO_3^- \rightarrow Cl^- + NO_3(aq)$	1D8/(cw·Na)	[9] [2]
509	$Br(aq) + Br(aq) \rightarrow Br_2(aq)$	1D9/(cw·Na)	[9] [2]
510	$Br_2^- + Br_2^- \rightarrow Br_2(aq) + Br^- + Br^-$	1.7D9/(cw·Na)	[9] [2]
511	$Br^- + O_3(aq) \rightarrow BrO^-$	210.0·exp(-4450.0·(1D0/T-1D0/298D0))/(cw·Na)	[9] [2]
512	$Br(aq) + HO_2(aq) \rightarrow Br^-$	1.6D8/(cw·Na)	[9] [2]
513	$Br(aq) + H_2O_2(aq) \rightarrow Br^- + HO_2(aq)$	4D9/(cw·Na)	[9] [2]
514	$Br_2(aq) + HO_2(aq) \rightarrow Br_2^-$	1.1D8/(cw·Na)	[9] [2]
515	$Br_2(aq) + O_2^- \rightarrow Br_2^-$	5.6D9/(cw·Na)	[9] [2]
516	$Br_2(aq) + H_2O_2(aq) \rightarrow Br^- + Br^-$	1.3D3/(cw·Na)	[9] [2]
517	$Br_2^- + OH(aq) \rightarrow Br^- + HOBr(aq)$	1D9/(cw·Na)	[9] [2]
518	$Br_2^- \rightarrow Br^- + Br^- + OH(aq)$	$[OH^-]$·1.1D4	[9] [2]
519	$Br_2^- + HO_2(aq) \rightarrow Br^- + Br^-$	4.4D9/(cw·Na)	[9] [2]
520	$Br_2^- + HO_2(aq) \rightarrow Br_2(aq) + H_2O_2(aq)$	4.4D9/(cw·Na)	[9] [2]
521	$Br_2^- + O_2^- \rightarrow Br^- + Br^-$	1.7D8/(cw·Na)	[9] [2]
522	$Br_2^- + H_2O_2(aq) \rightarrow Br^- + Br^- + HO_2(aq)$	1D5/(cw·Na)	[9] [2]
523	$Br_3^- + HO_2(aq) \rightarrow Br_2^- + Br^-$	1D7/(cw·Na)	[9] [2]
524	$Br_3^- + O_2^- \rightarrow Br_2^- + Br^-$	3.8D9/(cw·Na)	[9] [2]
525	$BrO(aq) + BrO(aq) \rightarrow BrO_2^- + BrO^-$	2.8D9/(cw·Na)	[9] [2]
526	$BrO_2^- + BrO(aq) \rightarrow BrO_2(aq) + BrO^-$	4D8/(cw·Na)	[9] [2]
527	$Br_2^- + BrO_2^- \rightarrow Br^- + Br^- + BrO_2(aq)$	8D7/(cw·Na)	[9] [2]
528	$BrO_2^- + OH(aq) \rightarrow BrO_2(aq)$	1.8D9/(cw·Na)	[9] [2]

[1] MCMv3.3.1 ; [2] Hoffmann et al. (2016) ; [3] Wu et al. (2014) ; [4] Berndt et al. (2019) ; [5] Kukui et al. (2003)

[6] Atkinson et al. (2007) ; [7] Sander et al. (2006) ; [8] Atkinson et al. (2008) ; [9] Braeuer et al. (2013) ; [10] Jacobson (2005)

[11] Demore et al. (1997) ; [12] Berndt et al. (2020) ; [13] Kahan et al. (2012) ; [14] Burkholder et al. (2015)

[E] Estimate based on equilibrium coefficients ; [C] Based on pKa value from COSMO*therm* ; [A] Assumed

. . . multiphase DMS mechanism continued

#	Reaction	Rate	Ref.
529	HOBr(aq) + OH(aq) → BrO(aq)	2D9/(cw·Na)	[9] [2]
530	BrO$^-$ + OH(aq) → BrO(aq)	4.5D9/(cw·Na)	[9] [2]
531	HOBr(aq) + HO_2(aq) → Br(aq)	1D9/(cw·Na)	[9] [2]
532	HOBr(aq) + $O_2{}^-$ → Br(aq)	3.5D9/(cw·Na)	[9] [2]
533	BrO$^-$ + $O_2{}^-$ → Br(aq)	2D8/(cw·Na)	[9] [2]
534	HOBr(aq) + H_2O_2(aq) → Br$^-$	3.5D6/(cw·Na)	[9] [2]
535	BrO$^-$ + H_2O_2(aq) → Br$^-$	2D5/(cw·Na)	[9] [2]
536	$Br_2{}^-$ + $HSO_3{}^-$ → Br$^-$ + Br$^-$ + $SO_3{}^-$	5D7·exp(-780.0·(1D0/T-1D0/298D0))/(cw·Na)	[9] [2]
537	$Br_2{}^-$ + $SO_3{}^{2-}$ → Br$^-$ + Br$^-$ + $SO_3{}^-$	3.3D7·exp(-650.0·(1D0/T-1D0/298D0))/(cw·Na)	[9] [2]
538	Br$^-$ + $SO_4{}^-$ → Br(aq) + $SO_4{}^{2-}$	2.1D9/(cw·Na)	[9] [2]
539	HOBr(aq) + $SO_3{}^{2-}$ → Br$^-$ + $HSO_4{}^-$	5D9/(cw·Na)	[9] [2]
540	HOBr(aq) + $HSO_3{}^-$ → Br$^-$ + $HSO_4{}^-$	5D9/(cw·Na)	[9] [2]
541	Br$^-$ + HSO5$^-$ → HOBr(aq) + $SO_4{}^{2-}$	1D0·exp(-5338.0·(1D0/T-1D0/298D0))/(cw·Na)	[9] [2]
542	Br$^-$ + NO_3(aq) → Br(aq) + $NO_3{}^-$	3.8D9/(cw·Na)	[9] [2]
543	$Br_2{}^-$ + $NO_2{}^-$ → Br$^-$ + Br$^-$ + NO_2(aq)	1.2D7·exp(-1720.0·(1D0/T-1D0/298D0))/(cw·Na)	[9] [2]
544	Br$^-$ + NO_2kat$^-$ → $BrNO_2$(aq)	1D10/(cw·Na)	[9] [2]
545	Br$^-$ + $BrNO_2$(aq) → Br_2(aq) + $NO_2{}^-$	2.55D4/(cw·Na)	[9] [2]
546	$Br_2{}^-$ + $Cl_2{}^-$ → Br_2(aq) + Cl$^-$ + Cl$^-$	4D9/(cw·Na)	[9] [2]
547	Br$^-$ + HOCl(aq) → BrCl(aq)	1.3D6/(cw·Na)	[9] [2]
548	Br$^-$ + ClO$^-$ → BrCl(aq)	3.65D10/(cw·Na)	[9] [2]
549	Br$^-$ + $ClNO_2$(aq) → BrCl(aq) + $NO_2{}^-$	5D6/(cw·Na)	[9] [2]
550	$BrNO_2$(aq) + Cl$^-$ → BrCl(aq) + $NO_2{}^-$	1D1/(cw·Na)	[9] [2]
551	Br(aq) + Br$^-$ → $Br_2{}^-$	1.2D10/(cw·Na)	[9] [2]
552	$Br_2{}^-$ → Br(aq) + Br$^-$	1.9D4	[9] [2]
553	Br_2(aq) + Br$^-$ → $Br_3{}^-$	9.6D8/(cw·Na)	[9] [2]
554	$Br_3{}^-$ → Br_2(aq) + Br$^-$	5.5D7	[9] [2]
555	Br_2(aq) → Br$^-$ + HOBr(aq)	m(H_2O)·1.7·exp(-7500.0·(1D0/T-1D0/298D0))	[9] [2]
556	Br$^-$ + HOBr(aq) → Br_2(aq)	[H^+]·1.6D10/((cw·Na))	[9] [2]
557	HBr(aq) → Br$^-$	5D11	[9] [2]
558	Br$^-$ → HBr(aq)	[H^+]·5D2	[9] [2]
559	HOBr(aq) → BrO$^-$	1D2	[9] [2]
560	BrO$^-$ → HOBr(aq)	[H^+]·5D10	[9] [2]
561	Br$^-$ + OH(aq) → BrOH$^-$	1.1D10/(cw·Na)	[9] [2]
562	BrOH$^-$ → Br$^-$ + OH(aq)	3.3D7	[9] [2]
563	Br(aq) → BrOH$^-$	[OH^-]·1.3D10 + m(H_2O)·2.45D-2	[9] [2]
564	BrOH$^-$ → Br(aq)	4.2D6 + [H^+]·4.4D10	[9] [2]
565	BrOH$^-$ + Br$^-$ → $Br_2{}^-$	1.9D8/(cw·Na)	[9] [2]

[1] MCMv3.3.1 ; [2] Hoffmann et al. (2016) ; [3] Wu et al. (2014) ; [4] Berndt et al. (2019) ; [5] Kukui et al. (2003)

[6] Atkinson et al. (2007) ; [7] Sander et al. (2006) ; [8] Atkinson et al. (2008) ; [9] Braeuer et al. (2013) ; [10] Jacobson (2005)

[11] Demore et al. (1997) ; [12] Berndt et al. (2020) ; [13] Kahan et al. (2012) ; [14] Burkholder et al. (2015)

[E] Estimate based on equilibrium coefficients ; [C] Based on pKa value from COSMO*therm* ; [A] Assumed

…multiphase DMS mechanism continued

#	Reaction	Rate	Ref.
566	$Br_2^- \rightarrow BrOH^- + Br^-$	$[OH^-]\cdot 2.7D6$	[9] [2]
567	$HOBr(aq) + HOBr(aq) \rightarrow Br^- + HBrO_2(aq)$	$2D\text{-}5/(cw\cdot Na)$	[9] [2]
568	$Br^- + HBrO_2(aq) \rightarrow HOBr(aq) + HOBr(aq)$	$[H^+]\cdot 3D6/((cw\cdot Na))$	[9] [2]
569	$HBrO_2(aq) \rightarrow BrO_2^-$	6.3D5	[9] [2]
570	$BrO_2^- \rightarrow HBrO_2(aq)$	$[H^+]\cdot 5D10$	[9] [2]
571	$HOBr(aq) + HBrO_2(aq) \rightarrow Br^- + BrO_3^-$	$3.2D0/(cw\cdot Na)$	[9] [2]
572	$Br^- + BrO_3^- \rightarrow HOBr(aq) + HBrO_2(aq)$	$([H^+]^{2D0})\cdot 2.0D0/((cw\cdot Na))$	[9] [2]
573	$HBrO_2(aq) + HBrO_2(aq) \rightarrow HOBr(aq) + BrO_3^-$	$3D3/(cw\cdot Na)$	[9] [2]
574	$HOBr(aq) + BrO_3^- \rightarrow HBrO_2(aq) + HBrO_2(aq)$	$[H^+]\cdot 1D\text{-}8/((cw\cdot Na))$	[9] [2]
575	$Br_2O_4(aq) \rightarrow BrO_3^- + HBrO_2(aq)$	$m(H_2O)\cdot 2.2D3$	[9] [2]
576	$BrO_3^- + HBrO_2(aq) \rightarrow Br_2O_4(aq)$	$[H^+]\cdot 42.0D0/((cw\cdot Na))$	[9] [2]
577	$Br_2O_4(aq) \rightarrow BrO_2(aq) + BrO_2(aq)$	7.4D4	[9] [2]
578	$BrO_2(aq) + BrO_2(aq) \rightarrow Br_2O_4(aq)$	$1.4D9/(cw\cdot Na)$	[9] [2]
579	$BrCl(aq) \rightarrow HOBr(aq) + Cl^-$	1D5	[9] [2]
580	$HOBr(aq) + Cl^- \rightarrow BrCl(aq)$	$[H^+]\cdot 5.6D9/((cw\cdot Na))$	[9] [2]
581	$BrCl^- \rightarrow Br^- + Cl(aq)$	1.9D3	[9] [2]
582	$Br^- + Cl(aq) \rightarrow BrCl^-$	$1.2D10/(cw\cdot Na)$	[9] [2]
583	$BrCl^- \rightarrow Br(aq) + Cl^-$	6.1D4	[9] [2]
584	$Br(aq) + Cl^- \rightarrow BrCl^-$	$1D8/(cw\cdot Na)$	[9] [2]
585	$BrCl^- + Br^- \rightarrow Br_2^- + Cl^-$	$8D9/(cw\cdot Na)$	[9] [2]
586	$Br_2^- + Cl^- \rightarrow BrCl^- + Br^-$	$4.3D6/(cw\cdot Na)$	[9] [2]
587	$BrCl^- + Cl^- \rightarrow Cl_2^- + Br^-$	$1.1D2/(cw\cdot Na)$	[9] [2]
588	$Cl_2^- + Br^- \rightarrow BrCl^- + Cl^-$	$4D9/(cw\cdot Na)$	[9] [2]
589	$Br_2Cl^- \rightarrow BrCl(aq) + Br^-$	4.3D5	[9] [2]
590	$BrCl(aq) + Br^- \rightarrow Br_2Cl^-$	$7.7D9/(cw\cdot Na)$	[9] [2]
591	$Br_2Cl^- \rightarrow Br_2(aq) + Cl^-$	3.8D4	[9] [2]
592	$Br_2(aq) + Cl^- \rightarrow Br_2Cl^-$	$5D4/(cw\cdot Na)$	[9] [2]
593	$BrCl_2^- \rightarrow BrCl(aq) + Cl^-$	1.7D5	[9] [2]
594	$BrCl(aq) + Cl^- \rightarrow BrCl_2^-$	$1D6/(cw\cdot Na)$	[9] [2]
595	$BrCl_2^- \rightarrow Br^- + Cl_2(aq)$	9D3	[9] [2]
596	$Br^- + Cl_2(aq) \rightarrow BrCl_2^-$	$6D9/(cw\cdot Na)$	[9] [2]
597	$Br^- + ClOH^- \rightarrow BrCl^-$	$1D9/(cw\cdot Na)$	[9] [2]
598	$BrCl^- \rightarrow Br^- + ClOH^-$	$[OH^-]\cdot 3D6$	[9] [2]
599	$BrOH^- + Cl^- \rightarrow BrCl^-$	$1.9D8/(cw\cdot Na)$	[9] [2]
600	$BrCl^- \rightarrow BrOH^- + Cl^-$	$[OH^-]\cdot 2D7$	[9] [2]
601	$IODINE(aq) + IODINE(aq) \rightarrow IODINE2(aq)$	$1.1D10/(cw\cdot Na)$	[9] [2]
602	$IODINE(aq) + I_2^- \rightarrow I3^-$	$6.5D9/(cw\cdot Na)$	[9] [2]

[1] MCMv3.3.1 ; [2] Hoffmann et al. (2016) ; [3] Wu et al. (2014) ; [4] Berndt et al. (2019) ; [5] Kukui et al. (2003)

[6] Atkinson et al. (2007) ; [7] Sander et al. (2006) ; [8] Atkinson et al. (2008) ; [9] Braeuer et al. (2013) ; [10] Jacobson (2005)

[11] Demore et al. (1997) ; [12] Berndt et al. (2020) ; [13] Kahan et al. (2012) ; [14] Burkholder et al. (2015)

[E] Estimate based on equilibrium coefficients ; [C] Based on pKa value from COSMO*therm* ; [A] Assumed

. . . multiphase DMS mechanism continued

#	Reaction	Rate	Ref.
603	I_2^- + I_2^- → I3$^-$ + I^-	2.5D9/(cw·Na)	[9] [2]
604	I^- + O_3(aq) → HOI(aq)	2.17D9·exp(-8790.0·(1D0/T-1D0/298D0))/(cw·Na)	[9] [2]
605	IODINE2(aq) + HO_2(aq) → I_2^-	6D9/(cw·Na)	[9] [2]
606	IODINE2(aq) + O_2^- → I_2^-	6D9/(cw·Na)	[9] [2]
607	I3$^-$ + HO_2(aq) → I_2^- + I^-	2.5D8/(cw·Na)	[9] [2]
608	I3$^-$ + O_2^- → I_2^- + I^-	2.5D8/(cw·Na)	[9] [2]
609	HIO_2(aq) + H_2O_2(aq) → IO_3^-	6D1/(cw·Na)	[9] [2]
610	IO_2^- + H_2O_2(aq) → IO_3^-	6D1/(cw·Na)	[9] [2]
611	IO(aq) + IO(aq) → HOI(aq) + HIO_2(aq)	1.5D9/(cw·Na)	[9] [2]
612	IODINE2(aq) + HSO_3^- → I^- + I^- + HSO_4^-	1D6/(cw·Na)	[9] [2]
613	HOI(aq) + $SO_3^{\ 2-}$ → I^- + HSO_4^-	5D9/(cw·Na)	[9] [2]
614	HOI(aq) + HSO_3^- → I^- + HSO_4^-	5D9/(cw·Na)	[9] [2]
615	I^- + ICl(aq) → IODINE2(aq) + Cl^-	1.1D9/(cw·Na)	[9] [2]
616	I^- + HOCl(aq) → ICl(aq)	3.5D11/(cw·Na)	[9] [2]
617	I^- + HOBr(aq) → IBr(aq)	5D9/(cw·Na)	[9] [2]
618	HOI(aq) + Cl_2(aq) → HIO_2(aq) + Cl^- + Cl^-	1D6/(cw·Na)	[9] [2]
619	HOI(aq) + HOCl(aq) → HIO_2(aq) + Cl^-	5D5/(cw·Na)	[9] [2]
620	HOI(aq) + HOBr(aq) → HIO_2(aq) + Br^-	1D6/(cw·Na)	[9] [2]
621	HIO_2(aq) + HOCl(aq) → IO_3^- + Cl^-	1.5D3/(cw·Na)	[9] [2]
622	IO_2^- + HOCl(aq) → IO_3^- + Cl^-	1.5D3/(cw·Na)	[9] [2]
623	HIO_2(aq) + HOBr(aq) → IO_3^- + Br^-	1D6/(cw·Na)	[9] [2]
624	IO_2^- + HOBr(aq) → IO_3^- + Br^-	1D6/(cw·Na)	[9] [2]
625	IODINE(aq) + I^- → I_2^-	9.1D9/(cw·Na)	[9] [2]
626	I_2^- → IODINE(aq) + I^-	6.7D4	[9] [2]
627	IODINE2(aq) + I^- → I3$^-$	6.2D9/(cw·Na)	[9] [2]
628	I3$^-$ → IODINE2(aq) + I^-	8.7D6	[9] [2]
629	HI(aq) → I^-	5D11	[9] [2]
630	I^- → HI(aq)	[H$^+$]·156D0	[9] [2]
631	HOI(aq) → IO^-	1.58D0	[9] [2]
632	IO^- → HOI(aq)	[H$^+$]·5D10	[9] [2]
633	HOI(aq) + I^- → IODINE2(aq)	[H$^+$]·4.4D12/((cw·Na))	[9] [2]
634	IODINE2(aq) → HOI(aq) + I^-	3D0	[9] [2]
635	HOI(aq) + HOI(aq) → HIO_2(aq) + I^-	25D0/(cw·Na)	[9] [2]
636	HIO_2(aq) + I^- → HOI(aq) + HOI(aq)	[H$^+$]·2D10/((cw·Na))	[9] [2]
637	HOI(aq) + HOI(aq) → IO_2^- + I^-	25D0/(cw·Na)	[9] [2]
638	IO_2^- + I^- → HOI(aq) + HOI(aq)	([H$^+$]^{2D0})·2D10/((cw·Na))	[9] [2]
639	HIO_2(aq) → IO_2^-	1.26D9	[9] [2]

[1] MCMv3.3.1 ; [2] Hoffmann et al. (2016) ; [3] Wu et al. (2014) ; [4] Berndt et al. (2019) ; [5] Kukui et al. (2003)

[6] Atkinson et al. (2007) ; [7] Sander et al. (2006) ; [8] Atkinson et al. (2008) ; [9] Braeuer et al. (2013) ; [10] Jacobson (2005)

[11] Demore et al. (1997) ; [12] Berndt et al. (2020) ; [13] Kahan et al. (2012) ; [14] Burkholder et al. (2015)

[E] Estimate based on equilibrium coefficients ; [C] Based on pKa value from COSMO*therm* ; [A] Assumed

. . . multiphase DMS mechanism continued

#	Reaction	Rate	Ref.
640	$IO_2^- \rightarrow HIO_2(aq)$	$[H^+]\cdot 5D10$	[9] [2]
641	$HIO_3(aq) \rightarrow IO_3^-$	8.5D9	[9] [2]
642	$IO_3^- \rightarrow HIO_3(aq)$	$[H^+]\cdot 5D10$	[9] [2]
643	$HIO_2(aq) + HOI(aq) \rightarrow IO_3^- + I^-$	$2.4D2/(cw\cdot Na)$	[9] [2]
644	$IO_3^- + Iion \rightarrow HIO_2(aq) + HOI(aq)$	$([H^+]^{2D0})\cdot 1.2D3/((cw\cdot Na))$	[9] [2]
645	$IO_2^- + HOI(aq) \rightarrow IO_3^- + I^-$	$2.4D2/(cw\cdot Na)$	[9] [2]
646	$IO_3^- + I^- \rightarrow IO_2^- + HOI(aq)$	$[H^+]\cdot 1.2D3/((cw\cdot Na))$	[9] [2]
647	$IO_2^- + IODINE2(aq) \rightarrow IO_3^- + I^- + I^-$	$5.5D\text{-}5/(cw\cdot Na)$	[9] [2]
648	$IO_3^- + I^- + I^- \rightarrow IO_2^- + IODINE2(aq)$	$([H^+]^{2D0})\cdot 4.2D8/((cw\cdot Na)^{2D0})$	[9] [2]
649	$IBr(aq) + I^- \rightarrow IODINE2(aq) + Br^-$	$2D9/(cw\cdot Na)$	[9] [2]
650	$IODINE2(aq) + Br^- \rightarrow IBr(aq) + I^-$	$4.74D3/(cw\cdot Na)$	[9] [2]
651	$HOI(aq) + Cl^- \rightarrow ICl(aq)$	$[H^+]\cdot 2.9D10/((cw\cdot Na))$	[9] [2]
652	$ICl(aq) \rightarrow HOI(aq) + Cl^-$	2.4D6	[9] [2]
653	$HOI(aq) + Br^- \rightarrow IBr(aq)$	$[H^+]\cdot 4.1D12/((cw\cdot Na))$	[9] [2]
654	$IBr(aq) \rightarrow HOI(aq) + Br^-$	8D5	[9] [2]
655	$ICl(aq) + Cl^- \rightarrow ICl_2^-$	$4.24D9/(cw\cdot Na)$	[9] [2]
656	$ICl_2^- \rightarrow ICl(aq) + Cl^-$	5.5D7	[9] [2]
657	$IBr(aq) + Br^- \rightarrow IBr_2^-$	$4.93D6/(cw\cdot Na)$	[9] [2]
658	$IBr_2^- \rightarrow IBr(aq) + Br^-$	1.7D5	[9] [2]
659	$ICl(aq) + Br^- \rightarrow IClBr^-$	$7.7D9/(cw\cdot Na)$	[9] [2]
660	$IClBr^- \rightarrow ICl(aq) + Br^-$	4.3D5	[9] [2]
661	$IBr(aq) + Cl^- \rightarrow IClBr^-$	$5D4/(cw\cdot Na)$	[9] [2]
662	$IClBr^- \rightarrow IBr(aq) + Cl^-$	3.8D4	[9] [2]
663	$DMS(aq) + O_3(aq) \rightarrow DMSO(aq)$	$8.61D8\cdot exp(\text{-}2600\cdot(1D0/T\text{-}1D0/298D0))/(cw\cdot Na)$	[2]
664	$DMS(aq) + OH(aq) \rightarrow DMSO(aq) + HO_2(aq)$	$1.9D10/(cw\cdot Na)$	[2]
665	$DMS(aq) + Cl_2^- \rightarrow CH_3SCH_3Cl(aq) + Cl^-$	$3D9/(cw\cdot Na)$	[2]
666	$DMS(aq) + Br_2^- \rightarrow CH_3SCH_3Br(aq) + Br^-$	$3.2D9/(cw\cdot Na)$	[2]
667	$DMS(aq) + H_2O_2(aq) \rightarrow DMSO(aq)$	$3.4D\text{-}2/(cw\cdot Na)$	[2]
668	$CH_3SCH_3Cl(aq) + O_2(aq) \rightarrow DMSO(aq) + ClO(aq)$	$2.41D3/(cw\cdot Na)$	[9] [2]
669	$CH_3SCH_3Br(aq) + O_2(aq) \rightarrow DMSO(aq) + BrO(aq)$	$6.02D2/(cw\cdot Na)$	[2]
670	$DMSO(aq) + O_3(aq) \rightarrow DMSO_2(aq)$	$3D0/(cw\cdot Na)$	[2]
671	$DMSO(aq) + OH(aq) \rightarrow MSIA(aq)$	$6.65D9\cdot exp(\text{-}1270\cdot(1D0/T\text{-}1D0/298D0))/(cw\cdot Na)$	[2]
672	$DMSO(aq) + SO_4^- \rightarrow DMSO^- + SO_4^{\ 2-}$	$2.97D9\cdot exp(\text{-}1440\cdot(1D0/T\text{-}1D0/298D0))/(cw\cdot Na)$	[2]
673	$DMSO(aq) + Cl(aq) \rightarrow CH_3SOCH_3Cl(aq)$	$6.3D9/(cw\cdot Na)$	[2]
674	$DMSO(aq) + Cl_2^- \rightarrow CH_3SOCH_3Cl(aq) + Cl^-$	$1.6D7/(cw\cdot Na)$	[2]
675	$DMSO(aq) + H_2O_2(aq) \rightarrow DMSO_2(aq)$	$2.75D\text{-}6/(cw\cdot Na)$	[2]
676	$DMSO^- + Br^- \rightarrow CH_3SOCH_3Br(aq)$	$5D9/(cw\cdot Na)$	[2]

[1] MCMv3.3.1 ; [2] Hoffmann et al. (2016) ; [3] Wu et al. (2014) ; [4] Berndt et al. (2019) ; [5] Kukui et al. (2003)

[6] Atkinson et al. (2007) ; [7] Sander et al. (2006) ; [8] Atkinson et al. (2008) ; [9] Braeuer et al. (2013) ; [10] Jacobson (2005)

[11] Demore et al. (1997) ; [12] Berndt et al. (2020) ; [13] Kahan et al. (2012) ; [14] Burkholder et al. (2015)

[E] Estimate based on equilibrium coefficients ; [C] Based on pKa value from COSMO*therm* ; [A] Assumed

. . . multiphase DMS mechanism continued

#	Reaction	Rate	Ref.
677	$CH_3SOCH_3Br(aq) + Br^- \rightarrow DMSO(aq) + Br_2^-$	2.6D8/(cw·Na)	[2]
678	$CH_3SOCH_3Cl(aq) \rightarrow MSIA(aq) + HCl(aq)$	m(H_2O)·1D7	[2]
679	$CH_3SOCH_3OH(aq) \rightarrow MSIA(aq)$	1D7	[2]
680	$DMSO_2(aq) + OH(aq) \rightarrow CH_3SO_2CH_2(aq)$	1.77D7·exp(-1690·(1D0/T-1D0/298D0))/(cw·Na)	[2]
681	$DMSO_2(aq) + SO_4^- \rightarrow CH_3SO_2CH_2(aq) + SO_4^{2-}$	3.95D6·exp(-1360·(1D0/T-1D0/298D0))/(cw·Na)	[2]
682	$DMSO_2(aq) + Cl(aq) \rightarrow CH_3SO_2CH_2(aq) + HCl(aq)$	8.2D5/(cw·Na)	[2]
683	$DMSO_2(aq) + Cl_2^- \rightarrow CH_3SO_2CH_2(aq) + HCl(aq) + Cl^-$	8.24D3/(cw·Na)	[2]
684	$DMSO_2(aq) + O_2(aq) \rightarrow CH_3SO_2CH_2O_2(aq)$	2D9/(cw·Na)	[2]
685	$CH_3SO_2CH_2O_2(aq) + RO_2(aq) \rightarrow CH_3SO_2(aq) + HCHO(aq)$	7D3/(cw·Na)	[2]
686	$MSIA(aq) + O_3(aq) \rightarrow CH_3SO_3H(aq)$	3.5D7/(cw·Na)	[2]
687	$MSIA(aq) + OH(aq) \rightarrow CH_3SO_3H_2(aq)$	6D9/(cw·Na)	[2]
688	$CH_3SO_2^- + OH(aq) \rightarrow CH_3SO_2(aq)$	0.9·1.2D10/(cw·Na)	[2]
689	$CH_3SO_2^- + OH(aq) \rightarrow HSO_3^-$	0.1·1.2D10/(cw·Na)	[2]
690	$CH_3SO_2^- + SO_4^- \rightarrow CH_3SO_2(aq) + SO_4^{2-}$	1D9/(cw·Na)	[2]
691	$CH_3SO_2^- + Cl_2^- \rightarrow CH_3SO_2(aq) + Cl^- + Cl^-$	8D8/(cw·Na)	[2]
692	$CH_3SO_2^- + H_2O_2(aq) \rightarrow CH_3SO_3^-$	1.2D-2/(cw·Na)	[2]
693	$CH_3SO_2^- + O_3(aq) \rightarrow CH_3SO_3^-$	2D6/(cw·Na)	[2]
694	$CH_3SO_3H_2(aq) + O_2(aq) \rightarrow CH_3SO_3H(aq) + HO_2(aq)$	1.2D9/(cw·Na)	[2]
695	$CH_3SO_3H(aq) + OH(aq) \rightarrow CH_2SO_3H(aq)$	1.5D7/(cw·Na)	[2]
696	$CH_3SO_3^- + OH(aq) \rightarrow CH_2SO_3^-$	1.29D7·exp(-2630·(1D0/T-1D0/298D0))/(cw·Na)	[2]
697	$CH_3SO_3^- + SO_4^- \rightarrow CH_3SO_3(aq) + SO_4^{2-}$	1.13D4·exp(-2490·(1D0/T-1D0/298D0))/(cw·Na)	[2]
698	$CH_3SO_3^- + Cl(aq) \rightarrow CH_3SO_3(aq) + Cl^-$	4.9D5/(cw·Na)	[2]
699	$CH_3SO_3^- + Cl_2^- \rightarrow CH_3SO_3(aq) + Cl^- + Cl^-$	3.89D3/(cw·Na)	[2]
700	$CH_3SO_2(aq) + OH(aq) \rightarrow CH_3SO_3H(aq)$	1D10/(cw·Na)	[2]
701	$CH_3SO_2(aq) + O_3(aq) \rightarrow CH_3SO_3(aq)$	1.5D9/(cw·Na)	[2]
702	$CH_3SO_2(aq) + SO_3^{2-} \rightarrow CH_3SO_2^- + SO_4^{2-}$	1.7D9/(cw·Na)	[2]
703	$CH_3SO_2(aq) \rightarrow SO_2(aq)$	8.3D4	[2]
704	$CH_3SO_2(aq) + O_2(aq) \rightarrow CH_3SO_2O_2(aq)$	1.2D9/(cw·Na)	[2]
705	$CH_3SO_2(aq) + CH_3SO_2(aq) \rightarrow MSIA(aq) + CH_3SO_3H(aq)$	8D8/(cw·Na)	[2]
706	$CH_3SO_2O_2(aq) + CH_3SO_2^- \rightarrow CH_3SO_3^- + CH_3SO_3(aq)$	6.2D8/(cw·Na)	[2]
707	$CH_3SO_3(aq) + CH_3SO_2^- \rightarrow CH_3SO_3^- + CH_3SO_2(aq)$	1D8/(cw·Na)	[2]
708	$CH_3SO_3(aq) \rightarrow SO_3(aq)$	8.3D4	[2]
709	$CH_3SO_3(aq) + HO_2(aq) \rightarrow CH_3SO_3H(aq)$	8.3D5/(cw·Na)	[2]
710	$CH_2SO_3H(aq) + O_2(aq) \rightarrow O_2CH_2SO_3H(aq)$	2D9/(cw·Na)	[2]
711	$CH_2SO_3^- + O_2(aq) \rightarrow O_2CH_2SO_3^-$	2D9/(cw·Na)	[2]
712	$O_2CH_2SO_3^- \rightarrow HCHO(aq) + SO_3^-$	[H^+]·7D3	[2]
713	$MSIA(aq) \rightarrow CH_3SO_2^-$	1.2D8	[C]

[1] MCMv3.3.1 ; [2] Hoffmann et al. (2016) ; [3] Wu et al. (2014) ; [4] Berndt et al. (2019) ; [5] Kukui et al. (2003)

[6] Atkinson et al. (2007) ; [7] Sander et al. (2006) ; [8] Atkinson et al. (2008) ; [9] Braeuer et al. (2013) ; [10] Jacobson (2005)

[11] Demore et al. (1997) ; [12] Berndt et al. (2020) ; [13] Kahan et al. (2012) ; [14] Burkholder et al. (2015)

[E] Estimate based on equilibrium coefficients ; [C] Based on pKa value from COSMO*therm* ; [A] Assumed

. . . multiphase DMS mechanism continued

#	Reaction	Rate	Ref.
714	$CH_3SO_2^-$ → MSIA(aq)	$[H^+]$·5D10	[2]
715	CH_3SO_3H(aq) → $CH_3SO_3^-$	4.25D13	[C]
716	$CH_3SO_3^-$ → CH_3SO_3H(aq)	$[H^+]$·5D10	[2]
717	$O_2CH_2SO_3H$(aq) → $O_2CH_2SO_3^-$	3.65D12	[2]
718	$O_2CH_2SO_3^-$ → $O_2CH_2SO_3H$(aq)	$[H^+]$·5D10	[2]
719	Cl^- + $DMSO^-$ → CH_3SOCH_3Cl(aq)	1D10/(cw·Na)	[2]
720	CH_3SOCH_3Cl(aq) → Cl^- + $DMSO^-$	3.03D7	[2]
721	$DMSO^-$ → CH_3SOCH_3OH(aq)	m(H_2O)·1.25D5	[2]
722	CH_3SOCH_3OH(aq) → $DMSO^-$	$[H^+]$·5D10	[2]
723	HPMTF(aq) + OH(aq) → $HOOCH_2SCO$(aq)	1D10/(cw·Na)	[E*]
724	SO_2(aq) → HSO_3^-	1D12	[E][2]
725	HSO_3^- → SO_2(aq)	$[H^+]$·(1D12/(1.71D-2·exp(7.04D0·(298D0/T-1D0))))	[E][2]
726	HSO_3^- → SO_3^{2-}	1D12	[E][2]
727	SO_3^{2-} → HSO_3^-	$[H^+]$·(1D12/(5.99D-8·exp(3.74D0·(298D0/T-1D0))))	[E][2]
728	HSO_4^- → SO_4^{2-}	1D12	[E][2]
729	SO_4^{2-} → HSO_4^-	$[H^+]$·(1D12/(1.02D-2·(exp(8.85D0·(298D0/T-1D0)) +25.14·(1D0-298D0/T+log(298D0/T)))))	[E][2]
730	HO_2(aq) → O_2^-	1D12	[E][10]
731	O_2^- → HO_2(aq)	$[H^+]$·(1D12/3.5D-5)	[E] [10]
732	H_2O_2(aq) → HO_2^-	1D12	[E][10]
733	HO_2^- → H_2O_2(aq)	$[H^+]$·(1D12/(2.21D-12·exp(-12.52D0·(298D0/T-1D0))))	[E][10]
734	H_2O_2(aq) + HSO_3^- → HSO_4^-	($[H^+]$·(7.45D7·exp(-15.96D0·(298D0/T-1D0)))	[2]
735	HSO_3^- + HO_2(aq) → HSO_4^- + OH(aq)	4.35D5/(cw·Na)	[2]
736	SO_3^{2-} + HO_2(aq) → SO_4^{2-} + OH(aq)	5.65D5/(cw·Na)	[2]
737	HSO_3^- + O_2^- → HSO_4^- + OH(aq)	4.35D4/(cw·Na)	[2]
738	SO_3^{2-} + O_2^- → SO_4^{2-} + OH(aq)	5.65D4/(cw·Na)	[2]
739	HSO_3^- + OH(aq) → $SO5^-$	4.2D9·exp(-5.03D0·(298D0/T-1D0))/(cw·Na)	[2]
740	SO_3^{2-} + OH(aq) → $SO5^-$	4.6D9·exp(-5.03D0·(298D0/T-1D0))/(cw·Na)	[2]
741	SO_2(aq) + O_3(aq) → HSO_4^-	2.4D4/(cw·Na)	[2]
742	HSO_3^- + O_3(aq) → HSO_4^-	3.7D5·exp(-18.56D0·(298D0/T-1D0))/(cw·Na)	[2]
743	SO_3^{2-} + O_3(aq) → SO_4^{2-}	1.5D9·exp(-17.72D0·(298D0/T-1D0))/(cw·Na)	[2]
744	HSO_3^- + $SO5^-$ → $HSO5^-$ + $SO5^-$	3D5·exp(-10.4D0·(298D0/T-1D0))/(cw·Na)	[2]
745	SO_3^{2-} + $SO5^-$ → $HSO5^-$ + $SO5^-$	1.3D7·exp(-6.71D0·(298D0/T-1D0))/(cw·Na)	[2]
746	HSO_3^- + SO_4^- → HSO_4^- + $SO5^-$	1.3D9·exp(-5.03D0·(298D0/T-1D0))/(cw·Na)	[2]
747	SO_3^{2-} + SO_4^- → SO_4^{2-} + $SO5^-$	5.3D8·exp(-5.03D0·(298D0/T-1D0))/(cw·Na)	[2]
748	HSO_3^- + $HSO5^-$ → HSO_4^- + HSO_4^-	7.1D6·exp(-10.47D0·(298D0/T-1D0))/(cw·Na)	[2]
749	H_2O_2(aq) + OH(aq) → HO_2(aq)	2.7D7·exp(-5.7D0·(298D0/T-1D0))/(cw·Na)	[2]

[1] MCMv3.3.1 ; [2] Hoffmann et al. (2016) ; [3] Wu et al. (2014) ; [4] Berndt et al. (2019) ; [5] Kukui et al. (2003)

[6] Atkinson et al. (2007) ; [7] Sander et al. (2006) ; [8] Atkinson et al. (2008) ; [9] Braeuer et al. (2013) ; [10] Jacobson (2005)

[11] Demore et al. (1997) ; [12] Berndt et al. (2020) ; [13] Kahan et al. (2012) ; [14] Burkholder et al. (2015)

[E] Estimate based on equilibrium coefficients ; [C] Based on pKa value from COSMO*therm* ; [A] Assumed

…multiphase DMS mechanism continued

#	Reaction	Rate	Ref.
750	$H_2O_2(aq) + SO_4{}^- \rightarrow HO_2(aq) + SO_4^{2-}$	1.2D3·exp(-6.71D0·(298D0/T-1D0))/(cw·Na)	[2]
751	$OH(aq) + HO_2(aq) \rightarrow$ DUMMY	7D9·exp(-5.03D0·(298D0/T-1D0))/(cw·Na)	[2]
752	$OH(aq) + O_2{}^- \rightarrow$ DUMMY	1D10·exp(-5.03D0·(298D0/T-1D0))/(cw·Na)	[2]
753	$OH(aq) + HSO5^- \rightarrow SO5^-$	1.7D7·exp(-6.38D0·(298D0/T-1D0))/(cw·Na)	[2]
754	$O_2{}^- + O_3(aq) \rightarrow OH(aq)$	1.5D9·exp(-5.03D0·(298D0/T-1D0))/(cw·Na)	[2]
755	$HO_2(aq) + HO_2(aq) \rightarrow H_2O_2(aq)$	8.6D5·exp(-7.94D0·(298D0/T-1D0))/(cw·Na)	[2]
756	$HO_2(aq) + O_2{}^- \rightarrow H_2O_2(aq)$	1D8·exp(-5.03D0·(298D0/T-1D0))/(cw·Na)	[2]
757	$HO_2(aq) + SO_4{}^- \rightarrow SO_4^{2-}$	5D9·exp(-5.03D0·(298D0/T-1D0))/(cw·Na)	[2]
758	$O_2{}^- + SO_4{}^- \rightarrow SO_4^{2-}$	5D9·exp(-5.03D0·(298D0/T-1D0))/(cw·Na)	[2]
759	$O_2{}^- + SO5^- \rightarrow HSO5^-$	1D8·exp(-5.03D0·(298D0/T-1D0))/(cw·Na)	[2]
760	$SO5^- + SO5^- \rightarrow SO_4{}^- + SO_4{}^-$	6D8·exp(-5.03D0·(298D0/T-1D0))/(cw·Na)	[2]
761	$NH_3(aq) \rightarrow NH_4{}^-$	$[H^+]$·1D10	[E]
762	$NH_4{}^- \rightarrow NH_3(aq)$	1D10/(1.7882D9·exp(21.0200·(298D0/T-1D0)))	[E]
763	$SO_3(aq) \rightarrow HSO_4^-$	1D10	[A]
764	$Cl(aq) + Cl(aq) \rightarrow Cl_2(aq)$	8.75D7/(cw·Na)	[9] [2]

[1] MCMv3.3.1 ; [2] Hoffmann et al. (2016) ; [3] Wu et al. (2014) ; [4] Berndt et al. (2019) ; [5] Kukui et al. (2003)

[6] Atkinson et al. (2007) ; [7] Sander et al. (2006) ; [8] Atkinson et al. (2008) ; [9] Braeuer et al. (2013) ; [10] Jacobson (2005)

[11] Demore et al. (1997) ; [12] Berndt et al. (2020) ; [13] Kahan et al. (2012) ; [14] Burkholder et al. (2015)

[E] Estimate based on equilibrium coefficients ; [C] Based on pKa value from COSMO*therm* ; [A] Assumed

S1.1 Chamber wall effects

Table S2: Temperature dependant Henry's law solubility and wall mass accommodation coefficients . COSMO*therm* calculation were estimated at 298K and coupled with temperature dependence from other sources.

Type	H^{cp}	α_w	Ref.
Cl_2	9.15D-2·exp(2490D0·(1D0/T-1D0/298D0))	-	[1]
Cl	0.2D0	-	[1]
ClO	660D0·exp(5862D0·(1D0/T-1D0/298D0))	-	[1]
ClO_2	1D0·exp(-3300D0·(1D0/T-1D0/298D0))	-	[1]
HCl	1.1D0·exp(2020D0·(1D0/T-1D0/298D0))	-	[1]
HOCl	660D0·exp(5862D0·(1D0/T-1D0/298D0))	-	[1]
ClNO	5D-2	-	[1]
$ClNO_2$	4.6D-2	-	[1]
$ClNO_3$	2.1D5·exp(8700D0·(1D0/T-1D0/298D0))	-	[1]
Br_2	0.76D0·exp(4100D0·(1D0/T-1D0/298D0))	-	[1]
Br	1.2D0	-	[1]

[1] Braeuer et al. (2013) ; [2] Jacobson (2005) ; [3] Hoffmann et al. (2016)

[4] Kulmala and Laaksonen (1990) ; [C] COSMO*therm* with temperature dependence from Hoffmann et al. (2016); [A] Assumed

. . . Solubility continued

Type	H^{cp}	α_w	Ref.
BrO	93D0·exp(5862D0·(1D0/T-1D0/298D0))	-	[1]
$BrNO_2$	0.3	-	[1]
$BrNO_3$	2.1D5·exp(8700D0·(1D0/T-1D0/298D0))	-	[1]
$BrCl$	0.94D0·exp(5600D0·(1D0/T-1D0/298D0))	-	[1]
I_2	3D0·exp(4431D0·(1D0/T-1D0/298D0))	-	[1]
I	8D-2	-	[1]
IO	450D0·exp(5862D0·(1D0/T-1D0/298D0))	-	[1]
OIO	2.1D5·exp(8700D0·(1D0/T-1D0/298D0))	-	[1]
I_2O_2	2.1D5·exp(8700D0·(1D0/T-1D0/298D0))	-	[1]
HI	2.5D0·exp(9800D0·(1D0/T-1D0/298D0))	-	[1]
HOI	450D0·exp(5862D0·(1D0/T-1D0/298D0))	-	[1]
HIO_3	2.1D5·exp(8700D0·(1D0/T-1D0/298D0))	-	[1]
INO_2	2.1D5·exp(8700D0·(1D0/T-1D0/298D0))	-	[1]
INO_3	2.1D5·exp(8700D0·(1D0/T-1D0/298D0))	-	[1]
ICl	110D0·exp(5600D0·(1D0/T-1D0/298D0))	-	[1]
IBr	24D0·exp(5600D0·(1D0/T-1D0/298D0))	-	[1]
O_3	1.13D-2·exp(7.72·(298D0/T-1D0))	1D-7	[2]
OH	2.5D1·exp(22.21·(298D0/T-1D0))	1D-5	[2]
H_2O_2	9.1D2·101.325·exp(6600·(1D0/T-1D0/298D0))	1D0	[2]
DMS	0.56D0·exp(4480D0·(1D0/T-1D0/298D0))	1D-7	[3]
$DMSO$	1D7·exp(2580D0·(1D0/T-1D0/298D0))	1D-5	[3]
$DMSO_2$	1D7·exp(5390D0·(1D0/T-1D0/298D0))	1D-5	[3]
$MSIA$	1.68D9·exp(1760D0·(1D0/T-1D0/298D0))	1D-5	[C]
$HPMTF$	1.33D7	1D-5	[C]
SO_2	1.22D0*EXP(10.55*(298D0/TEMP-1D0))	1D-7	[2]
HO_2	2D3*EXP(22.28*(298D0/TEMP-1D0))	1D-5	[2]
NO_3	2.1D5*EXP(29.19*(298D0/TEMP-1D0))	1D-5	[2]
$HCHO$	3.46D0*EXP(8.19*(298D0/TEMP-1D0))	1D-5	[2]
NO_2	1D-2*EXP(8.38*(298D0/TEMP-1D0))	1D.7	[2]
O_2	1.3D-3	1D-5	[2]
SO_3	1D5	1D-5	[A]
NH_3	57.6*EXP(13.79*(298./TEMP-1D0) -5.39*(1D0+log(298./TEMP)-298./TEMP))	1D0	[2]
HNO_3	2.1D5·exp(8700.0·(1D0/T-1D0/298.15))	1D0	[2]
H_2SO_4	1D0/(98D-3·exp(-11.695D0+10156D0·(1D0/360.15D0-1D0/T +0.38D0/545D0·(1D0+log(360.15/T)-360.15/T))))	1D0	[4]
MSA	1.13D11·exp(1760D0·(1D0/T-1D0/298D0))	1D0	[C]

[1] Braeuer et al. (2013) ; [2] Jacobson (2005) ; [3] Hoffmann et al. (2016)

[4] Kulmala and Laaksonen (1990) ; [C] COSMO*therm* with temperature dependence from Hoffmann et al. (2016); [A] Assumed

S2 Model setup and additional results

S2.1 Chamber compaction and dilution due to instrument sampling

We simulated the gradual dilution of the smog chamber because of the instrument sampling and air entrainment from outside the chamber. The Teflon bag in AURA is mounted in a fixed metal frame. Based on the observations of the smog chamber we estimate that the chamber volume can be compressed from initially 5 m^3 to a minimum volume of 3 m^3 because of the instrument sampling. In the model we simulate the chamber volume compaction and gradually increasing air entrainment using a simplified parameterization which describe the fraction of the sampled air that result in a decreasing chamber volume:

$$f_{\text{compaction}} = (V(t) - V_{\text{min}})/(V_0 - V_{\text{min}}) \tag{1}$$

(V(t)), (V$_{\text{min}}$) and (V$_0$) denote the chamber volume at time (t), the estimated minimum chamber volume (3 m^3) in AURA and the initial chamber volume (5 m^3) respectively. The remaining fraction of the sampled air ($1 - f_{\text{compaction}}$) was assumed to be particle free air mixed into the chamber from outside, which resulted in a gradual dilution of the species concentrations in the chamber.

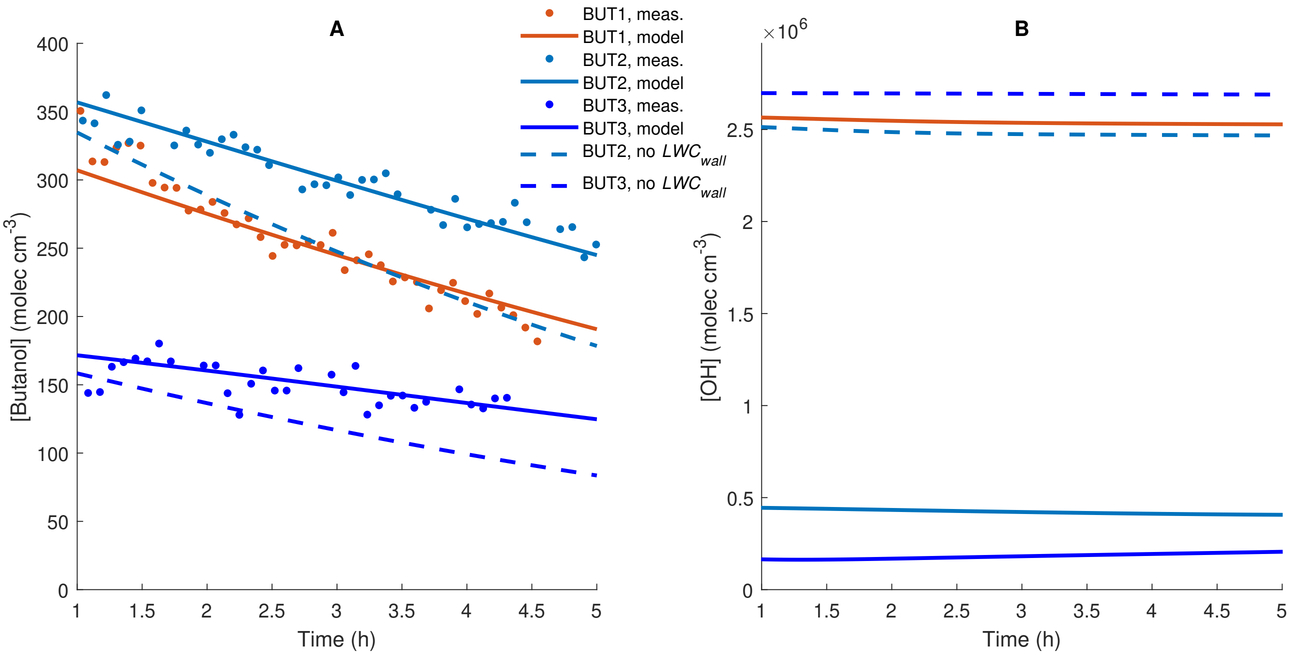

Figure S1. Model results and observations from three butanol experiments (BUT1-3). Panel **A**: Modelled and observed butanol concentrations. Panel **B**: Modelled OH concentration. BUT1: 293 K, RH $\sim$ 5 %; BUT2: 293 K, RH 50-60 %; BUT3: 273 K, RH 70-80 %. The dashed lines show the model results from simulations without a liquid water film on the chamber walls.

S2.2 Estimated wall liquid water content based on Butanol experiments

Fig. S1 shows the modelled and observed butanol decay and modelled OH concentrations during three different butanol experiments. In order to capture the observed butanol decay during humid experiments BUT2 and BUT3 we had to introduce a liquid water film corresponding to an effective liquid water content (LWC) of $\sim$30 g/m^3 and $\sim$500 g/m^3 on the chamber walls respectively. The LWC on the walls allow the highly water soluble H_2O_2, which serve as the main OH source, to be taken up efficiently on the chamber walls. The observed and modelled butanol loss rates are governed both by the chamber dilution and the OH oxidation. In the humid experiments (BUT2-3) the dilution is larger than in the dry experiment (BUT1) because of an inflow of 2 L/min of humidified air. In the dry experiment (BUT1) their is some indication that the butanol decay is slightly faster in the observations than in the model. This could possibly be a result of underestimated OH recycling in the MCMv3.3.1 butanol chemistry. When the model is run without any butanol the modelled OH concentration become $\sim$10 % larger. However, it may also be due to slightly underestimated chamber dilution in the model.

S2.3 COSMO*therm* calculations

We followed recommendations by Kurtén et al. (2018) in selecting conformers containing no intramolecular H-bonds as input for the COSMO*therm* calculations. This method has shown to give more accurate saturation vapour pressure estimates of multifunctional compounds that are able to form intramolecular H-bonds (Kurtén et al., 2018). The input files were computed at the BP/def2-TZVPD-FINE//BP/def-TZVP level of theory using the COSMO*conf* and TURBOMOLE programs (COSMO*conf*, 2013; TURBOMOLE, 2010).

Henry's law coefficients were calculated using COSMO*therm*-estimated saturation vapour pressure of the pure compound i (p_{sat}) and activity coefficient of compound i at infinite dilution in water (γ_i^w, with respect to pure compound reference state):

$$H_i^{cp} = \frac{1}{M_w \times p_{\mathrm{sat},i} \times \gamma_i^w} \tag{2}$$

This approach assumes low aqueous solubility for the compounds ($x_{\mathrm{sol},i}^w = 1/\gamma_i^w$), which means that the molar mass of the solution can be approximated using the molar mass of the solvent water (M_w). Table S3 shows the COSMO*therm*-estimated saturation vapour pressures and aqueous activity coefficients, as well as Henry's law coefficients calculated using the COSMO*therm* estimates.

Table S3. COSMO*therm*-estimated saturation vapour pressures, pKa and aqueous activity coefficients at 298.15 K, and Henry's law coefficients calculated from the two COSMO*therm* estimates.

	p_{sat} [atm]	γ^w	H^{cp} [mol atm^{-1} kg^{-1}]	pKa
HPMTF-hydrate	2.49×10^{-7}	2.80×10^{-1}	7.96×10^{8}	10.46
HPMTF	2.37×10^{-4}	1.76×10^{1}	1.33×10^{4}	10.30
MSA	4.16×10^{-7}	1.18	1.13×10^{8}	-2.93
MSIA	1.51×10^{-5}	2.18	1.69×10^{6}	2.62

S2.4 Sensitivity runs with variable wall liquid water content

To constrain the effect of different liquid water content on the chamber walls (LWC_{wall}), for the secondary aerosol formation from DMS, we performed several model sensitivity tests. Fig S2-S4 summarises the results from one dry experiment (DMS2) and the two humid experiments DMS6 and DMS7.

When the LWC_{wall} is lowered with one order of magnitude compared to the default model setup ($LWC_{wall} = 10^{-5}$ $\mathrm{gm^{-3}}$), for the dry experiment, the ammonia gas-phase concentration increases. This results in higher new particle formation (NPF) and total particle number concentration. The lower $_{wall}$ also prevent the uptake and oxidation of MSIA on the chamber walls, and thereby increases the formation of MSA and SA in the gas-phase and the secondary SA and MSA particle mass (PM) formation (Fig. S2B). The opposite effect is seen when the LWC_{wall} is increased compared to the default model setup.

For the humid experiments the LWC_{wall} serve as an efficient sink for the $\mathrm{H_2O_2(g)}$ which results in substantially lower $\mathrm{HO_2(g)}$ concentrations compared to the dry experiments. This promote the SA formation via thermal decomposition of $\mathrm{CH_3SO_3}$ in front of the MSA production via $\mathrm{CH_3SO_3 + HO_2}$. Thus, lowering the LWC_{wall} with one order of magnitude compared to the default model setup for experiment DMS6 result in lower SA and decreasing NPF (Fig. S3A), despite that the $\mathrm{NH_3(g)}$ concentration increases. This also results in overestimated MSA PM formation and underestimated $\mathrm{SO_4}$ PM formation (Fig. S3B). When the LWC_{wall} instead is increased with one order of magnitude compared to the default setup, the model underestimates the MSA PM and overestimates the $\mathrm{SO_4}$ PM in the end of the model simulation (Fig. S3B). Increasing LWC_{wall} also results in lower particle number concentrations. This time it is the $\mathrm{NH_3(g)}$ concentration which become the limiting factor for the NPF. Fig. S3 shows the model results from a simulation with $LWC_{wall} =$ 30 $\mathrm{gm^{-3}}$, i.e. the same LWC_{wall} as was estimated from the humid butanol experiment BUT2. With this LWC_{wall} value the modelled particle number concentration and $\mathrm{SO_4}$ PM are in close agreement with the observations, however the model underestimate the PM MSA with 20-30 %.

The increasing particle mass formation in the end of the simulations in experiment DMS6 is governed by the gradually increasing inflow of $\mathrm{NH_3(g)}$ rich air from outside the chamber, which result in a second weaker NPF event. The modelled PM mass increase is mainly a result of that the non-charged newly formed particles are less efficiently lost to the walls than the aged charged particles, and that the NPF increases the particle condensation sink. This tendency of increasing PM in the end of the experiment is not seen in the observations, which may indicate that the model overestimate the leakage of $\mathrm{NH_3(g)}$ into the chamber during the end of this experiment.

For the humid and cold experiment DMS7 the modelled particle number concentration and $\mathrm{SO_4}$ PM are relatively insensitive to different LWC_{wall} values (Fig. S4). However, the model strongly overestimates the MSA PM if we use the same LWC_{wall} as for the default DMS6 model setup, i.e. $LWC_{wall} \geq 10$ $\mathrm{gm^{-3}}$. The closest agreement between the modelled and measured MSA is found when the $LWC_{wall} \geq 500$ $\mathrm{gm^{-3}}$, i.e. similar LWC_{wall} as was estimated from the humid and cold butanol experiment BUT3 (Fig. S1).

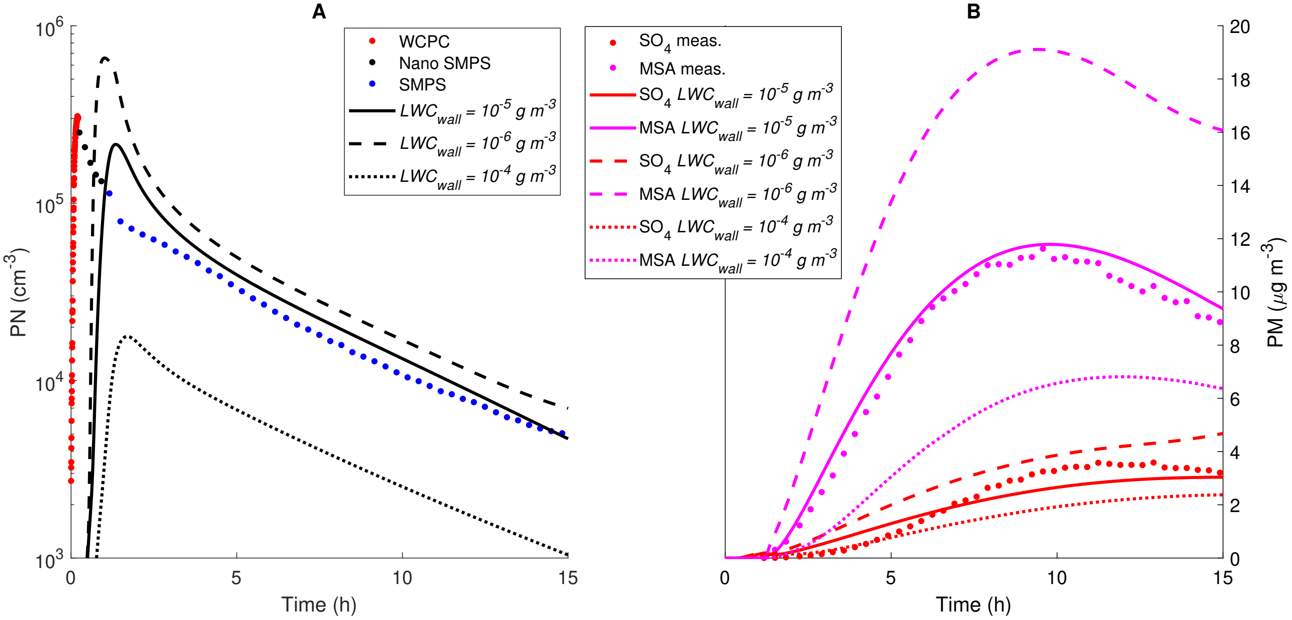

Figure S2. Modelled and measured particle number concentration (panel **A**) and particle MSA and SO_4 mass concentrations (panel **B**) for the dry chamber experiment DMS2. The model results are from different sensitivity runs with different LWC on the chamber walls.

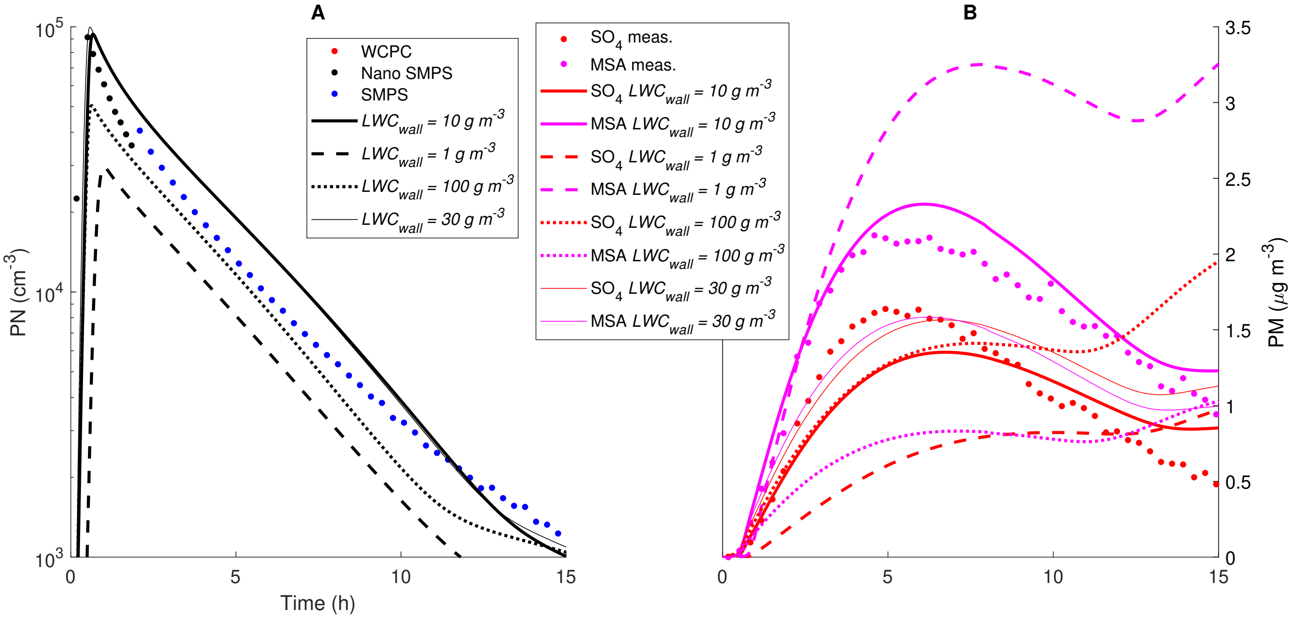

Figure S3. Modelled and measured particle number concentration (panel **A**) and particle MSA and SO_4 mass concentrations (panel **B**) for the humid chamber experiment DMS6. The model results are from different sensitivity runs with different LWC on the chamber walls.

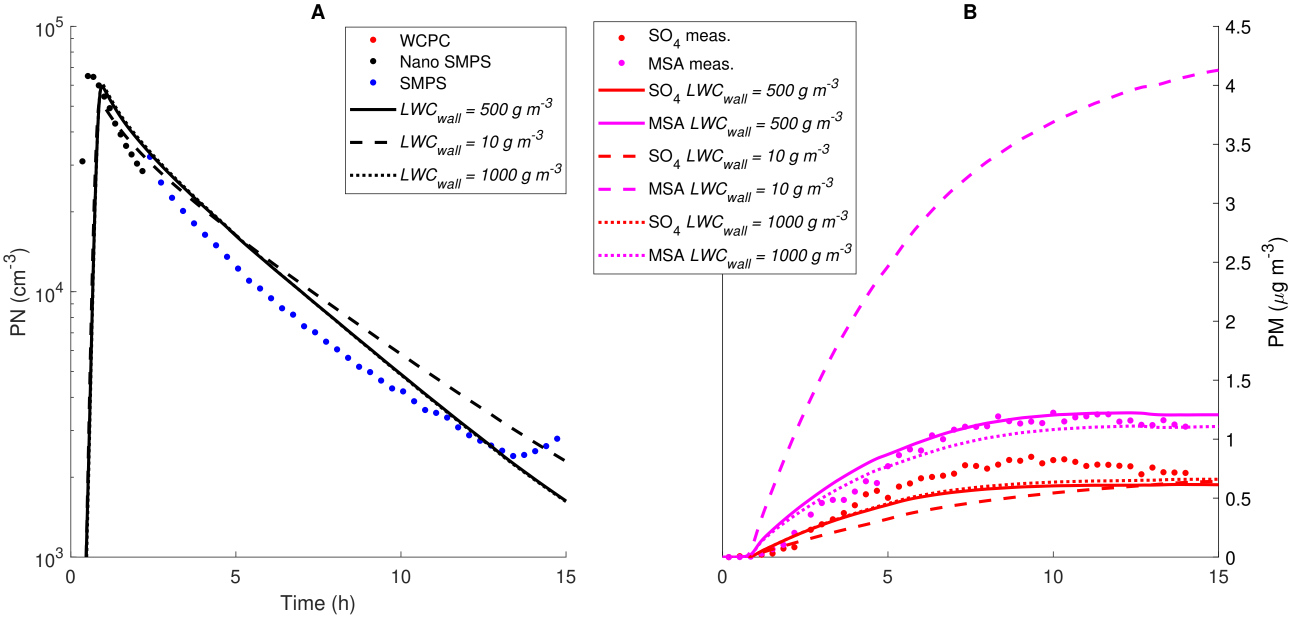

Figure S4. Modelled and measured particle number concentration (panel **A**) and particle MSA and SO_4 mass concentrations (panel **B**) for the humid and cold chamber experiment DMS7. The model results are from different sensitivity runs with different LWC on the chamber walls.

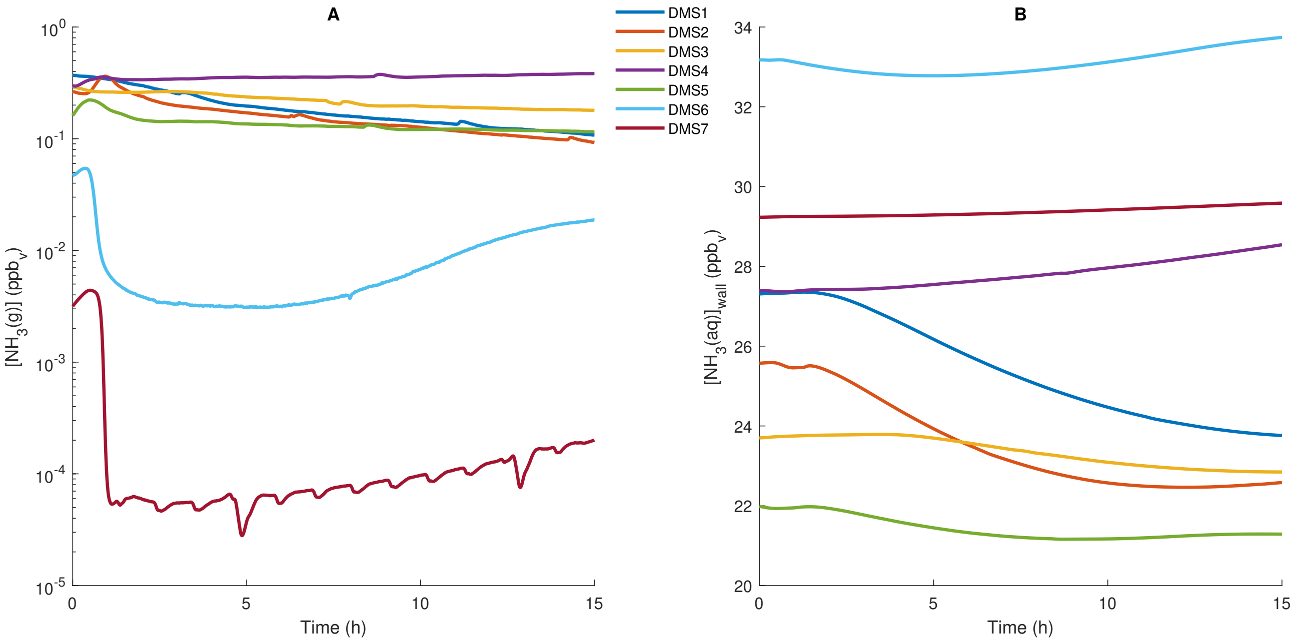

Figure S5. Modelled $\mathrm{NH_3}$ concentration in the gas-phase (panel **A**) and on the chamber walls (panel **B**) for all base case model simulations of experiments DMS1-7.

S2.5 Modelled $\mathrm{NH_3}$ concentrations

Figure S5 shows the modelled $\mathrm{NH_3}$ concentration in the gas-phase (Fig. S5A) and on the walls (Fig. S5B) for all simulated DMS experiments. The $\mathrm{NH_3(g)}$ concentration is governed by the loss of $\mathrm{NH_3(g)}$ to the aerosol particle phase, the acidity of the wall liquid water and the leakage of $\mathrm{NH_3(g)}$ into the chamber. In experiment DMS1, DMS2, DMS3 and DMS5 the aerosol particle condensation sink term is greater than the inflow of $\mathrm{NH_3(g)}$ into the chamber which result in gradually decreasing $\mathrm{NH_3}$ concentration both in the gas-phase and on the chamber walls. In DMS5, the experiment with lowest DMS concentration, the particle condensation sink of $\mathrm{NH_3(g)}$ is always smaller than the inflow of $\mathrm{NH_3(g)}$, which result in gradually increasing $\mathrm{NH_3}$ concentrations in the gas-phase and on the walls. In the humid experiments DMS6 and DMS7 the condensation sink term dominates over the influx of $\mathrm{NH_3}$ during the onset of the NPF in the chamber, while during the end of the experiments the inflow of $\mathrm{NH_3(g)}$ gradually increases the $\mathrm{NH_3}$ concentration in the gas-phase and on the walls. The very low $\mathrm{NH_3(g)}$ concentration in DMS7 compared to the other experiments is a result of the thick liquid water film on the walls and the low temperature. The ripples in the modelled $\mathrm{NH_3(g)}$ concentrations, mainly observed in DMS7, is caused by small temperature fluctuations of ± 1 K.

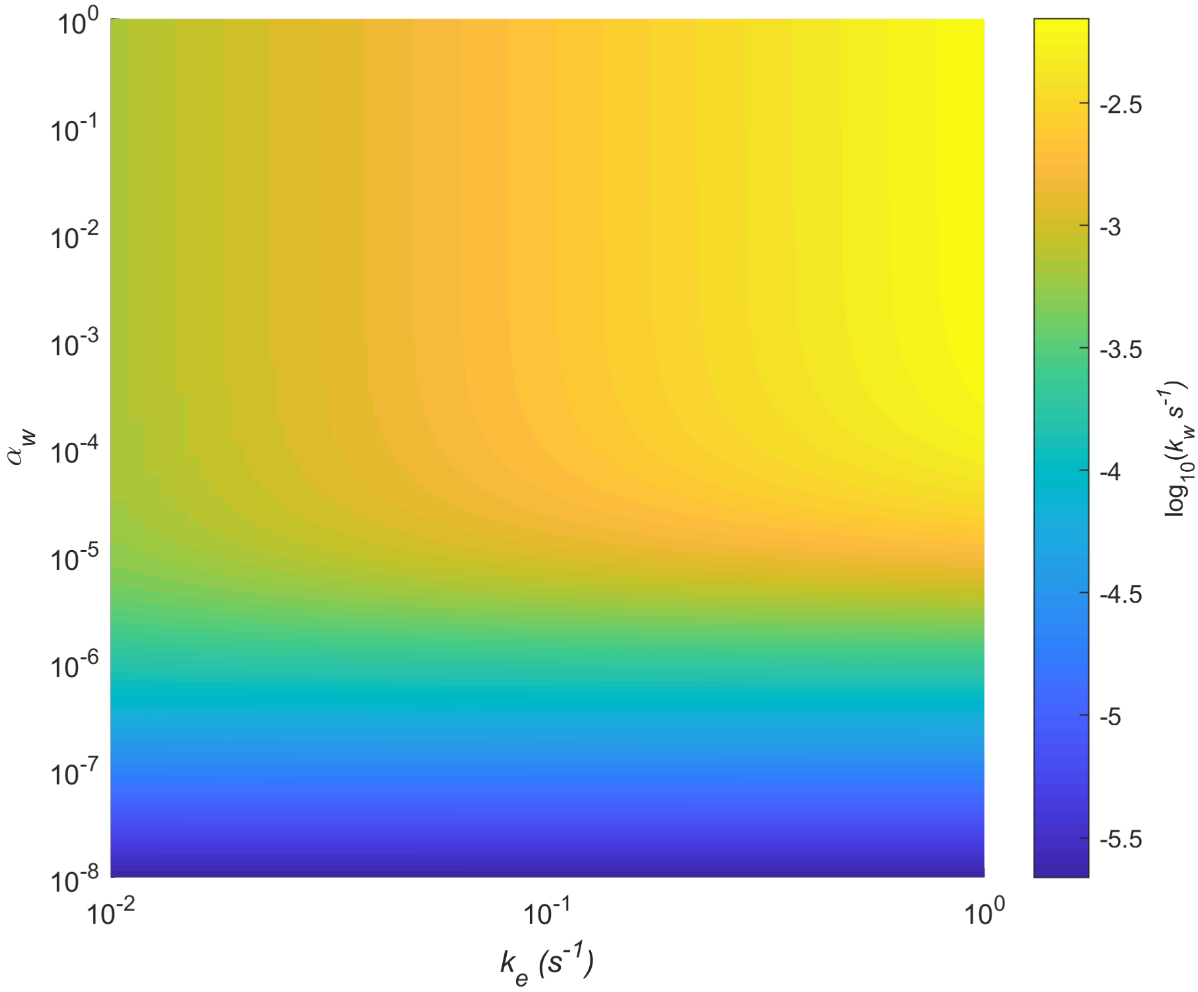

Figure S6. First order gas wall losses in a 5 m^3 smog chamber with a surface areas to volume ratio corresponding to a completely inflated AURA smog chamber. The wall loss rates were calculated with theory proposed by McMurry and Grosjean (1985) for a molecule with a diffusion coefficient (D) = 10^{-5} m^{2}s^{-1} and wall mass accommodation coefficients in the range 10^{-8} to 1.0

S2.6 Wall loss rates of gases

70 Figure S6 shows how the first order gas wall loss rates (k_w) varies as a function of the coefficient of eddy diffusion (k_e) and the wall mass accommodation α_w. The wall loss rates were derived with the theory proposed by McMurry and Grosjean (1985) (Eq. 1). For the AURA model simulations performed in this work we used a relatively low (k_e) of 0.02 s^{-1} motivated by a previous AURA smog chamber study which estimated first order wall losses of highly oxygenated organic molecules (HOM) (Quéléver et al., 2019).

S2.6.1 Sensitivity runs with variable O_3 wall uptake

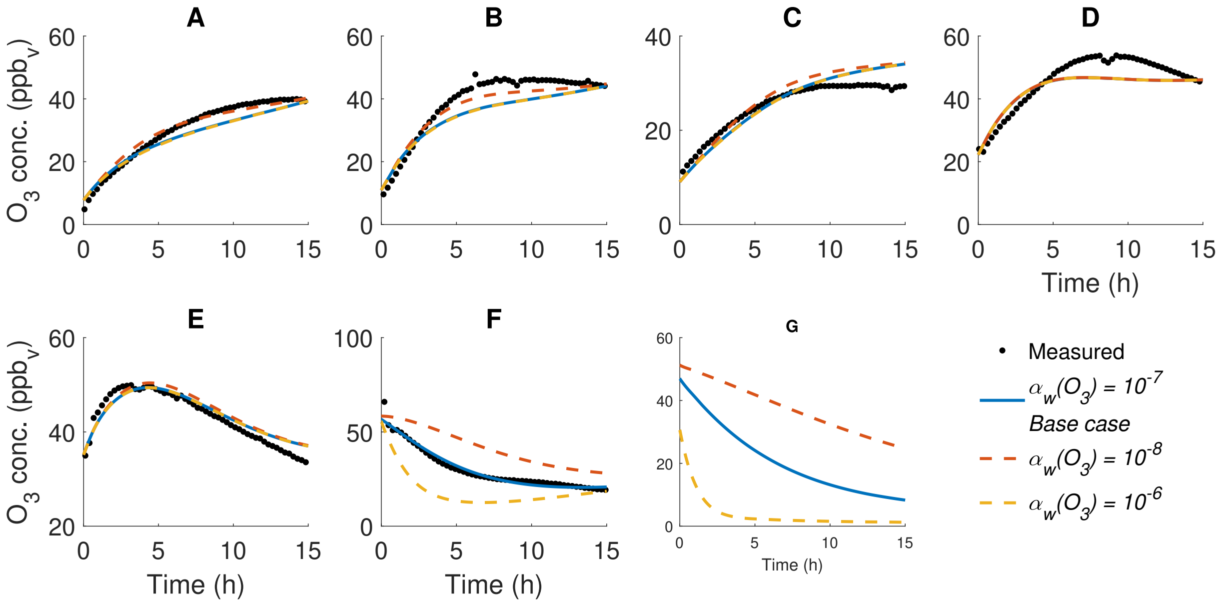

Figure S7. Measured and modelled O_3 concentration for different O_3 α_w. Panel **A**-**G** shows results from experiments DMS1-7.

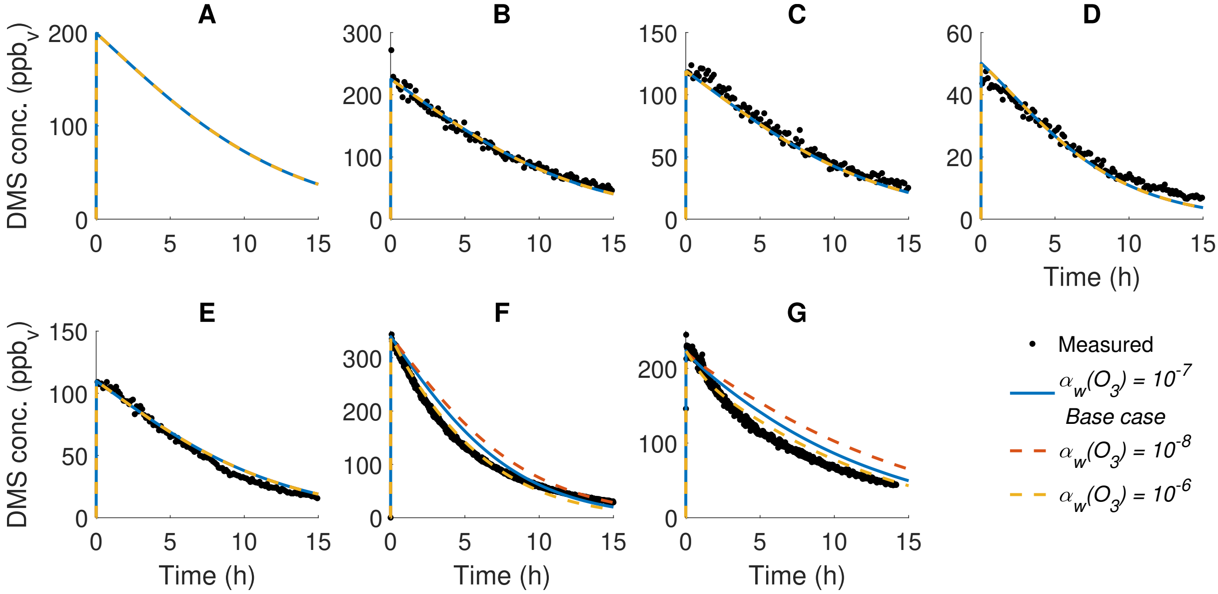

Figure S8. Measured and modelled DMS concentration for different O_3 α_w. Panel **A**-**G** shows results from experiments DMS1-7.

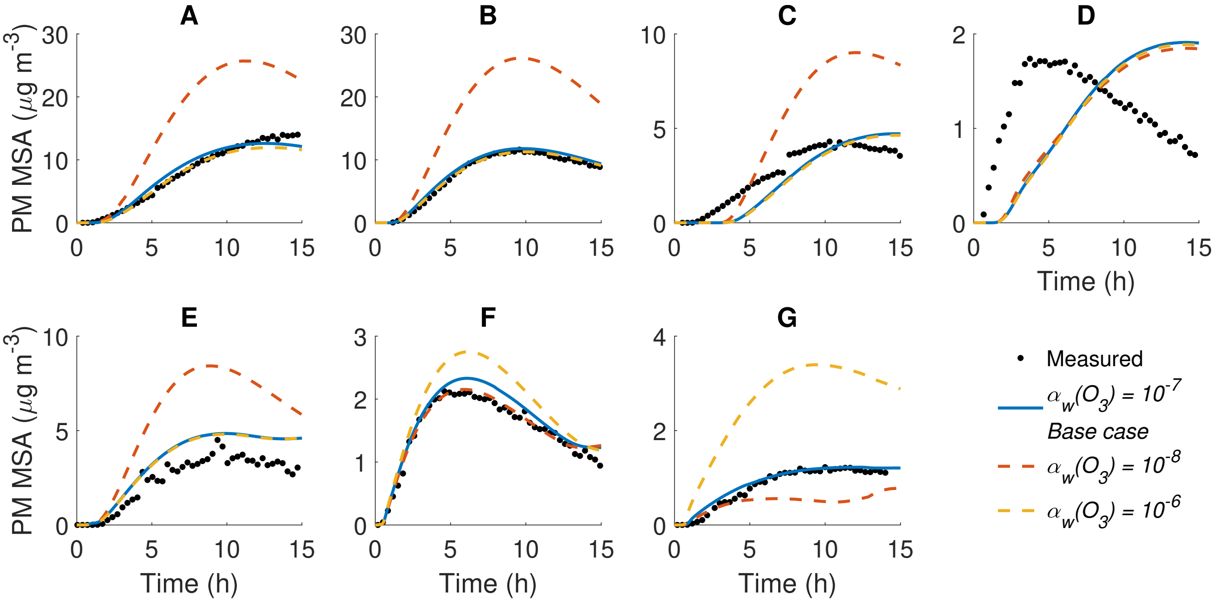

Figure S9. Measured and modelled MSA PM for different O_3 α_w. Panel **A**-**G** shows results from experiments DMS1-7.

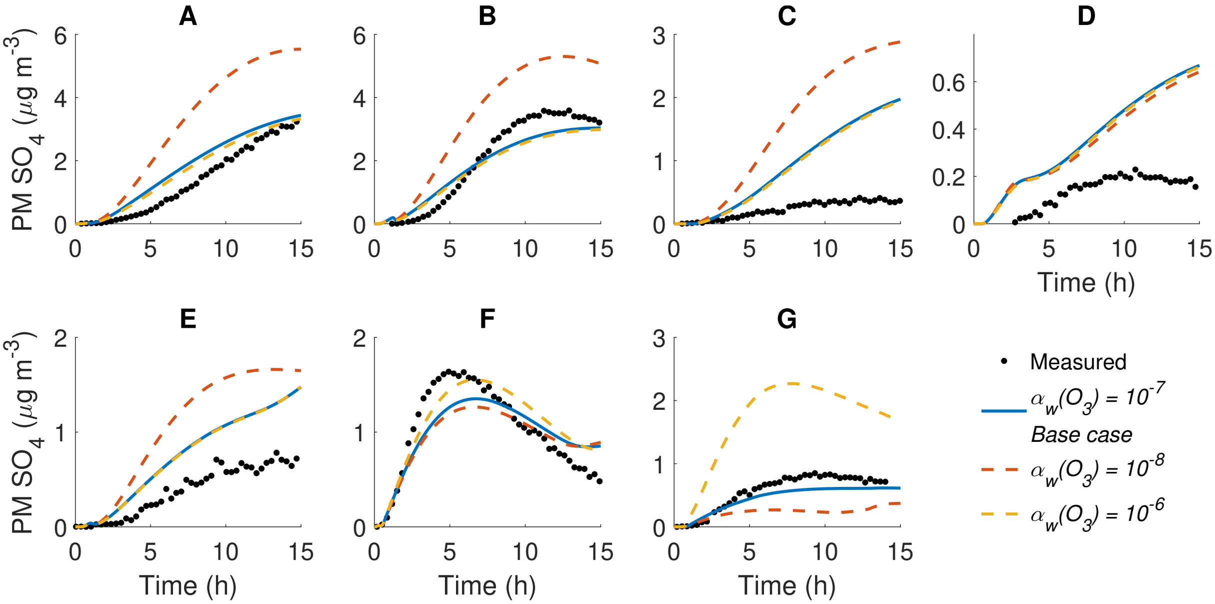

Figure S10. Measured and modelled SO_4 PM for different O_3 α_w. Panel **A**-**G** shows results from experiments DMS1-7.

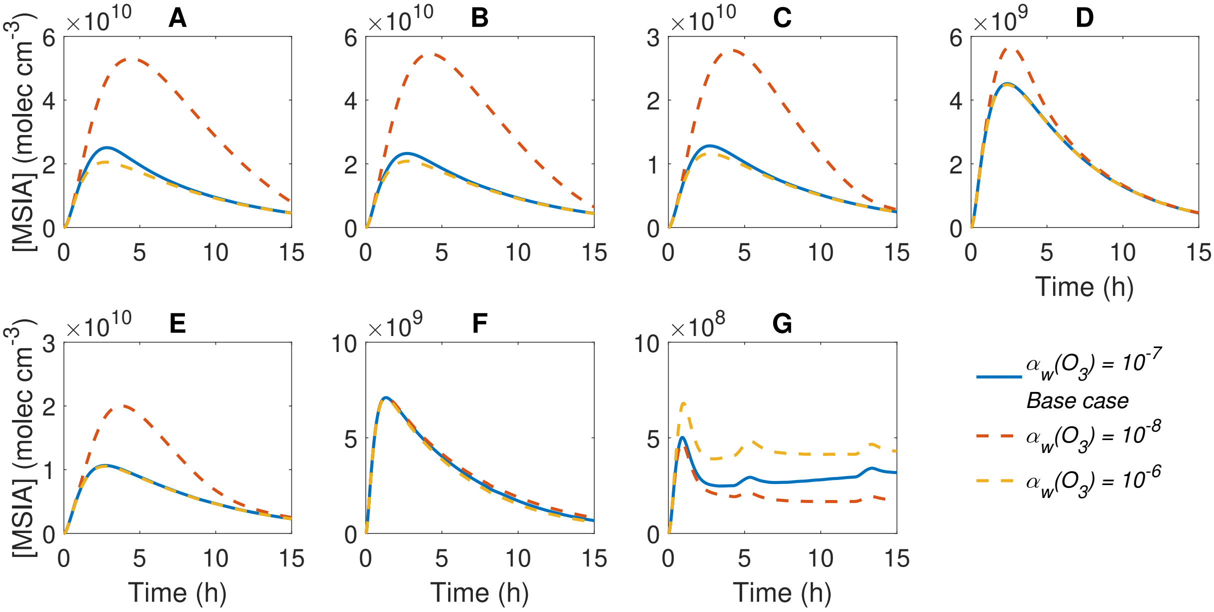

Figure S11. Modelled MSIA concentration for different O_3 α_w. Panel **A**-**G** shows results from experiments DMS1-7.

S2.6.2 Sensitivity runs with variable SO_2 wall uptake

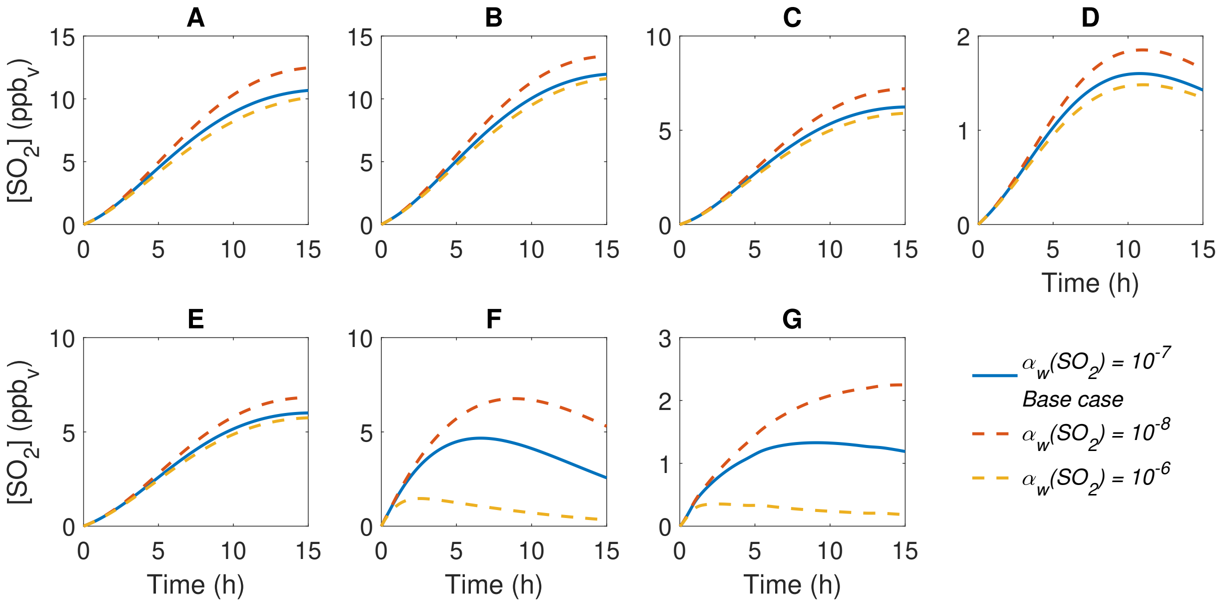

Figure S12. Modelled SO_2 concentration for different SO_2 α_w. Panel **A**-**G** shows results from experiments DMS1-7.

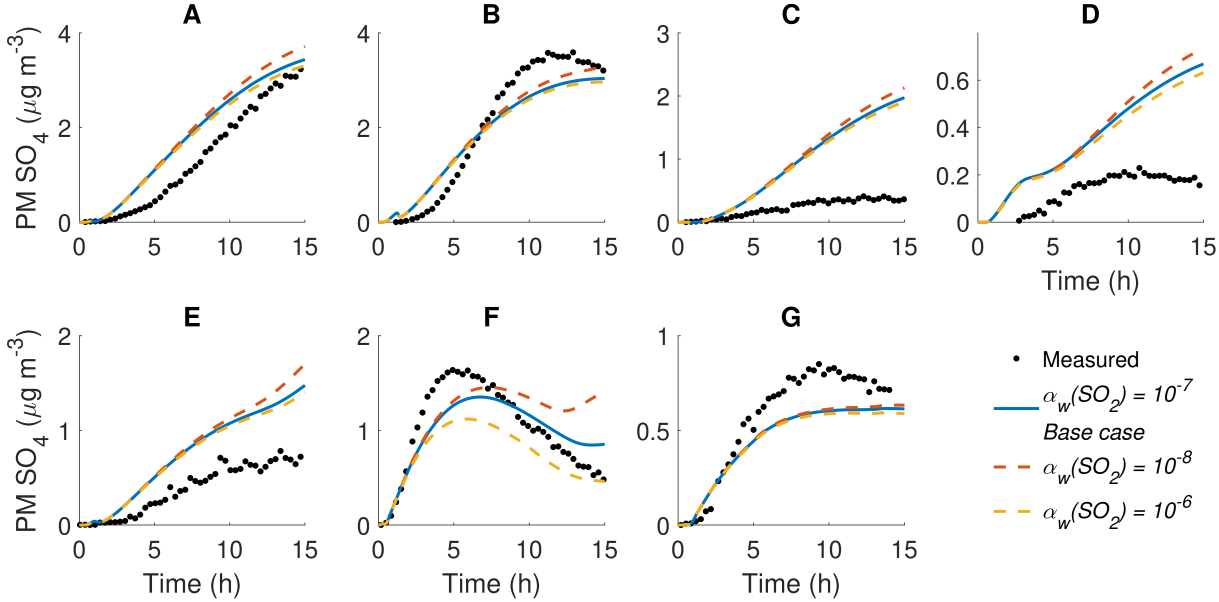

Figure S13. Measured and modelled SO_4 PM for different SO_2 α_w. Panel **A**-**G** shows results from experiments DMS1-7.

S2.6.3 Sensitivity runs with variable DMS wall uptake

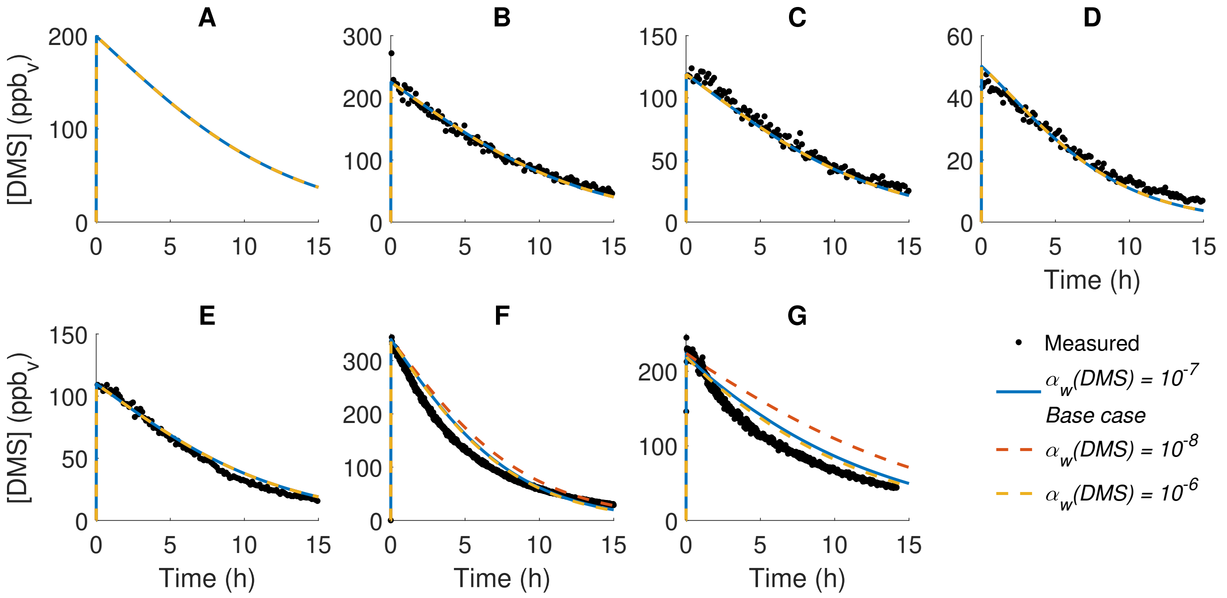

Figure S14. Measured and modelled DMS concentration for different DMS α_w. Panel **A**-**G** shows results from experiments DMS1-7.

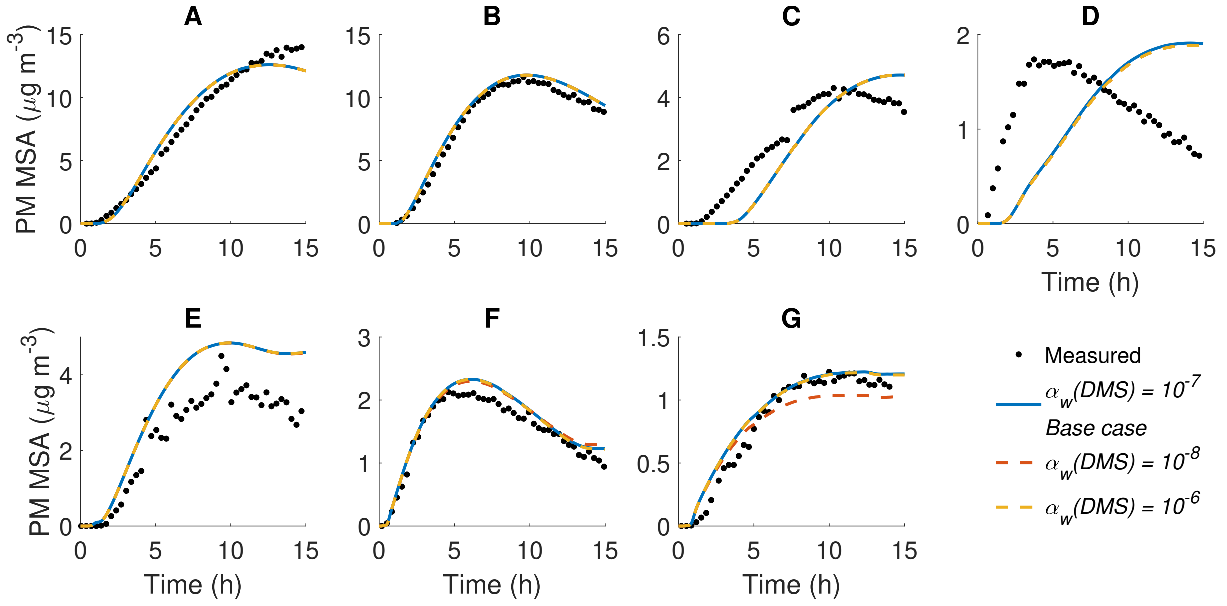

Figure S15. Measured and modelled MSA PM for different DMS α_w. Panel **A**-**G** shows results from experiments DMS1-7.

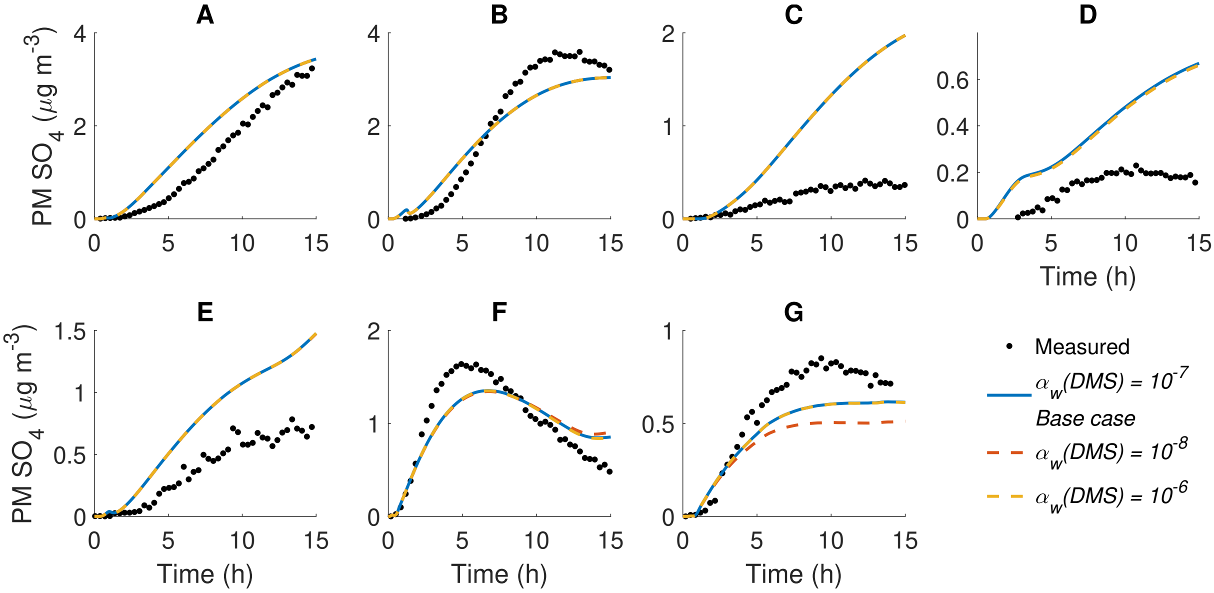

Figure S16. Measured and modelled $\mathrm{SO_4}$ PM for different $\mathrm{DMS}\ \alpha_w$. Panel **A**-**G** shows results from experiments DMS1-7.

S2.6.4 Sensitivity runs with variable DMSO, $\mathrm{DMSO_2}$, MSIA and HPMTF wall uptake

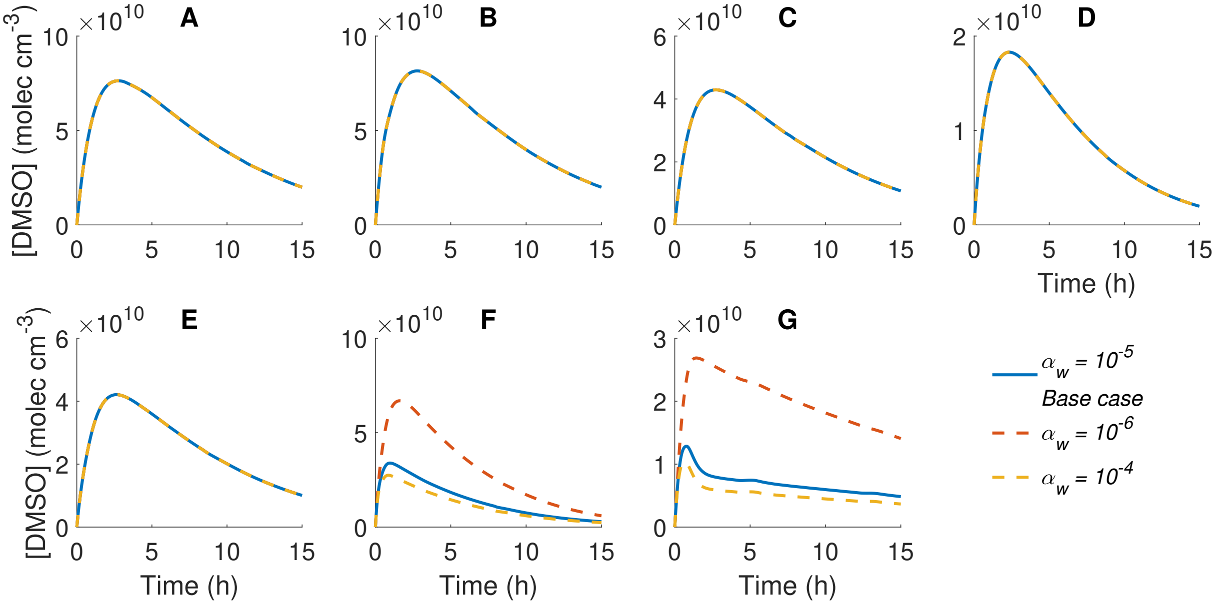

Figure S17. Modelled DMSO concentration for different α_w for the intermediate DMS oxidation products DMSO, $\mathrm{DMSO_2}$, MSIA and HPMTF. Panel **A**-**G** shows results from experiments DMS1-7.

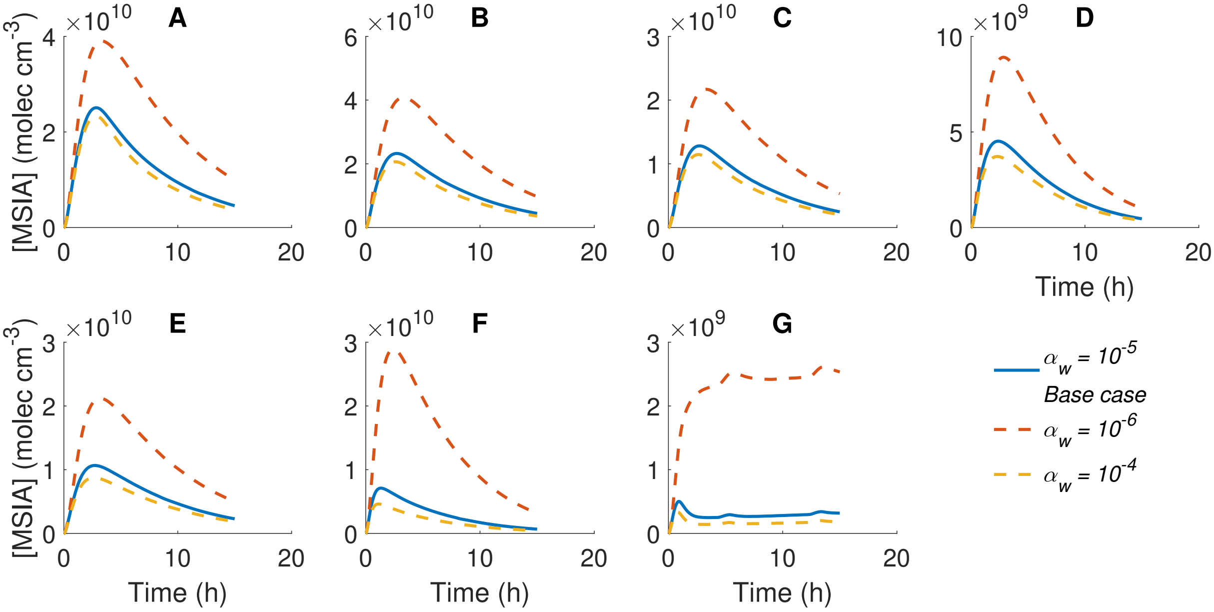

Figure S18. Modelled MSIA concentration for different α_w for the intermediate DMS oxidation products DMSO, $\mathrm{DMSO_2}$, MSIA and HPMTF. Panel **A**-**G** shows results from experiments DMS1-7.

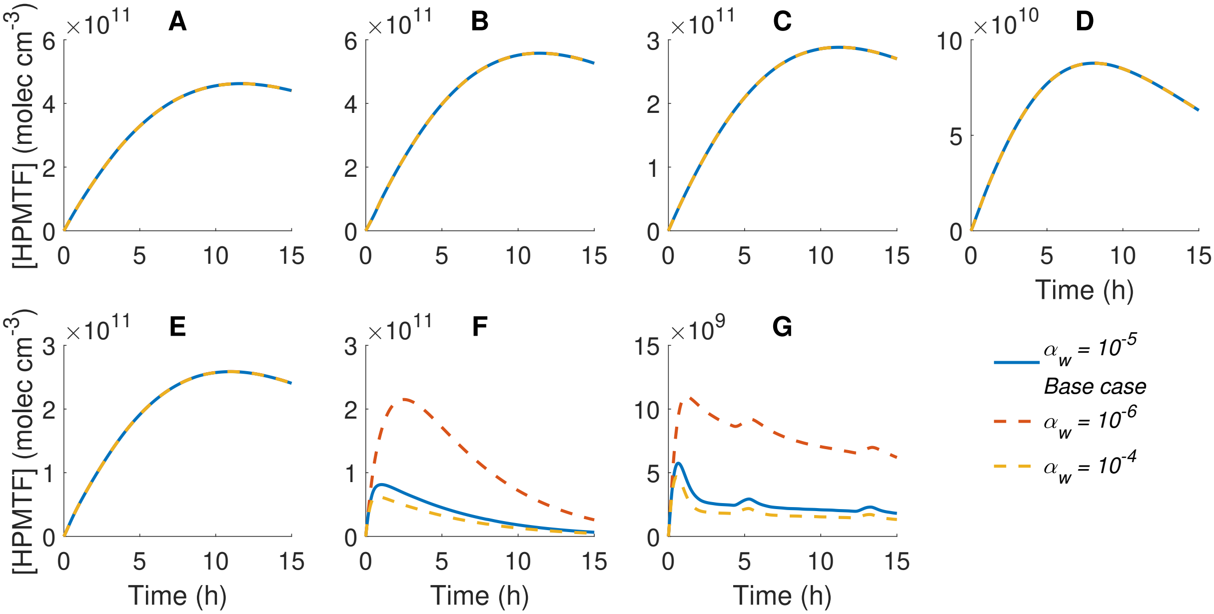

Figure S19. Modelled HPMTF concentration for different α_w for the intermediate DMS oxidation products DMSO, $\mathrm{DMSO_2}$, MSIA and HPMTF. Panel **A**-**G** shows results from experiments DMS1-7.

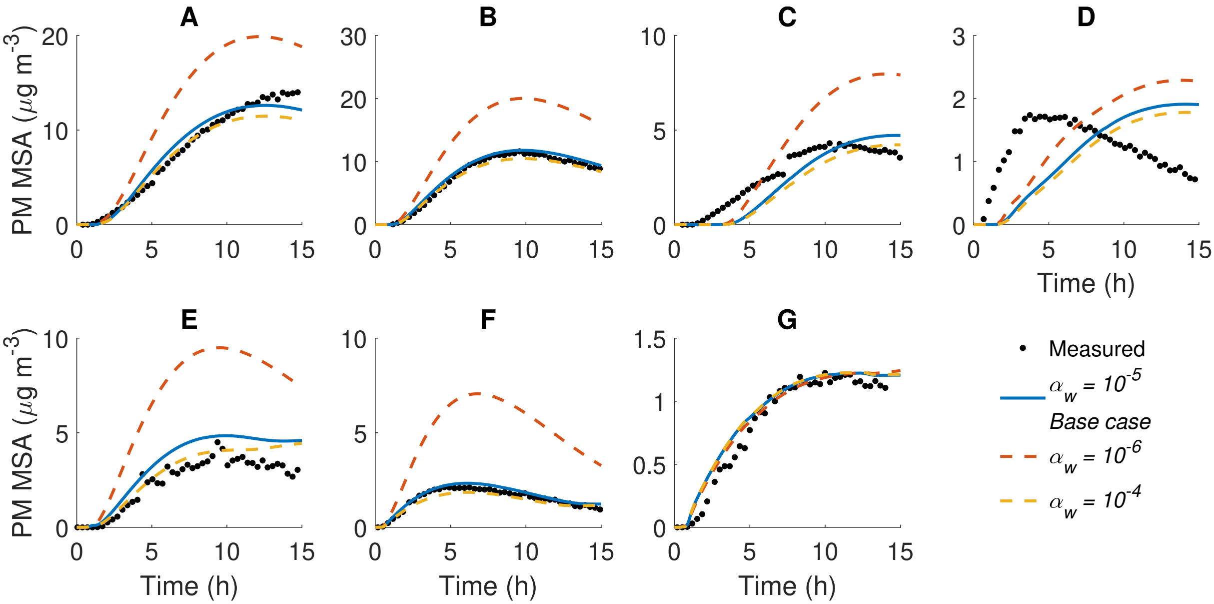

Figure S20. Measured and modelled MSA PM for different α_w for the intermediate DMS oxidation products DMSO, $\mathrm{DMSO_2}$, MSIA and HPMTF. Panel **A**-**G** shows results from experiments DMS1-7.

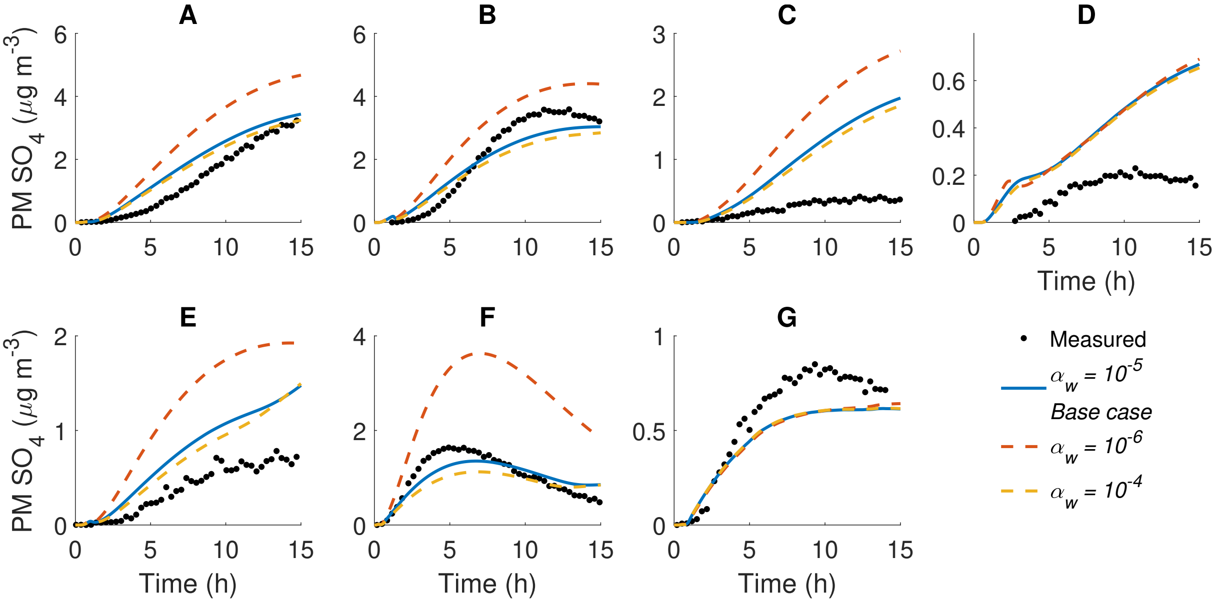

Figure S21. Measured and modelled $\mathrm{SO_4}$ PM for different α_w for the intermediate DMS oxidation products DMSO, $\mathrm{DMSO_2}$, MSIA and HPMTF. Panel **A**-**G** shows results from experiments DMS1-7.

S2.7 Gas partitioning between the gas-phase and liquid film on the chamber walls

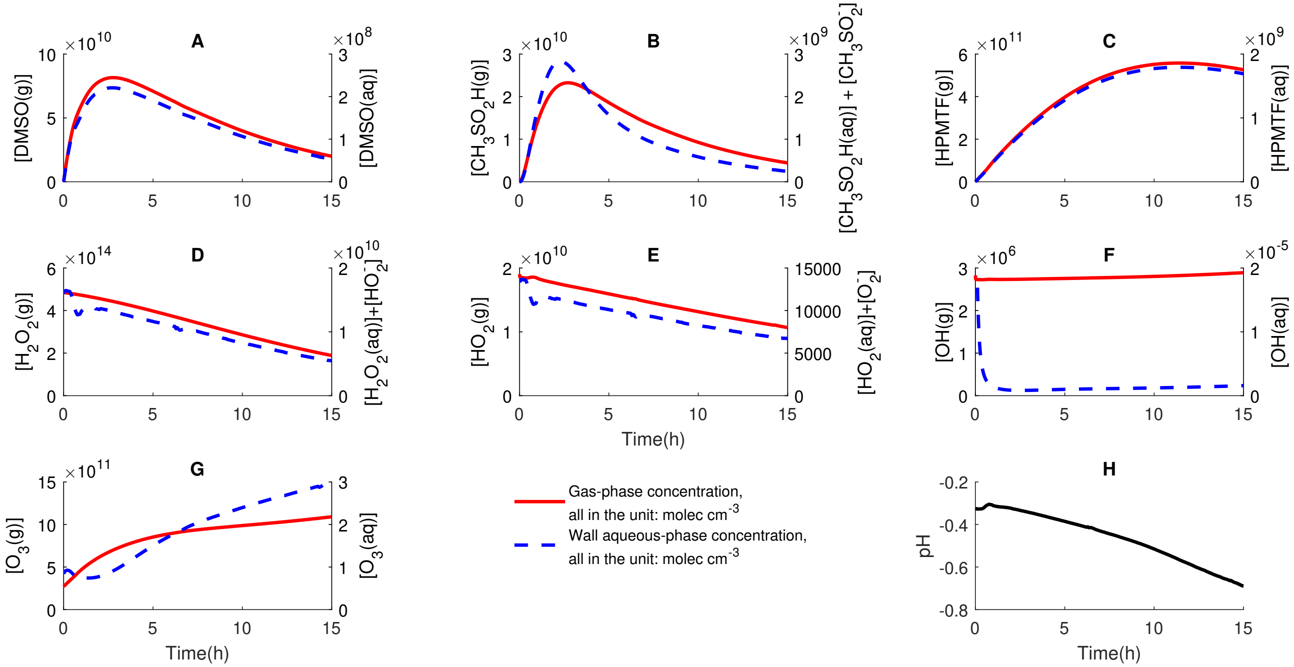

Figure S22. Modelled concentrations of the DMS oxidation products DMSO, MSIA (CH_3SO_2H) and HPMTF (panel **A**-**C**), and oxidation agents H_2O_2, HO_2, OH and O_3 (panel **D**-**G**) in the gas-phase (left y-axis) and in the chamber wall liquid water film (LWC_{wall}) (right y-axis) for the dry experiment DMS2. Panel **H** shows the modelled pH (acidity) in the liquid water film. All concentrations are given in molecules/(cm^3air).

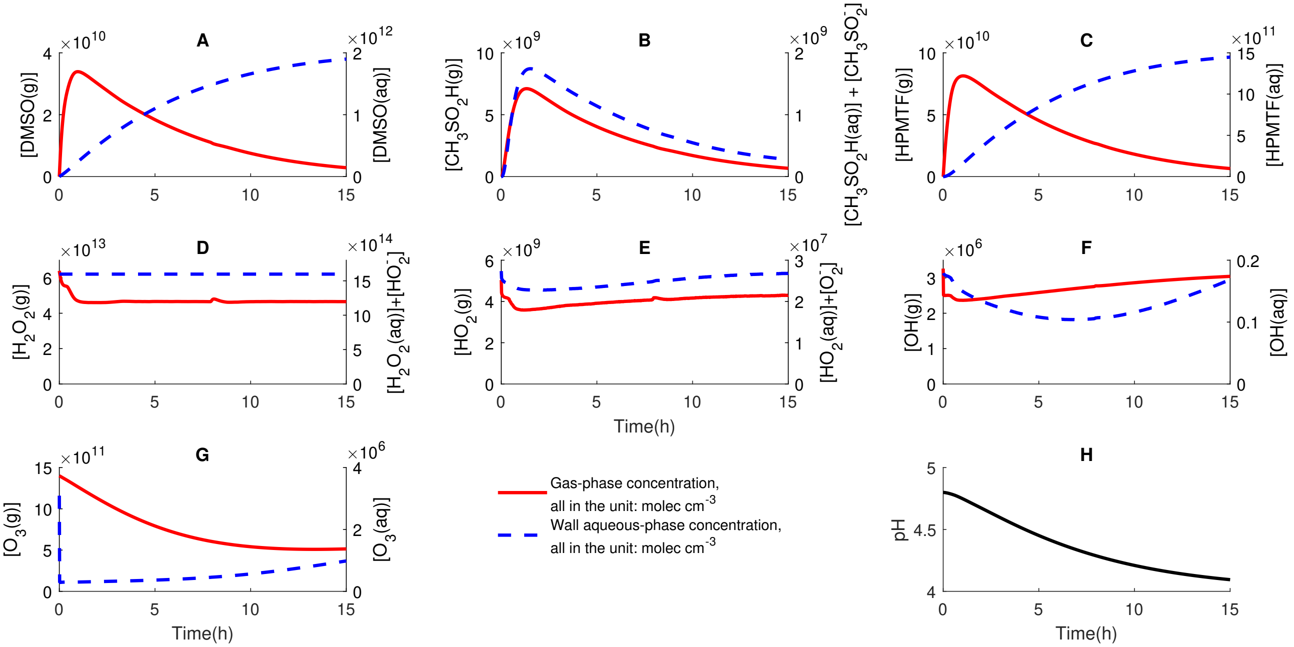

Figure S23. Modelled concentrations of the DMS oxidation products DMSO, MSIA ($\mathrm{CH_3SO_2H}$) and HPMTF (panel **A**-**C**), and oxidation agents $\mathrm{H_2O_2}$, $\mathrm{HO_2}$, OH and $\mathrm{O_3}$ (panel **D**-**G**) in the gas-phase (left y-axis) and in the chamber wall liquid water film (LWC_{wall}) (right y-axis) for the humid experiment DMS6. Panel **H** shows the modelled pH (acidity) in the liquid water film. All concentrations are given in $\mathrm{molecules/(cm^3air)}$.

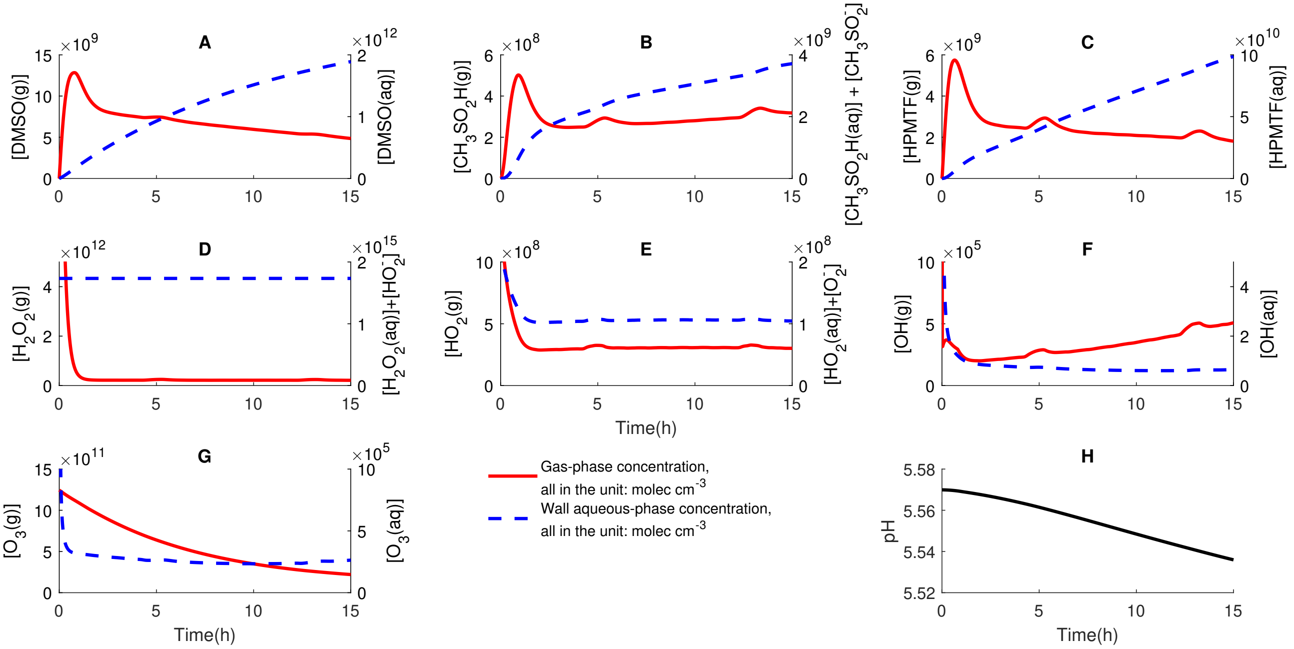

Figure S24. Modelled concentrations of the DMS oxidation products DMSO, MSIA ($\mathrm{CH_3SO_2H}$) and HPMTF (panel **A**-**C**), and oxidation agents $\mathrm{H_2O_2}$, $\mathrm{HO_2}$, OH and $\mathrm{O_3}$ (panel **D**-**G**) in the gas-phase (left y-axis) and in the chamber wall liquid water film (LWC_{wall}) (right y-axis) for the humid and cold experiment DMS7. Panel **H** shows the modelled pH (acidity) in the liquid water film. All concentrations are given in $\mathrm{molecules/(cm^3 air)}$.

S2.8 Wall loss for particles

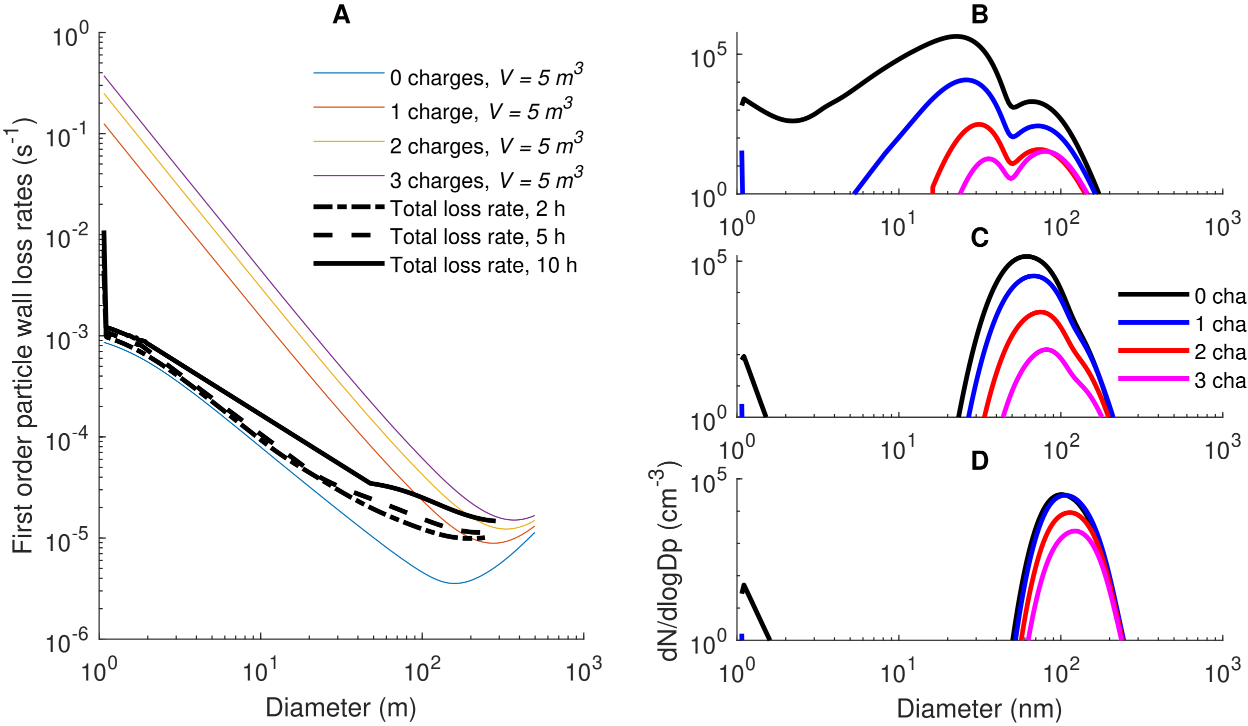

Figure S25. Example of modelled particle wall loss rates (panel **A**) and particle charge distributions after 2, 5 and 10 hours (panel **B**, **C** and **D**) for exp. DMS2. The modelled effective total particle wall loss rates take into account the fraction of particles with different number of elemental charges in each size bin. The high effective wall loss rate at the smallest particle size is a result of the relatively large fraction of charged molecules clusters that form new particles in the model. However, these particles are rapidly lost to the chamber walls and almost all nucleation mode aerosol particles above this size are non-charged.

80 S3 Results

S3.1 Chamber experiments

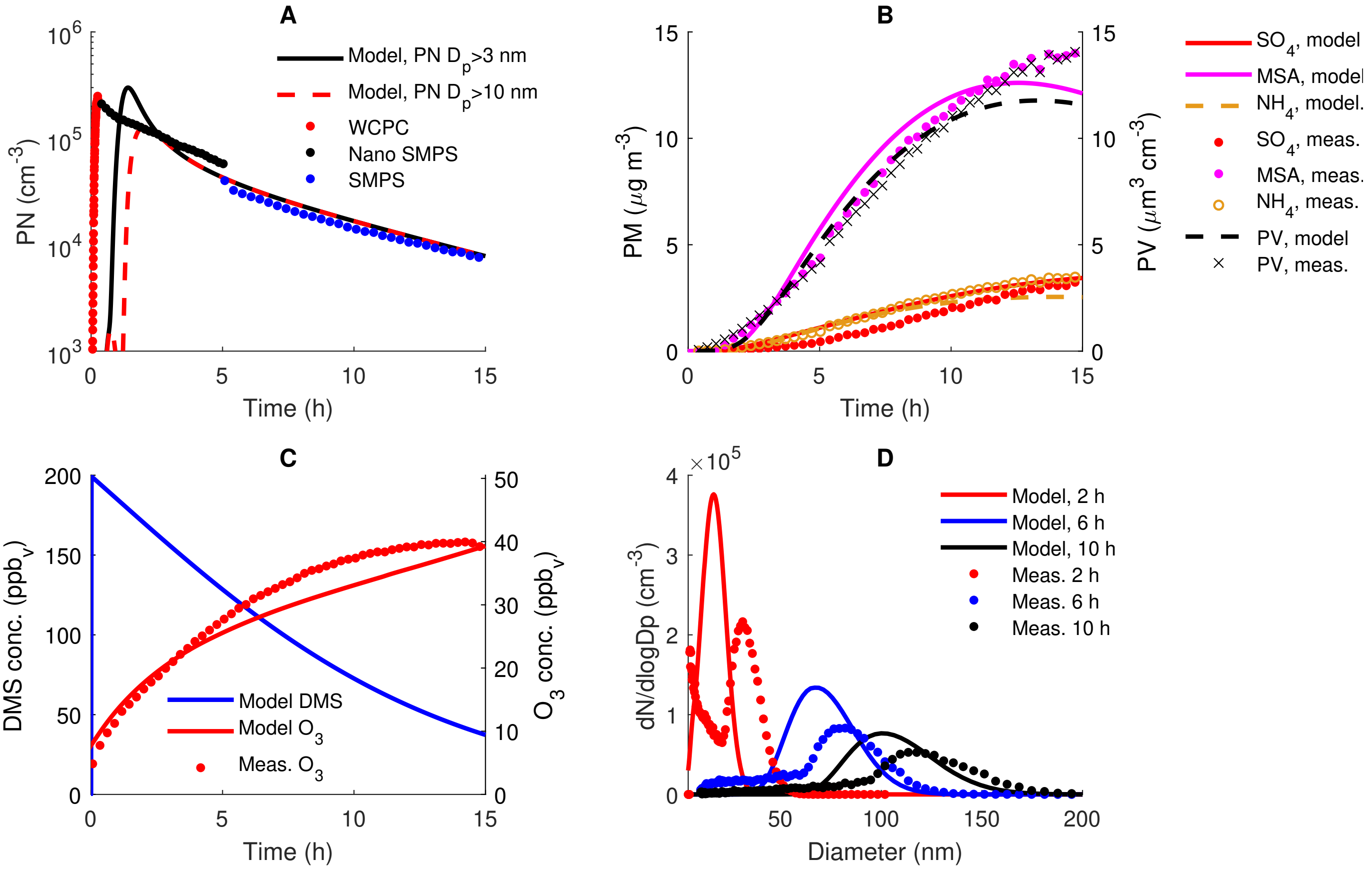

Figure S26. Model and measurement results from the dry DMS experiment DMS1. Panel **A**: measured and modelled particle number concentrations; Panel **B**: measured and modelled particle mass concentrations; Panel **C**: measured and modelled DMS and O_3 concentrations; and Panel **D**: measured and modelled particle number size distributions.

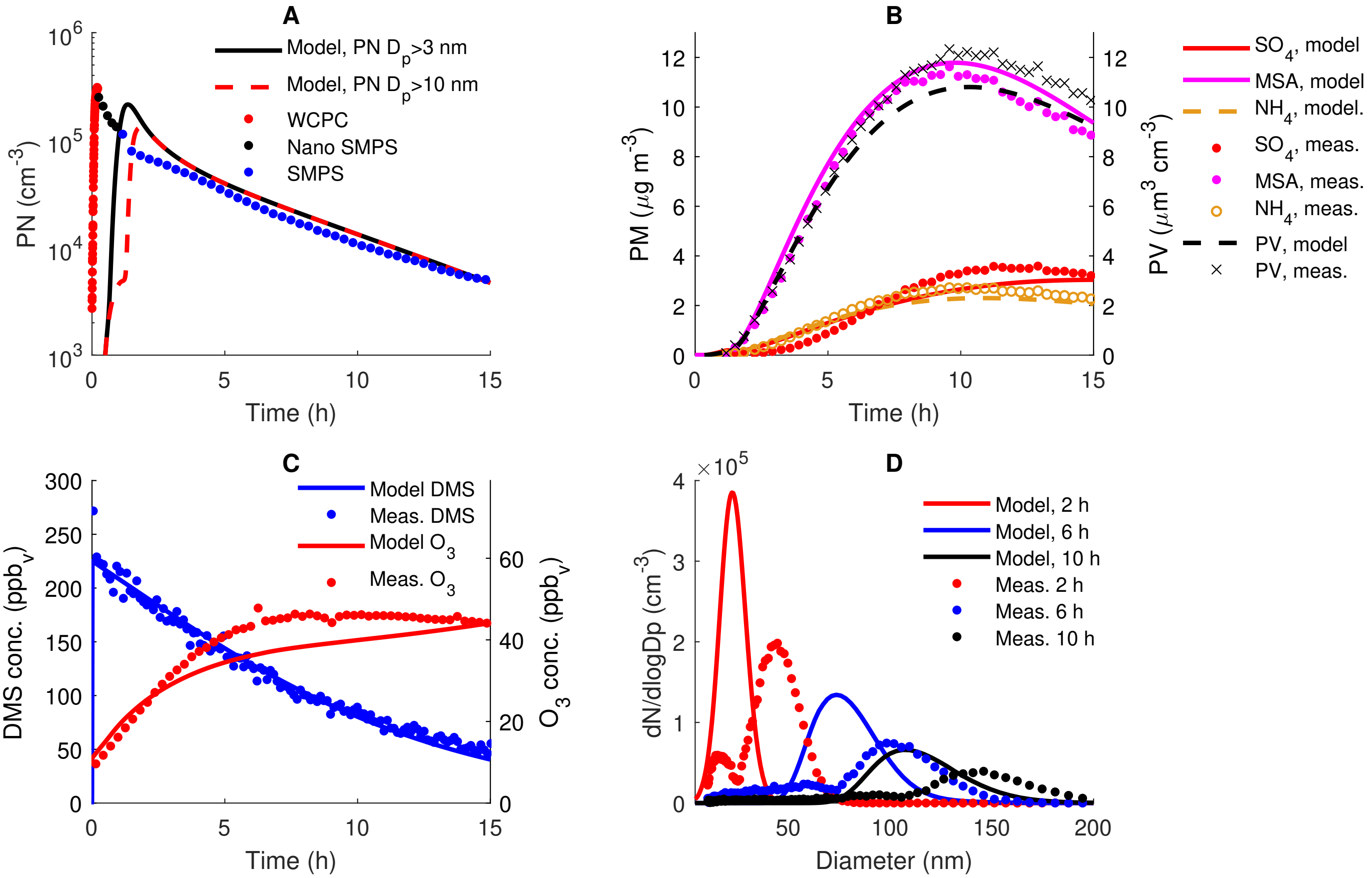

Figure S27. Model and measurement results from the dry DMS experiment DMS2. Panel **A**: measured and modelled particle number concentrations; Panel **B**: measured and modelled particle mass concentrations; Panel **C**: measured and modelled DMS and O_3 concentrations; and Panel **D**: measured and modelled particle number size distributions.

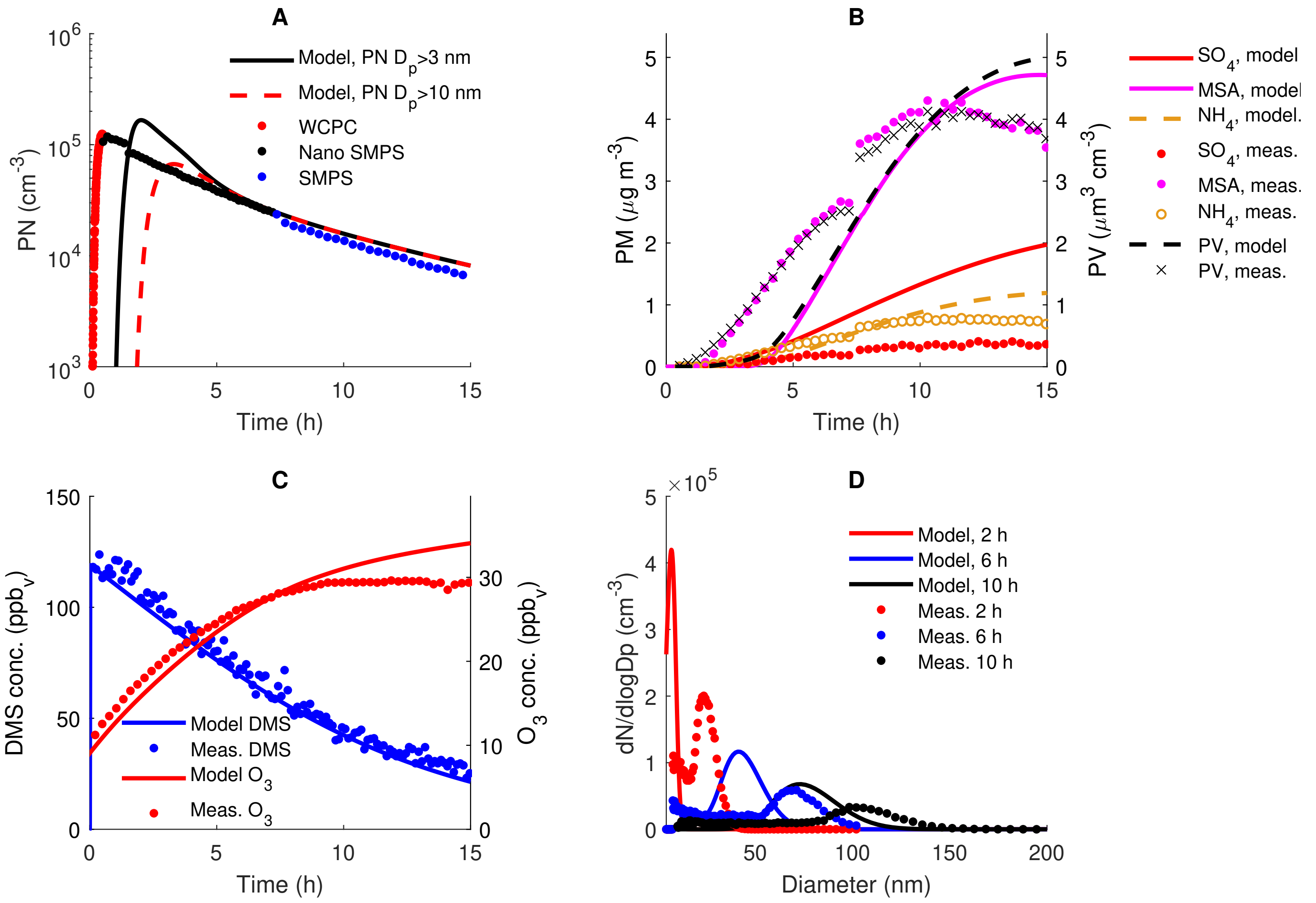

Figure S28. Model and measurement results from the dry DMS experiment DMS3. Panel **A**: measured and modelled particle number concentrations; Panel **B**: measured and modelled particle mass concentrations; Panel **C**: measured and modelled DMS and O_3 concentrations; and Panel **D**: measured and modelled particle number size distributions.

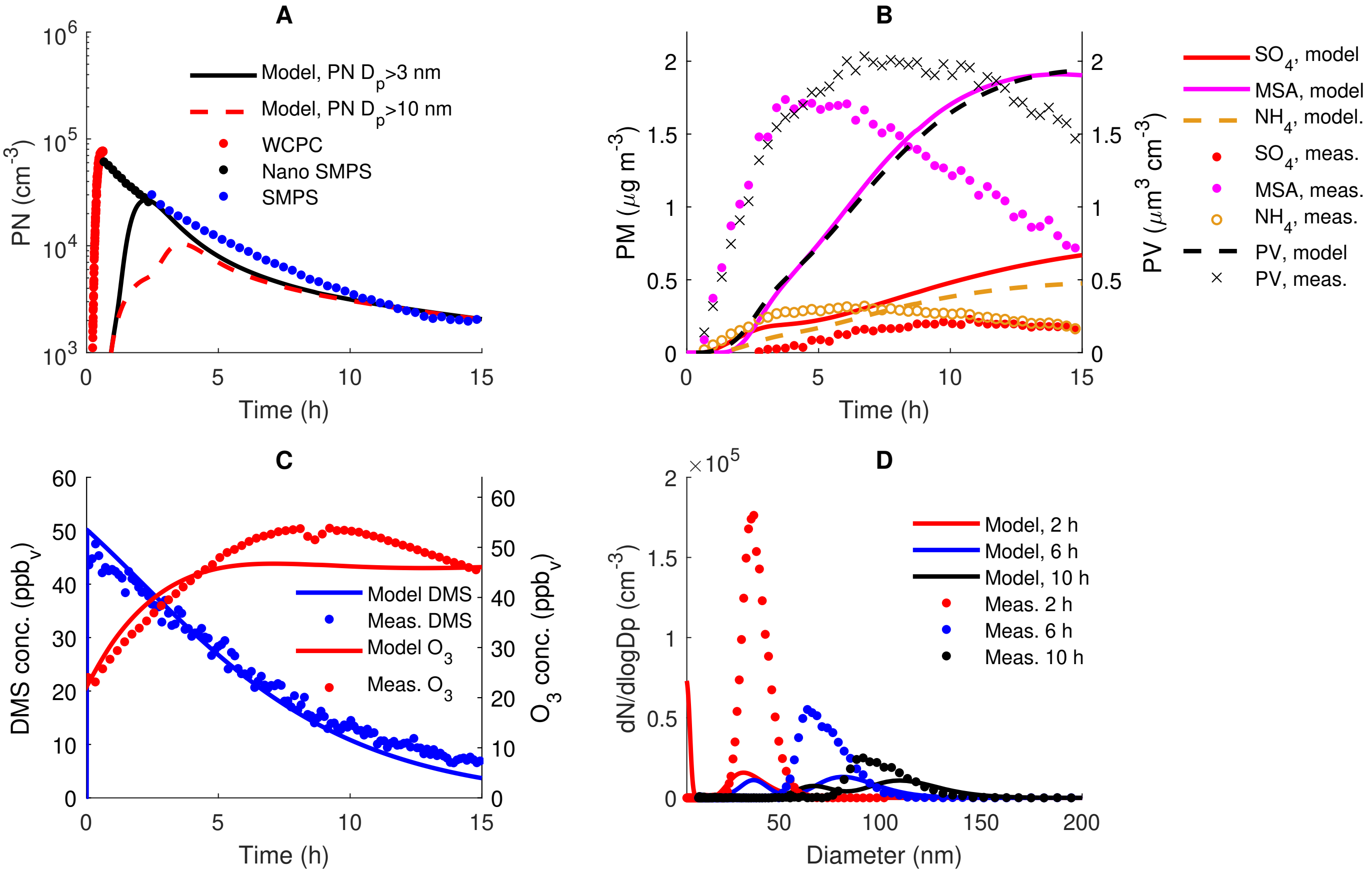

Figure S29. Model and measurement results from the dry DMS experiment DMS4. Panel **A**: measured and modelled particle number concentrations; Panel **B**: measured and modelled particle mass concentrations; Panel **C**: measured and modelled DMS and O_3 concentrations; and Panel **D**: measured and modelled particle number size distributions.

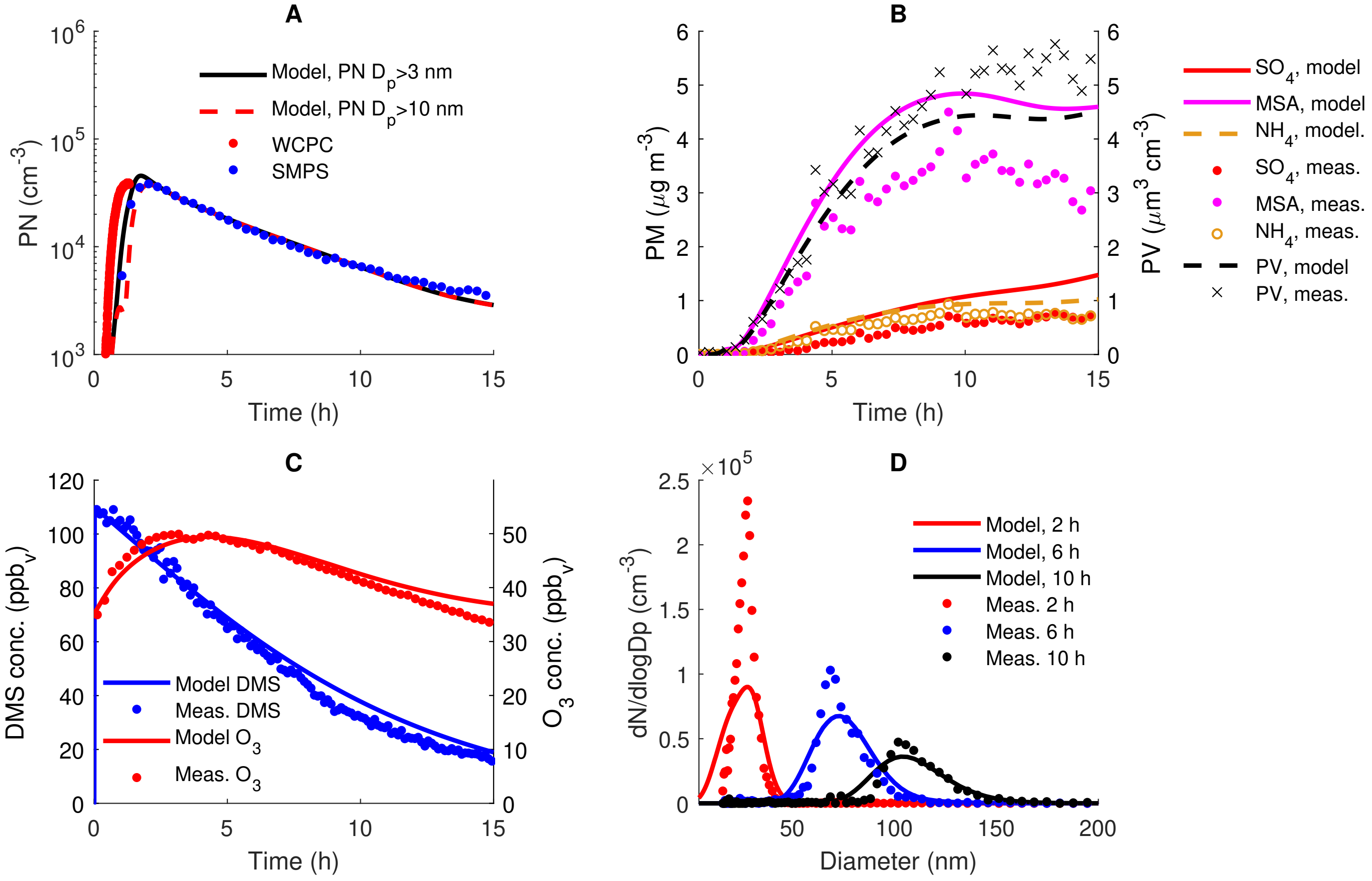

Figure S30. Model and measurement results from the dry DMS experiment DMS5. Panel **A**: measured and modelled particle number concentrations; Panel **B**: measured and modelled particle mass concentrations; Panel **C**: measured and modelled DMS and O_3 concentrations; and Panel **D**: measured and modelled particle number size distributions.

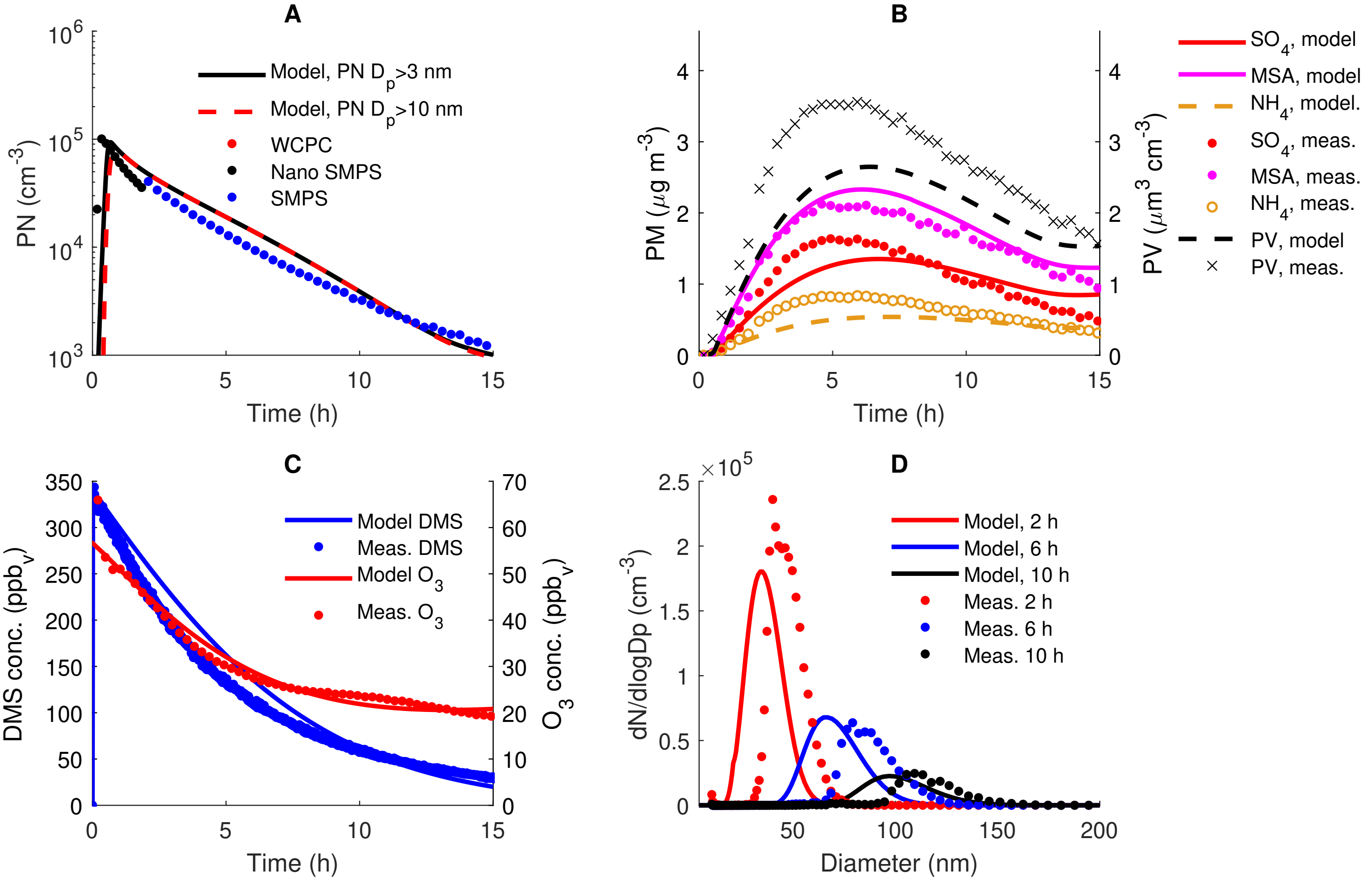

Figure S31. Model and measurement results from the humid DMS experiment DMS6. Panel **A**: measured and modelled particle number concentrations; Panel **B**: measured and modelled particle mass concentrations; Panel **C**: measured and modelled DMS and O_3 concentrations; and Panel **D**: measured and modelled particle number size distributions.

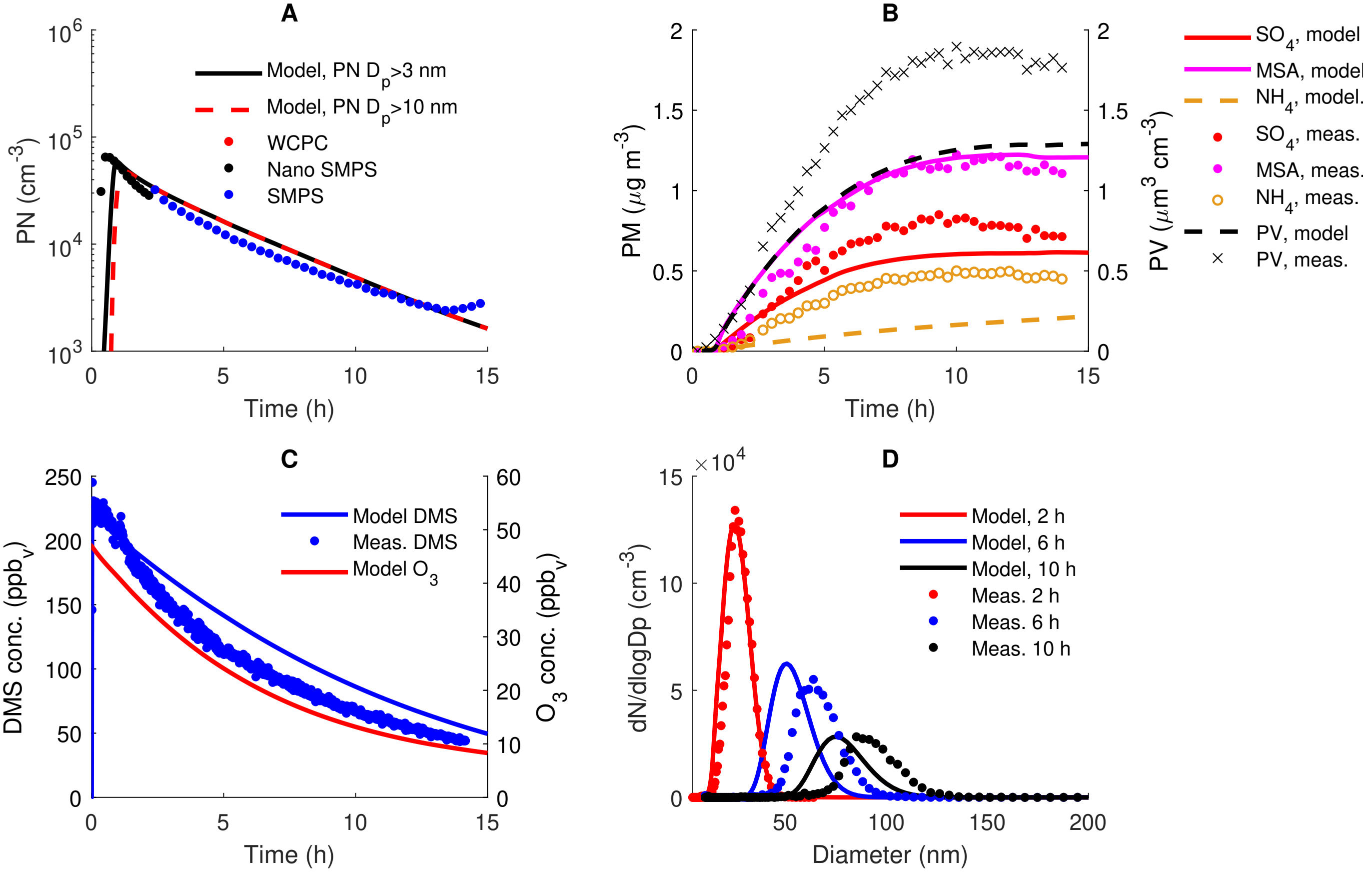

Figure S32. Model and measurement results from the humid and cold DMS experiment DMS7. Panel **A**: measured and modelled particle number concentrations; Panel **B**: measured and modelled particle mass concentrations; Panel **C**: measured and modelled DMS and O_3 concentrations; and Panel **D**: measured and modelled particle number size distributions.

S3.2 HMPTF and MSIA gas-phase chemistry

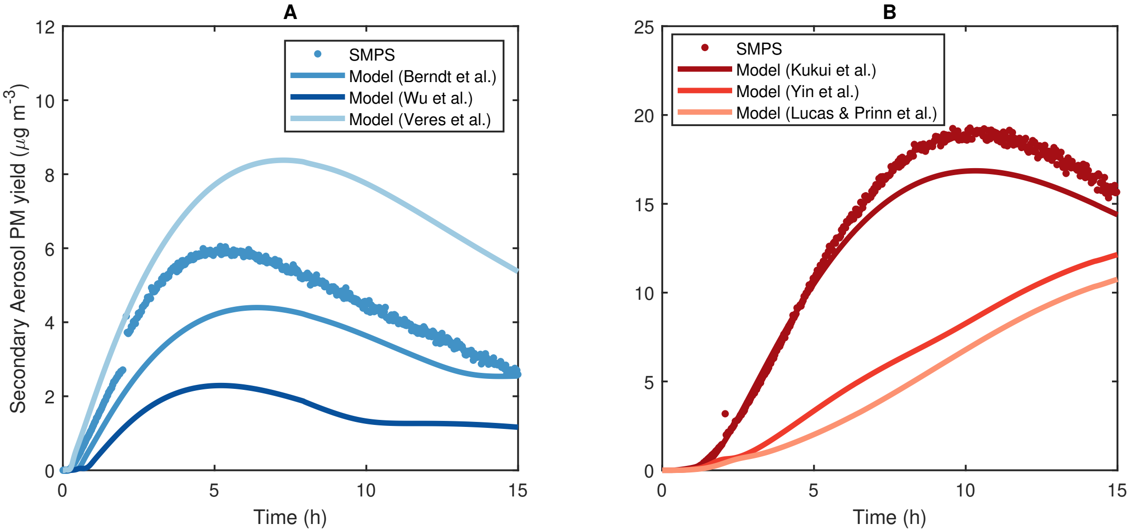

Figure S33. Modelled and measured (SMPS) PM using the $\mathrm{CH_3SCH_2OO}$ radical autoxidation rate from Berndt et al. (2019), Veres et al. (2020) or Yin et al. (1990), panel **A**, and the $\mathrm{MSIA + OH}$ oxidation rate by Kukui et al. (2003), Yin et al. (1990) or Lucas and Prinn (2002), panel **B**. Model runs are color-coded by their reaction constant - a strong color denoting a high value.

S3.3 Atmospheric implication

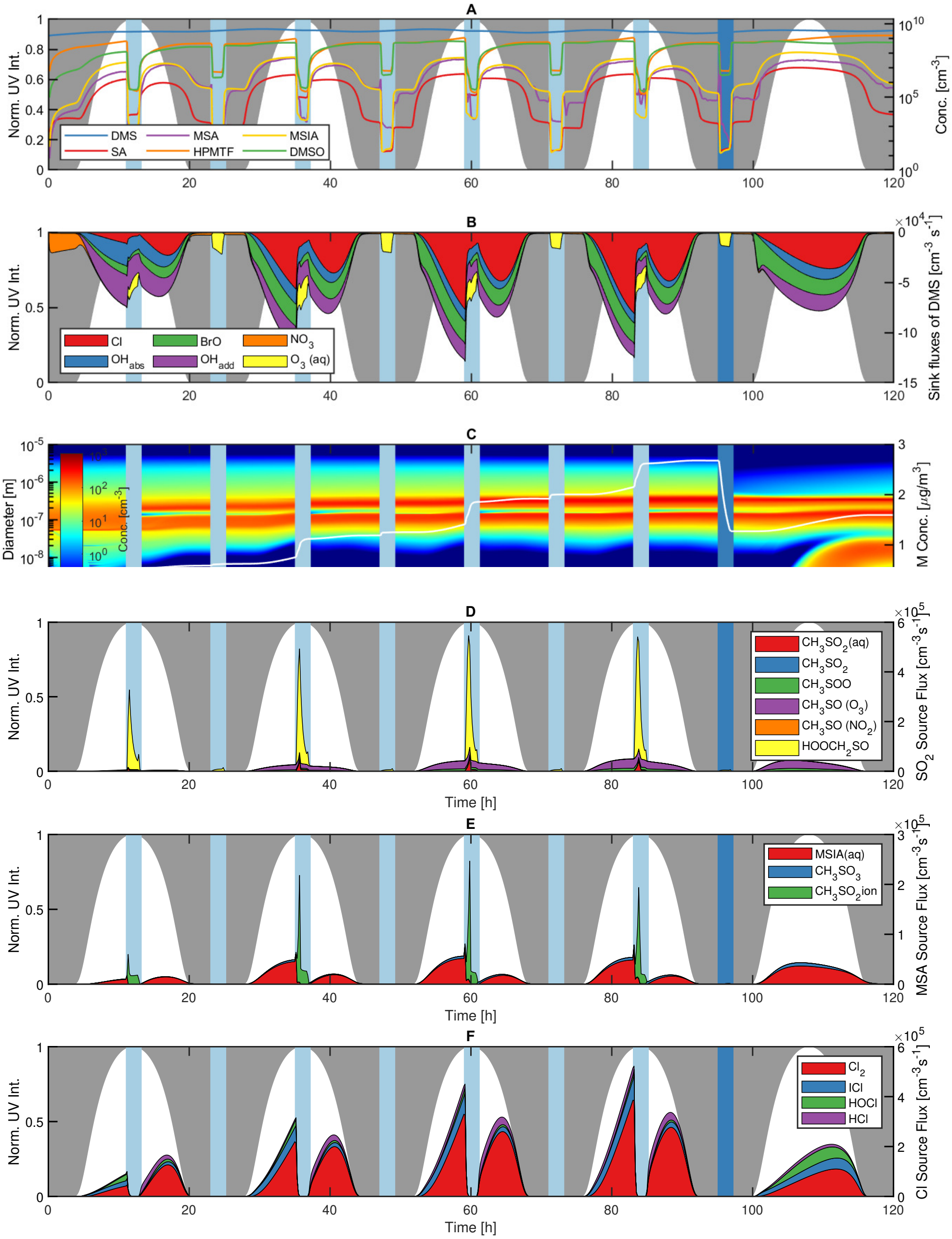

Figure S34. Modelled DMS oxidation and subsequent PM production related to the PolAtm sensitivity run. Panel **A** illustrates the evolution of DMS, SA, MSA, HMPTF, MSIA and DMSO gas-phase concentrations, **B** the sink fluxes of DMS due to Cl, OH, BrO, NO_3 and O_3 and **C** the number size distribution and secondary aerosol PM production. Panel **D**, **E** and **F** denote the source flux of SO_2, MSA and Cl, respectively. Light blue areas denote in-cloud period, in which rain events are represented as dark blue. Night and daytime periods are represented by the normalised UV-intensity and marked by grey and white areas, respectively.

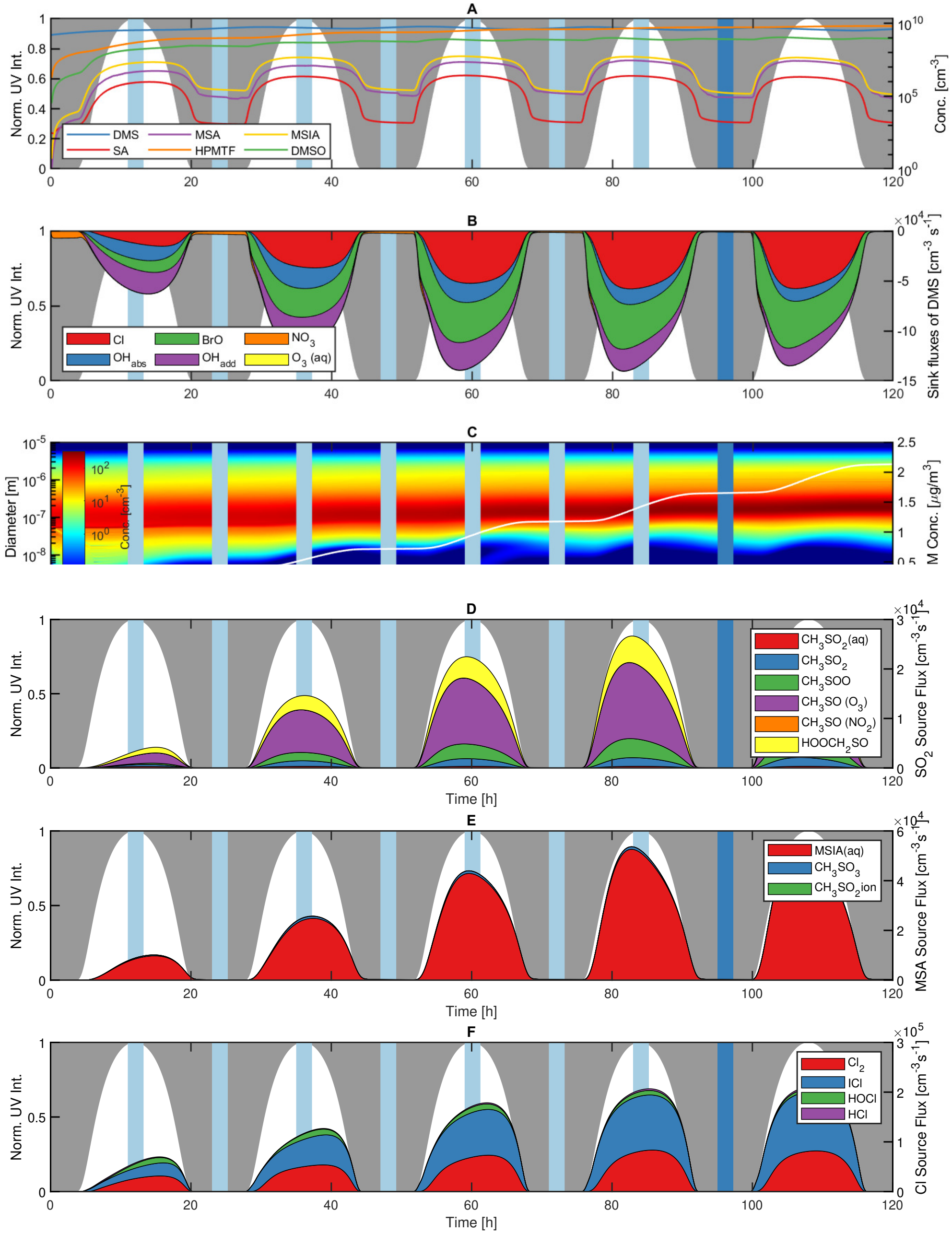

Figure S35. Modelled DMS oxidation and subsequent PM production related to the woCloudAtm sensitivity run. Panel **A** illustrates the evolution of DMS, SA, MSA, HMPTF, MSIA and DMSO gas-phase concentrations, **B** the sink fluxes of DMS due to Cl, OH, BrO, NO_3 and O_3 and **C** the number size distribution and secondary aerosol PM production. Panel **D**, **E** and **F** denote the source flux of SO_2, MSA and Cl, respectively. Light blue areas denote in-cloud period, in which rain events are represented as dark blue. Night and daytime periods are represented by the normalised UV-intensity and marked by grey and white areas, respectively.

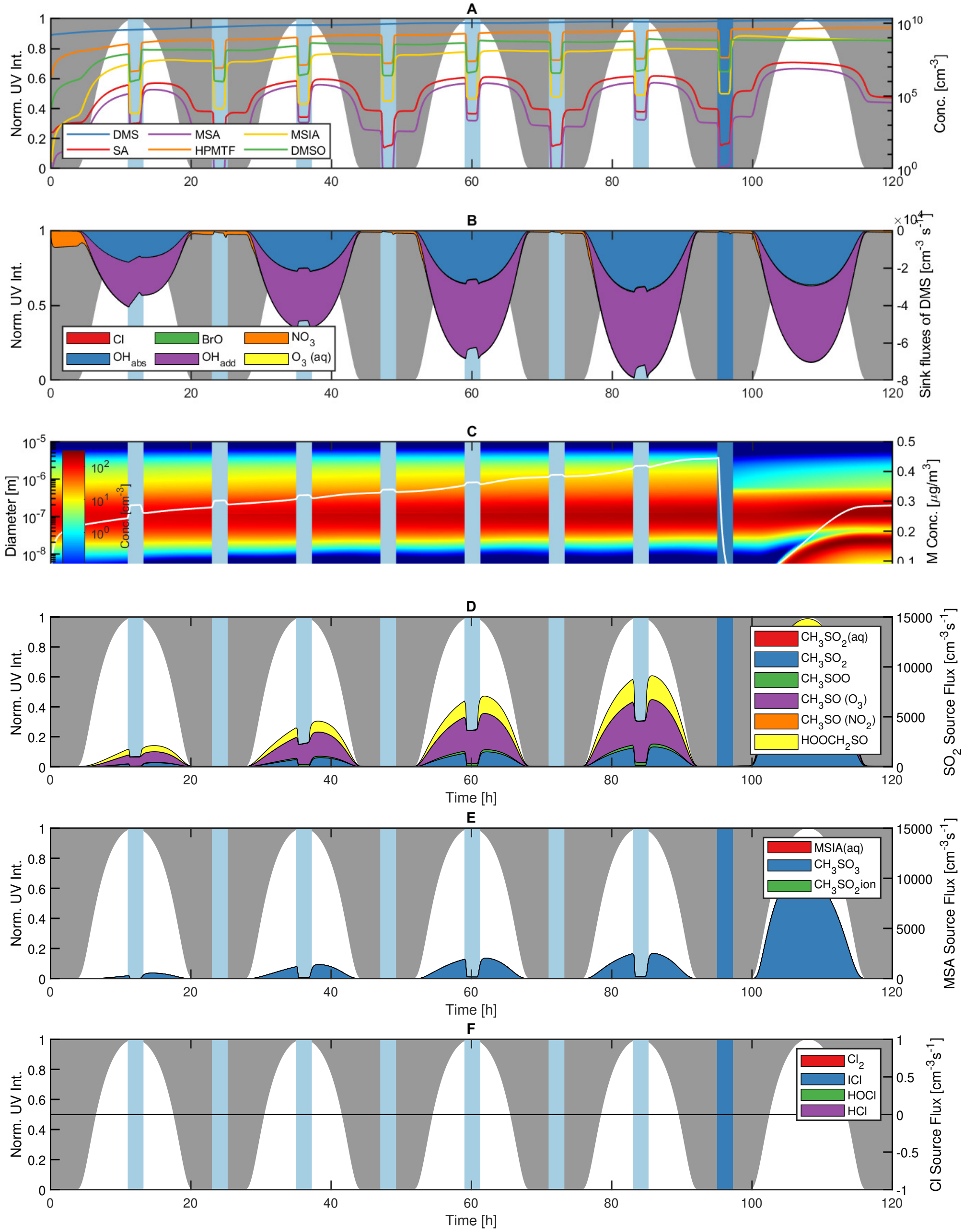

Figure S36. Modelled DMS oxidation and subsequent PM production related to the woAqAtm sensitivity run. Panel **A** illustrates the evolution of DMS, SA, MSA, HMPTF, MSIA and DMSO gas-phase concentrations, **B** the sink fluxes of DMS due to Cl, OH, BrO, NO_3 and O_3 and **C** the number size distribution and secondary aerosol PM production. Panel **D**, **E** and **F** denote the source flux of SO_2, MSA and Cl, respectively. Light blue areas denote in-cloud period, in which rain events are represented as dark blue. Night and daytime periods are represented by the normalised UV-intensity and marked by grey and white areas, respectively.

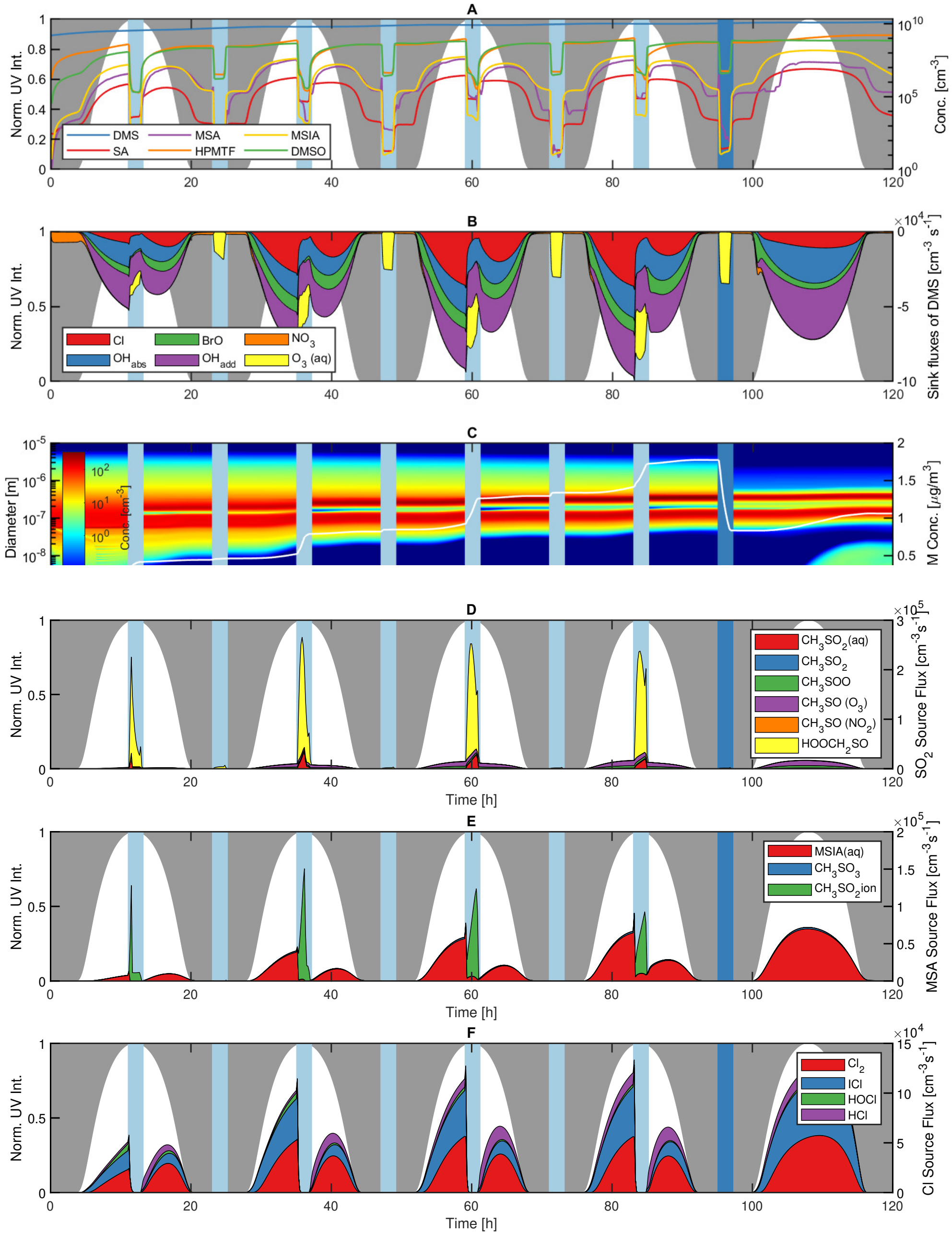

Figure S37. Modelled DMS oxidation and subsequent PM production related to the lowWindAtm sensitivity run. Panel **A** illustrates the evolution of DMS, SA, MSA, HMPTF, MSIA and DMSO gas-phase concentrations, **B** the sink fluxes of DMS due to Cl, OH, BrO, NO_3 and O_3 and **C** the number size distribution and secondary aerosol PM production. Panel **D**, **E** and **F** denote the source flux of SO_2, MSA and Cl, respectively. Light blue areas denote in-cloud period, in which rain events are represented as dark blue. Night and daytime periods are represented by the normalised UV-intensity and marked by grey and white areas, respectively.

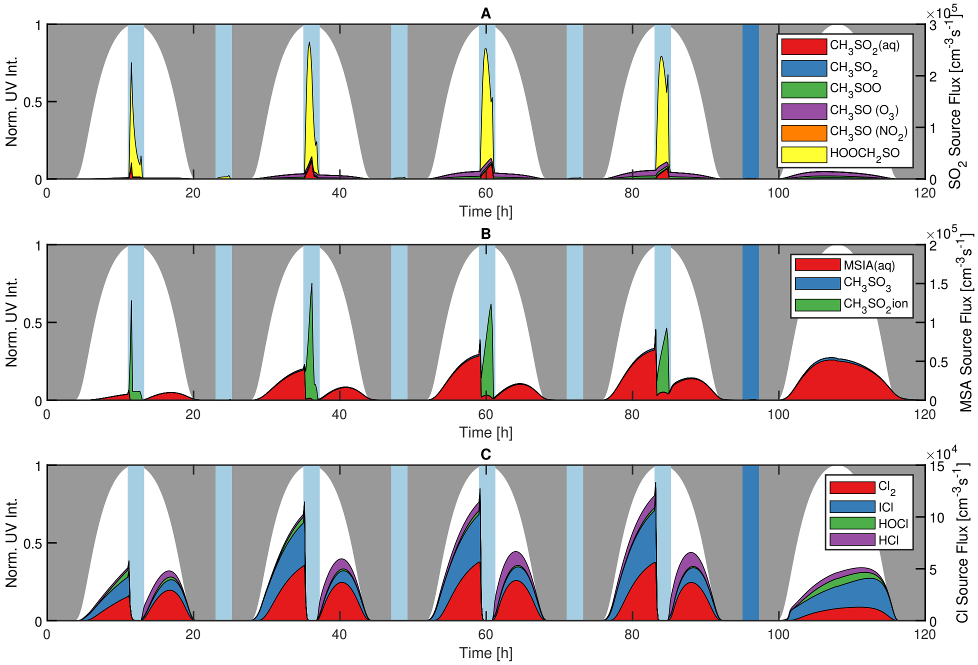

Figure S38. Modelled DMS oxidation realted to the AtmMain base run. Panel **A**, **B** and **C** denote the source flux of SO_2, MSA and Cl, respectively. Light blue areas denote in-cloud period, in which rain events are represented as dark blue. Night and daytime periods are represented by the normalised UV-intensity and marked by grey and white areas, respectively.

References

Atkinson, R., Baulch, D., Cox, R., Crowley, J., Hampson, R., Hynes, R., Jenkin, M., Rossi, M., and Troe, J.: Evaluated kinetic and photochemical data for atmospheric chemistry: Volume III - Gas phase reactions of inorganic halogens, Atmospheric Chemistry and Physics, 7, https://doi.org/10.5194/acp-7-981-2007, 2007.

Atkinson, R., Baulch, D., Cox, R., Crowley, J., Hampson, R., Hynes, R., Jenkin, M., Rossi, M., J, T., and Wallington, T.: Evaluated kinetic and photochemical data for atmospheric chemistry: Volume IV–gas phase reactions of organic halogen species, Atmospheric Chemistry and Physics, 8, https://doi.org/10.5194/acp-8-4141-2008, 2008.

Berndt, T., Scholz, W., Mentler, B., Fischer, L., Hoffmann, E., Tilgner, A., Hyttinen, N., Prisle, N. L., Hansel, A., and Herrmann, H.: Fast Peroxy Radical Isomerization and OH Recycling in the Reaction of OH Radicals with Dimethyl Sulfide, The Journal of Physical Chemistry Letters, 2019, https://doi.org/10.1021/acs.jpclett.9b02567, 2019.

Berndt, T., Chen, J., Møller, K. H., Hyttinen, N., Prisle, N. L., Tilgner, A., Hoffmann, E. H., Herrmann, H., and Kjaergaard, H. G.: SO2 formation and peroxy radical isomerization in the atmospheric reaction of OH radicals with dimethyl disulfide, Chem. Commun., 56, 13 634–13 637, https://doi.org/10.1039/D0CC05783E, http://dx.doi.org/10.1039/D0CC05783E, 2020.

Braeuer, P., Tilgner, A., Wolke, R., and Herrmann, H.: Mechanism development and modelling of tropospheric multiphase halogen chemistry: The CAPRAM Halogen Module 2.0 (HM2), JOURNAL OF ATMOSPHERIC CHEMISTRY, 70, 19–52, https://doi.org/10.1007/s10874-013-9249-6, 2013.

Burkholder, J. B., Sander, S. P., Abbatt, J., Barker, J. R., Huie, R. E., Kolb, C. E., Kurylo, M. J., Orkin, V. L., Wilmouth, D. M., and H., W. P.: Chemical Kinetics and Photochemical Data for Use in Atmospheric Studies, Evaluation No. 18, JPL Publication, 15-10, https://doi.org/http://jpldataeval.jpl.nasa.gov, 2015.

COSMO*conf*: version 4.3, COSMO*logic* GmbH & Co. KG., Leverkusen, Germany, 2013.

Demore, W., Sander, S., Golden, D., Hampson, R., Kurylo, M., Howard, C., Ravishankara, A., Kolb, C., and Molina, M.: Chemical Kinetics and Photochemical Data for Use in Stratospheric Modeling, JPL Publication, 90, 1997.

Hoffmann, E. H., Tilgner, A., Schrödner, R., Bräuer, P., Wolke, R., and Herrmann, H.: An advanced modeling study on the impacts and atmospheric implications of multiphase dimethyl sulfide chemistry, Proceedings of the National Academy of Sciences, 113, 11 776–11 781, https://doi.org/10.1073/pnas.1606320113, https://www.pnas.org/content/113/42/11776, 2016.

Jacobson, M. Z.: Fundamentals of Atmospheric Modelling (2nd edition), Cambridge University Press, Cambridge, United Kingdom and New York, NY, USA, 2005.

Kahan, T., Washenfelder, R., Vaida, V., and Brown, S.: Cavity-Enhanced Measurements of Hydrogen Peroxide Absorption Cross Sections from 353 to 410 nm, The journal of physical chemistry. A, 116, 5941–7, https://doi.org/10.1021/jp2104616, 2012.

Kukui, A., Borissenko, D., Laverdet, G., and Bras, G.: Gas-Phase Reactions of OH Radicals with Dimethyl Sulfoxide and Methane Sulfinic Acid Using Turbulent Flow Reactor and Chemical Ionization Mass Spectrometry, Journal of Physical Chemistry A, 107, https://doi.org/10.1021/jp0276911, 2003.

Kulmala, M. and Laaksonen, A.: Binary nucleation of water–sulfuric acid system: Comparison of classical theories with different H2SO4 saturation vapor pressures, The Journal of Chemical Physics, 93, 696–701, https://doi.org/10.1063/1.459519, https://doi.org/10.1063/1.459519, 1990.

Kurtén, T., Hyttinen, N., D'Ambro, E. L., Thornton, J., and Prisle, N. L.: Estimating the saturation vapor pressures of isoprene oxidation products $C_5H_{12}O_6$ and $C_5H_{10}O_6$ using COSMO-RS, Atmos. Chem. Phys., 18, 17 589–17 600, https://doi.org/10.5194/acp-18-17589-2018, 2018.

Lucas, D. D. and Prinn, R. G.: Mechanistic studies of dimethylsulfide oxidation products using an observationally constrained model, Journal of Geophysical Research: Atmospheres, 107, ACH 12–1–ACH 12–26, https://doi.org/10.1029/2001JD000843, https://agupubs.onlinelibrary.wiley.com/doi/abs/10.1029/2001JD000843, 2002.

McMurry, P. H. and Grosjean, D.: Gas and Aerosol Wall Losses in Teflon Film Smog Chambers, Environ. Sci. Technol., Vol. 19, No. 12,, 19, 1176–1182, 1985.

Quéléver, L. L. J., Kristensen, K., Jensen, L. N., Rosati, B., Teiwes, R., Daellenbach, K. R., Peräkylä, O., Roldin, P., Bossi, R., Pedersen, H. B., Glasius, M., Bilde, M., and Ehn, M.: Effect of temperature on the formation of highly oxygenated organic molecules (HOMs) from alpha-pinene ozonolysis, Atmos. Chem. Phys., 19, 7609—7625, https://doi.org/10.5194/acp-19-7609-2019, 2019.

Sander, S., Friedl, R., Golden, D., Kurylo, M., Moortgat, G., Wine, P., Ravishankara, A., Kolb, C., Molina, M., Finlayson-Pitts, B., Huie, R., and Orkin, V.: Chemical Kinetics and Photochemical Data for Use in Atmospheric Studies, JPL Publication, 06–2, 2006.

TURBOMOLE: Version 7.11, a development of University of Karlsruhe and Forschungszentrum Karlsruhe GmbH, TURBOMOLE GmbH, 2010.

Veres, P. R., Neuman, J. A., Bertram, T. H., Assaf, E., Wolfe, G. M., Williamson, C. J., Weinzierl, B., Tilmes, S., Thompson, C. R., Thames, A. B., Schroder, J. C., Saiz-Lopez, A., Rollins, A. W., Roberts, J. M., Price, D., Peischl, J., Nault, B. A., Møller, K. H., Miller, D. O., Meinardi, S., Li, Q., Lamarque, J.-F., Kupc, A., Kjaergaard, H. G., Kinnison, D., Jimenez, J. L., Jernigan, C. M., Hornbrook, R. S., Hills, A., Dollner, M., Day, D. A., Cuevas, C. A., Campuzano-Jost, P., Burkholder, J., Bui, T. P., Brune, W. H., Brown, S. S., Brock, C. A., Bourgeois, I., Blake, D. R., Apel, E. C., and Ryerson, T. B.: Global airborne sampling reveals a previously unobserved dimethyl sulfide oxidation mechanism in the marine atmosphere, Proceedings of the National Academy of Sciences, 117, 4505–4510, https://doi.org/10.1073/pnas.1919344117, https://www.pnas.org/content/117/9/4505, 2020.

Wu, R., Wang, S., and Wang, L.: A New Mechanism for The Atmospheric Oxidation of Dimethyl Sulfide. The Importance of Intramolecular Hydrogen Shift in CH3SCH2OO Radical., The journal of physical chemistry. A, 119, https://doi.org/10.1021/jp511616j, 2014.

Yin, F., Grosjean, D., Flagan, R. C., and Seinfeld, J. H.: Photooxidation of dimethyl sulfide and dimethyl disulfide. II: Mechanism evaluation, Journal of Atmospheric Chemistry, 11, 365–399, https://doi.org/10.1007/BF00053781, https://doi.org/10.1007/BF00053781, 1990.